



CZECH TECHNICAL UNIVERSITY IN PRAGUE

Faculty of Civil Engineering

Department of Steel and Timber Structures

**NUMERICAL CALCULATION OF WELDS
IN STRUCTURES FROM HIGH-STRENGTH STEEL**

**NUMERICKÝ VÝPOČET SVARŮ
KONSTRUKCÍ Z VYSOKOPEVNOSTNÍ OCELI**

DOCTORAL THESIS

Ing. Abhishek Ghimire

Doctoral study programme: Civil Engineering
Branch of study: Integral Safety

Doctoral thesis tutor: prof. František Wald, CSc.

Prague, 2023

<https://doi.org/10.14311/dis.fsv.2023.018>

Dedicated to all my family members and especially to my daughter Anvi (Puku)

ACKNOWLEDGEMENT

I would like to express my deep appreciation and gratitude to my supervisor, Prof. František Wald, CSc. He has provided invaluable supervision, guidance, advice, constant support, and unwavering interest throughout my Ph.D. studies.

I also thank the team of the Department of Steel and Timber Structures and the Faculty of Civil Engineering for their support and guidance during my Ph.D. journey. I would also like to thank Ing. Matyáš Kožich, Ing. Vojtěch Stančík, Ph.D. for their support during the experiment. The work prepared under the project TAČR Merlion III FW01010392, Pokročilý návrh konstrukčních detailů/prvků pomocí strojového učení, Advanced design of structural details/elements using machine learning.

I am incredibly grateful to my family for their unwavering support and assistance throughout my Ph.D. studies. My wife, Anjita Khanal, deserves the most thanks for her unwavering support, forbearance, and patience that have contributed significantly to this endeavor.

Lastly, I am grateful to everyone who contributed in any capacity to this project.

Ing. Abhishek Ghimire
December 2023, Prague

ABSTRACT

High strength steels (HSS) have become more prevalent in the steel market in recent years, bringing environmental benefits in sustainable construction. These steel grades have better tensile strength, toughness, and weldability than traditional steel grades. Steel yield strength continues to increase due to new production processes, which is critical for structural integrity in industries that use welding as a primary technique. The strength of welded joints can be determined by classical or finite element analysis (FEA) based on design guidelines. Numerical modeling is a reliable tool for designing the system and its components, and recently developed welding modeling techniques can save time and effort in fatigue design. However, there is a need for established methods to determine the resistance of welds in structural steels using numerical design models.

The prEN 1993-1-14:2021 standard provides two methods for finite element analysis-based design: numerical design calculation (NDC) and numerical simulation (NS). The objective of this study is to develop a numerical design model to evaluate the strength of fillet welds made of high strength structural steels for use in steel structures. The model uses NDC to calculate the weld strength of HSS transverse fillet lap welds. It is tested and validated using experimental, analytical, and finite element results. The study also determines the strain limit for HSS transverse and longitudinal fillet lap welds, the deformation capacity of transverse fillet lap welds, and provides benchmark examples for NDC.

This study focuses on the NDC method, which uses the Regular Inclined Shell Element Model (RISEM) in the Finite Element Method (FEM) to evaluate weld strength. NDC follows standardized procedures and uses shell elements to provide reliable and economical results with minimal computational requirements. However, it does not account for residual stresses and weld shrinkage. The inclined shell element in RISEM represents the geometry and stiffness of welds and controls their stresses in the plane. The study recommends the use of a common inclined shell element with rigid members to accurately represent the geometry and stiffness of fillet welds. A new strength criterion is proposed based on the stresses on the inclined shell element, using the uniform equivalent stress as an indicator. The validity of the method is confirmed by comparing RISEM and test results using finite element (FE) simulation.

The proposed design model helps engineers to accurately and efficiently determine the strength of HSS welded joints in combination with FEM. The deformation capacity of HSS transverse fillet lap welds is always less than 1 mm, as measured by Digital Image Correlation (DIC). The fracture surface area more accurately represents the weld strength than the effective theoretical area. The predicted strength based on EC3 and AISC is more conservative than the test strength. However, the expected weld strength calculated using AISC provides a better prediction value.

The NDC uses a RISEM to determine weld strength by limiting ultimate stresses. Tests and calculation results have shown that the RISEM weld resistance is 1.60 times higher than the analytical model (AM) in prEN1993-1-8:2020 for transverse welds. The reason for this may be the assumption of uniform stress distribution in the weld. However, in the case of longitudinal welds, the variance is only 11%. The plastic strain was limited to 5% in order to simplify the design resistance of transverse and longitudinal fillet welds, which allows to calculate the design resistance of the weld without laboratory material tests in the FE model, using only three primary parameters (E , f_y , and f_u). Benchmark examples for transverse and longitudinal fillet welds made of S700 MC Plus-OK AristoRod 13.12 were performed with a 5% plastic strain limit. The RISEM results show good agreement with the AM in both welding configurations, with a maximum difference from the AM of 11%.

RISEM can be used as an economical design model for welded joints. However, the scope of work is limited to certain types of fillet lap welds. Further investigations on different weld configurations of fillet welds of high strength structural steels can ensure the applicability of the design

models. This calculation approach could also be extended to other welded connections, such as long welds, ribbed plate connections, and connections to unstiffened flanges, which could greatly increase the reliability of the proposed model.

Keywords: Steel structures, Design, Analytical model, Numerical calculation, High-strength steel, Weld resistance, Deformation capacity, Ductility, Inclined shell element, Regular inclined shell element model, Digital image correlation, Stress integration method, Strain limit

CONTENTS

ACKNOWLEDGEMENT	3
ABSTRACT.....	4
LIST OF ABBREVIATIONS	9
NOMENCLATURE	10
CHAPTER 1: INTRODUCTION	12
1.1 Background	12
1.2 Overview	12
CHAPTER 2: LITERATURE REVIEW	14
2.1 High-strength steel.....	14
2.1.1 General	14
2.1.2 Historical development of high-strength steels	14
2.1.3 Advantages and application of high-strength structural steels	14
2.1.4 Welding of high-strength steel	15
2.2 Design rules	17
2.2.1 European standard.....	17
2.2.2 US standard AISC 360-16.....	20
2.3 Experimental research.....	22
2.4 Numerical modeling of welds	31
2.5 Basic concepts of digital image correlation techniques	32
2.6 Strain limit	33
CHAPTER 3: OBJECTIVES.....	34
CHAPTER 4: EXPERIMENT	35
4.1 Material information	35
4.1.1 Base metal	35
4.1.2 Filler metal	38
4.2 Specimen information	41
4.2.1 General	41
4.2.2 Geometry and Configuration.....	41
4.3 Test setup and the measurement	43
4.3.1 Measurement of force and displacement.....	43
4.3.2 Measurement of fracture surface area	44
4.4 Results: Strength	45
4.5 Results: Deformation capacity and ductility	47

CHAPTER 5: ANALYTICAL MODEL	51
5.1 Material information	51
5.3 Specimen information	51
5.4 Analytical calculation: Weld resistance	52
CHAPTER 6: FINITE ELEMENT MODEL.....	54
6.1 Specimen information	54
6.2 Solid model	54
6.2.1 Material model	54
6.2.2 Finite element modelling.....	55
6.2.3 Mesh sensitivity study	56
6.2.4 Validation of solid model.....	57
6.3 Shell model	59
6.3.1 Material model	59
6.3.2 Finite element modelling.....	59
6.3.3 Mesh sensitivity study	61
6.3.4 Verification of shell with solid model.....	63
6.3.5 Verification of shell with analytical model	65
CHAPTER 7: NUMERICAL DESIGN CALCULATION.....	67
7.1 Strength criterion of fillet welded connection.....	67
7.1.1 Maximum equivalent stress method.....	67
7.1.2 Stress integration method	69
7.2 Results.....	72
CHAPTER 8: VALIDATION AND VERIFICATION	74
8.1 Validation of numerical calculations	74
8.2 Verification of numerical calculations	77
8.3 Benchmark examples	78
CHAPTER 9: PLASTIC STRAIN.....	82
9.1 General.....	82
9.2 Numerical model.....	82
9.2.1 Minimum elongation at failure.....	82
9.2.2 Evaluation the purposed strain limits	83
9.2.3 Verification	84
9.3 Benchmark examples	86
CHAPTER 10: SUMMARY AND OUTLOOK.....	91
10.1 Summary	91

10.2 Outlook	92
REFERENCE.....	93
Annex 1 Detail measurement of the specimen.....	98
Annex 2 Material properties	101
Annex 3 Displacement and strain vs. time.....	104
Annex 4 Force-Deformation curve	109
Annex 5 Strength vs. strain.....	112
Annex 6 Summary of experimental results.....	115
Annex 7 Summary of analytical calculation	116
Annex 8 Summary of numerical design calculation	117
LIST OF TABLES	118
LIST OF FIGURES	120

LIST OF ABBREVIATIONS

AM	Analytical model
ASD	Allowable strength design
CEV	Carbon equivalent value
DIC	Digital image correlation
FE	Finite element
FEA	Finite element analysis
FEM	Finite element model
HSS	High-strength steel
HSSs	High-strength steels
L	Longitudinal weld
LRFD	Load and resistance factor design
NDC	Numerical design calculation
NS	Numerical simulation
RISEM	Regular inclined shell element model
T	Transverse weld
TS	Transverse welded specimen
UHSS	Ultimate high-strength steel
UTS	Ultimate tensile strength

NOMENCLATURE

a	Throat thickness of the weld [mm]
A_{th}	Theoretical surface area of weld [mm ²]
A_{fr}	Fracture surface area of weld [mm ²]
F_u	Ultimate load capacity [kN]
A_{BM}	Cross-sectional area of the base metal [mm ²]
A_{we}	Effective area of the weld [mm ²]
b_1	Width of base plate [mm]
b_2	Width of cover plate [mm]
E	Young's modulus of elasticity [GPa]
F_{EXX}	Filler metal classification strength [MPa]
F_{nBM}	Nominal stress of the base metal [MPa]
F_{nw}	Nominal stress of the weld metal [MPa]
f_u	Material ultimate tensile stress [MPa]
F_{Ed}	Applied force [kN]
$F_{W,Ed}$	Design value of the weld force per unit length [kN]
$F_{W,Rd}$	Design weld resistance per unit length [kN]
$F_{w,Rd,T}$	Design weld resistance of transverse weld [kN]
$F_{w,Rd,L}$	Design weld resistance of longitudinal weld [kN]
$f_{u,PM}$	Nominal ultimate tensile strength of the parent metal [MPa]
$f_{u,FM}$	Nominal ultimate tensile strength of filler metal [MPa]
$f_{vw,d}$	Design shear strength of the weld [kN]
f_y	Material yield stress [MPa]
L	Length of the weld [mm]
L_j	Overall length of the lap [mm]
R_n	Nominal weld stress [MPa]
R_{RISEM}	Design resistance of regular inclined shell element model [kN]
R_{nwl}	Total nominal strength of longitudinally loaded fillet welds [MPa]
R_{nwt}	Total nominal strength of transversely loaded fillet welds [MPa]
t_1	Thickness of base plate [mm]
t_2	Thickness of cover plate [mm]

w	shear leg of weld [mm]
β	Reduction factor [-]
β_w	Correlation factor depends on the grade of steel [-]
β_{wL}	Reduction factor for long weld [-]
$\beta_{w,mod}$	Modified correlation factor that depends on the filler metal strength [-]
$\beta_{w,mod,mix}$	Correlation factor for mixed connections [-]
δ_u	Deformation capacity [mm]
ε_u	Ultimate strain [%]
ε_{eff}^{in}	Effective strain in the inclined shell element [%]
θ	Angle between the longitudinal direction of the force and the weld [°]
\emptyset	Resistance factor [-]
Ω	Safety factor [-]
γ_{M2}	Partial safety factor for the resistance of welds [-]
σ_{\perp}	The normal stress perpendicular to the throat [MPa]
σ_{\parallel}	The normal stress parallel to the axis of the weld [MPa]
σ_n	Normal stress acting on inclined shell element [MPa]
σ_x	Normal stress in x-direction [MPa]
σ_y	Normal stress in y-direction [MPa]
τ_{\perp}	The shear stress (In the plane of the throat) perpendicular to the axis of the weld [MPa]
τ_{\parallel}	The shear stress (in the plane of the throat) parallel to the axis of the weld [MPa]
τ_{θ}	Normal shear stress acting on inclined shell element [MPa]
τ_p	Shear stress acting parallelly on inclined plane [MPa]
τ_{xy}	Shear stress in y-direction [MPa]
τ_{yx}	Shear stress in x-direction [MPa]
σ_{eqv,max_T}	Maximum resultant equivalent stress acting on inclined shell element in FE shell model when a line of action of the force is perpendicular to the weld direction [MPa]
σ_{eqv,max_L}	Maximum resultant equivalent stress acting on inclined shell element in FE shell model when a line of action of the force is parallel to the weld direction [MPa]
σ_{eqv,in_T}	Equivalent uniform stress acting on inclined shell element in FE shell model when a line of action of the force is perpendicular to the weld direction [MPa]
σ_{eqv,in_L}	Equivalent uniform stress acting on inclined shell element in FE shell model when a line of action of the force is parallel to the weld direction [MPa]
$\sigma_{w,Ed}$	Weld stress [MPa]

CHAPTER 1: INTRODUCTION

1.1 Background

In steel construction, welding connections frequently join two or more metallic parts by fusing them and filling them with molten metal from an electrode [1]. Several types of welded connections, fillet welds, fillet welds all around, butt welds, plug welds, and flare groove welds, are used in the construction field based on their properties [2]. For building constructions, fillet and partial penetration connections are commonly employed. Therefore, a great deal of experimental and analytical research has been conducted to understand the behavior of fillet welds in predicting their strength and ductility [3].

High-strength steels (HSSs) have become more prevalent in the steel market in the past few years. Steel yield strength is constantly growing due to the continual development of new production processes [4]. Many steel industries are working to develop light and slender constructions of steel structures having good welding characteristics and high ductility [5]. High-strength steel (HSS) creates lighter structures requiring smaller foundations, reducing transportation and construction costs and releasing less CO₂ [4]. Structural integrity is one of the crucial aspects in many industrial sectors where welding is a primary technique for connection. It is necessary to ensure these welded connections' strength and sufficient ductility and toughness to redistribute stresses and internal forces when using HSS [6].

The strength of welded connections can be determined using classical analysis or finite element analysis (FEA) based on the details described in the respective design guidelines [7]. According to Krejsa et al. [8], numerical modeling is used interestingly in design practice by using an efficient software system that can provide valuable results regarding the reliability of the proposed approach and elements. Recently, various modeling techniques were developed for the design of welds in structural steels for fatigue design, which minimizes the modeling work effort and time. At the same time, these increase the level of accuracy in representing the welds [9].

1.2 Overview

The investigation of HSS transverse fillet lap-welded connection behavior is categorized as experimental, analytical, and numerical analysis. This study focuses on weld resistance and deformation capacity.

The work is structured as follows:

Chapter 2 reviews the literature for the current design guidelines, experimental studies, numerical modeling of welds, basic theory for digital image correlation (DIC) approaches, and the principle of strain limit for design purposes. Additionally, it discusses the distinctive qualities of HSSs, which are crucial for presenting the experimental results later.

The main objective of the current study is explained in Chapter 3, which includes the primary and secondary goals of the work.

The outcomes of experimental works are explained and interpreted in Chapter 4. This chapter thoroughly explains the specimen geometry, material details, test execution process, and test results.

Similarly, Chapter 5 covers the analytical model (AM) of a transverse fillet lap-welded connection made of HSS, along with the analytical calculation of weld resistance, which is then contrasted with the outcomes of a numerical design model.

The modeling of solid and shell element finite element models as well as its validation and verification procedure explain in Chapter 6.

Chapter 7 presents and elaborates on the proposed numerical design calculation (NDC) of the HSS welds. This chapter analyzes and interprets results regarding the weld's resistance, deformation capacity, and ductility.

Furthermore, Chapter 8 clearly defines the verification and validation of the proposed NDC. Benchmark examples of fillet welds are also given to ensure the suggested paradigm.

On top of that, a plastic strain design limit is introduced for transverse and longitudinal fillet lap-welded connections from HSS in Chapter 9. Benchmark examples are also agreed upon to ensure the suggested theory.

The final chapter, Chapter 10, summarizes the essential findings and results regarding the weld resistance, deformation capacity, and ductility of transverse fillet lap-welded connections composed of HSS and offers propositions for additional research with suggestions for future research work to broaden the applicability of design model.

CHAPTER 2: LITERATURE REVIEW

2.1 High-strength steel

2.1.1 General

The application of high-strength steel (HSS) increases interestingly in the structural steel field. It is always sensitive for the designer to compute the design resistance of connection in steel structures. The numerical design calculation (NDC) will help the engineers accurately and efficiently determine the resistance of welded connection from HSS in combination with a finite element model (FEM). The material and the welding procedure influence the strength of the welded connection. During the welding, great heat generation and extreme cooling speeds occurred, leading to structural changes and, thus, changes in the properties of the weld metal. This chapter introduces the historical development of HSS, its advantages, and its application to current issues. In addition to this, it explains the determination and influence of welding parameters.

2.1.2 Historical development of high-strength steels

The development of modern HSSs started in the second half of the sixties, when many grades began to be produced by heat treatment, initially hardening, followed by tempering. The thermomechanical rolling process developed in Japan in the mid-seventies. These two production processes are currently the most popular, resulting in products with different application areas due to their specific properties. The HSS characterizes a higher toughness, better weldability, cold formability, and the ability to withstand increased atmospheric corrosion compared to conventional steel. It also has a good performance in tensile strength. Nowadays, HSSs are used in a wide range, with a demand for lightweight design structures with increased structural performance [10]. Many steelmakers have carried out extensive studies about the welding of HSS, and they have recommended for welding of this steel [11].

2.1.3 Advantages and application of high-strength structural steels

The characteristics of high-strength structural steels include a high yield point, significant toughness at low temperatures, and excellent weldability. Utilizing HSSs offers numerous advantages compared to ordinary-strength steels. These include enhanced safety due to their superior strength in the elastic phase, improved cost-effectiveness through smaller member sizes, and reduced structural weight, resulting in decreased welding work. Most notably, the environment and ecology benefit from the reduced utilization of steel, welding, and coating materials, leading to lower consumption of non-renewable resources [12]. Using HSS grades reduces the cross-sectional area, reducing the dead weight. In addition, this process also impacts the costs of a steel structure. Reducing the cross-sections also enables larger assemblies and assembly units with lower transport and assembly costs simultaneously. Due to this, the manufacturing costs decrease with increasingly smaller wall thicknesses. As a result, modern structural steels enable the realization of innovative and economical steel structures. These HSSs can be used in planning highly stressed columns in industrial and multi-story buildings, trusses with large spans, and offshore structures. Thus, it is possible to meet planners' and engineers' needs for lightweight, cost-effective constructions while considering sustainability possible [13]. When using HSSs to construct lightweight structures, it is essential to consider how the service loading, material, geometry, and manufacturing method interact because durability is determined by this relationship [14]. In conclusion, modern types of HSS have great potential use for new practical and aesthetic structural solutions. Numerous applications in Europe and worldwide show that modern types of HSS enable very economical and sustainable solutions for bridges and building structures [15]–[18].

In the past few years, there has been evidence that using contemporary steel grades, like high-strength and weatherproof structural steels, can contribute to economic benefits, rapid construction, and the responsible utilization of natural resources. Structural steel's numerous advantages distinguish it from other materials, particularly reinforced concrete. These advantages include its exceptional ability to withstand tension and pressure, high modulus of elasticity, remarkable deformability, and unlimited recyclability at the end of its useful lifespan [13].

2.1.4 Welding of high-strength steel

The weldability of steel is mainly affected by its chemical composition. HSSs are weldable, and their welding characteristics vary slightly with the production route and individual characteristics of the HSS grade [19]. Weldability can be improved by reducing the hardness of the steel, and hardness can be reduced by lowering the carbon content during the manufacturing process [20]. Fine-grained structural steels are considered HSS, which has a higher yield point with high toughness value, and the carbon content of these steels is almost always below 0.2% [21]. To achieve the desired strength and toughness of the weld, the chemical composition of the filler material is fundamental [19].

2.1.4.1 Carbon equivalent value

The carbon equivalent value (CEV) is generally used to assess the weldability of steels. Several CEV formulae exist to measure the steel's hardenability, and given below (see Eq. 2.1) is the International Institute of Welding (III) definition of CEV used throughout Europe [19].

$$CEV = C + \frac{Mn}{6} + \frac{(Mo+Cr+V)}{5} + \frac{(Ni+Cu)}{15} \quad [\%] \quad (2.1)$$

where C is carbon content in wt. %, Mn is manganese content, Mo is molybdenum content, Cr is chromium content, V is vanadium content, Ni is nickel content, and Cu is copper content in wt. %.

A higher CEV generally leads to higher hardenability and a greater risk of hydrogen (cold) cracking in the welded joint [19]. The maximum permitted CEVs for high-strength plates in European product standards are given in Table 1 to Table 3.

Table 1 Maximum specified CEV for normalized HSS, EN 10025-3 [22].

Steel grade (N and NL)	Max. CEV in % for nominal product thickness [mm]		
	≤63	>63 and ≤100	>100 and ≤250
S420	0.48	0.50	0.52
S460	0.53	0.54	0.55

Table 2 Maximum specified CEV for thermomechanical rolled HSS, EN 10025-4 [23].

Steel grade (M and ML)	Max. CEV in % for nominal product thickness [mm]			
	≤16	>16 and ≤40	>40 and ≤63	>63 and ≤150
S420	0.43	0.45	0.46	0.47
S460	0.45	0.46	0.47	0.48
S500	0.47	0.47	0.47	0.48

Table 3 Maximum specified CEV for quenched and tempered HSS, EN 10025-6 [24].

Steel grade (Q, QL and QL1)	Max. CEV in % for nominal product thickness [mm]		
	≤50	>50 and ≤100	>100 and ≤200
S460	0.47	0.48	0.50
S500	0.47	0.70	0.70
S550	0.65	0.77	0.83
S620	0.65	0.77	0.83
S690	0.65	0.77	0.83

2.1.4.2 Welding consumables

Generally, welding consumables are chosen as per requirements of the strength and toughness of the weld. Baddoo and Chen [19] recommend using under-matched strength welding consumables to reduce the risk of hydrogen cold-cracking. However, if the tensile strength of the weld needs to be equal to or close to the strength of the parent metal, then matching filler metals are adopted.

2.1.4.3 Heat input

The heat input depends on the voltage, current, and welding speed (see Equation 2.2) [25]. Generally, low heat input prefers because of better toughness, increased strength, reduced deformation, lower residual stress, and a narrow heat-affected zone [19].

$$Q = kx E \quad (2.2)$$

$$E = \frac{Ux Ix 60}{vx1000} \quad (2.3)$$

where E is the arc energy, U is Voltage [V], I is current [A], v is welding speed [mm/min], and k is thermal efficiency (0.6 to 1.0), according to the welding method.

2.1.4.4 Cooling time $t_{8/5}$

The cooling time during the welding influences the properties of the weld connection. The cooling time $t_{8/5}$ means the time in seconds for the weld to cool down from 800° C to 500°C. This cooling rate is crucial because, this time, the material reforms microstructure, and the heat-affected zone's toughness, strength, and hardness are established [19].

If the cooling times are too short, there will be a risk of cold cracks [21]. Short cooling times also reduce the diffusion time in which the carbon can leave the iron lattice, and it is in the soluble form in the austenite, which no longer precipitates from the lattice. In addition, there are no holding times, so that no concentration compensation can occur. Thus, austenite is almost completely converted into very hard structural components such as Martensite or Bainite, which result in maximum hardness [13]. On the other hand, if the cooling time is too slow, further ferrite and pearlite components can be formed, leading to softening and, thus, a loss of strength [21]. According to [19], acceptable properties can usually be obtained with a cooling time between 5 to 20 seconds for HSSs up to S700 and reduced to 5 to 15 seconds for higher strengths. The cooling time $t_{8/5}$ can be determined according to EN 1011-2 [25] and presents the influences of it on different types of weld in Table 4.

Two-dimensional heat flow equation as per EN 1011-2 [25];


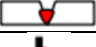


$$t_{8/5} = (4300 - 4.3T_0) \times 10^5 \times \frac{Q^2}{d^2} \times \left[\left(\frac{1}{500-T_0} \right)^2 - \left(\frac{1}{800-T_0} \right)^2 \right] \times F_2 \quad (2.4)$$

Three-dimensional heat flow equation as per EN 1011-2 [25];

$$t_{8/5} = (6700 - 5T_0) \times Q \times \left(\frac{1}{500-T_0} - \frac{1}{800-T_0} \right) \times F_3 \quad (2.5)$$

where $t_{8/5}$ is cooling time from 800°C to 500°C (sec), T_0 is working temperature (°C), d is the material thickness (mm), Q is heat input (kJ/mm), F_2 is shape factor for 2D heat flow, and F_3 is shape factor for 3D heat flow.

Table 4 Influence of the form of weld on the cooling time $t_{8/5}$ [25].

Weld type	Symbol	F_2	F_3
Weld		1.0	1.0
Butt weld		0.9	0.9
Corner weld		0.9-0.67	0.67
Angle T weld		0.45-0.67	0.67

2.2 Design rules

There are several analytical approaches followed internationally to design welds in structural steels. Much research was conducted to determine the proper design guidelines for the welding connection from normal and high-strength structural steel. This section briefly explains the design of weld connections from normal and high-strength structural steel based on European and US standards.

2.2.1 European standard

In Europe, the directional method and the mean stress methods are used to calculate the strength of fillet welded connection according to EN 1993-1-8:2006 [2]. The mean stress method is a simplification of the directional method. In the directional method, the forces transmitted by the weld are resolved into stress components σ_{\perp} , σ_{\parallel} , τ_{\perp} , and τ_{\parallel} within the area of the throat section because it is assumed to form the resisting and failing section, see Fig.1.

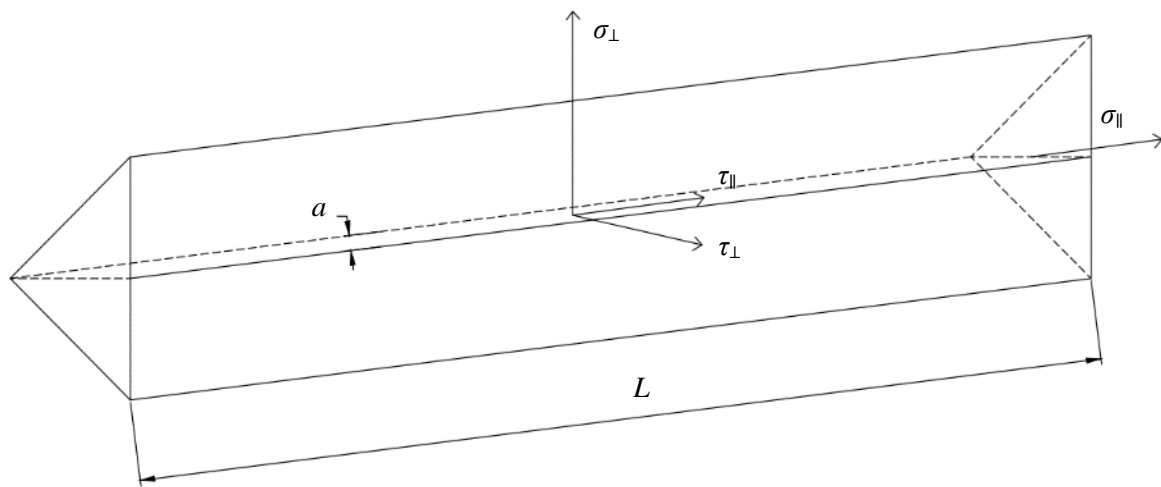


Fig. 1. Stresses on the throat section of fillet weld [2].

The normal and shear stress components are calculated from design loads assuming uniform stress distribution in the weld throat. However, the normal stress σ_{\parallel} parallel to the axis is not considered when verifying the design resistance of the weld [2].

The design resistance of the fillet weld should be taken as sufficient if the following conditions are satisfied:

$$\sigma_{w,Ed} = \sqrt{\sigma_{\perp}^2 + 3 \cdot \tau_{\perp}^2 + 3 \cdot \tau_{\parallel}^2} \leq \frac{f_u}{\beta_w \gamma_{M2}} \quad \text{and} \quad \sigma_{\perp} \leq \frac{0.9 \cdot f_u}{\gamma_{M2}} \quad (2.6)$$

where σ_{\perp} is the normal stress perpendicular to the throat, τ_{\perp} is the shear stress perpendicular to the axis of the weld, τ_{\parallel} is the shear stress parallel to the axis of the weld, f_u is tensile strength of the base metal (weaker part of the joined base metals), $\gamma_{M2}=1.25$ is the partial safety factor for the resistance of welds, β_w is the correlation factor depending on the grade of steel which ranges between 0.8 for mild steel and 1.0 for HSS in Table 5 [2].

The design resistance of a fillet weld may be assumed to be adequate if, at every point along its length, the resultant of all forces per unit length transmitted by the weld $F_{W,Ed}$ satisfy the following criteria:

$$F_{W,Ed} \leq F_{W,Rd} \quad (2.7)$$

where $F_{W,Ed}$ is the design value of the weld force per unit length; $F_{W,Rd}$ is the design weld resistance per unit length.

Independent with the orientation of the weld throat plane to the applied force on it, the design weld resistance per unit weld should be determined from Equation 2.8 given in EN 1993-1-8:2006 [2]:

$$F_{R,Ed} = f_{vw,d} \cdot a \quad (2.8)$$

where $f_{vw,d}$ is the design shear strength of the weld.

$$f_{vw,d} = \frac{f_u / \sqrt{3}}{\beta_w \gamma_{M2}} \quad (2.9)$$

where f_u , β_w , and γ_{M2} are defined earlier in Equation 2.6 and a = Effective throat thickness of the fillet weld, which should be taken as the height of the largest triangle (with equal or unequal legs) that can be inscribed within the fusion face and the weld surface, measured perpendicular to the outer side of this triangle and should not be less than 3 mm as per clauses 4.5.2 (1) and (2) in EN 1993-1-8:2006 [2].

Table 5 Correlation factor β_w depending on standard and steel grade [2].

Standard and steel grade			Correlation factor β_w
EN 10025	EN 10210	EN 10219	
S235 S235 W	S235 H	S235 H	0.80
S275 S275 N/NL S275 M/ML	S275 H S275 NH/NLH	S275 H S275 NH/NLH S275 MH/MLH	0.85
S355 S355 N/NL S355 M/ML S355 W	S355 H S355 NH/NLH	S355 H S355 NH/NLH S355 MH/MLH	0.90
S420 N/NL S420 M/ML		S420 MH/MLH	1.00
S460 N/NL S460 M/ML S460 Q/QL/QL1	S460 NH/NLH	S460 NH/NLH S460 MH/MLH	1.00

The strength of weld connection largely depends on the direction of applied force to the weld, which can be seen clearly in the given examples (see Table 6) of transverse and longitudinal welds to the direction of a force applied based on the EN 1993-1-8:2006 [2].

The design weld resistance of a connection with transverse fillet weld $F_{w,Rd,T}$ and longitudinal fillet weld $F_{w,Rd,L}$ can be determined by following functions:

$$F_{w,Rd,T} = \frac{f_u}{\sqrt{2} \cdot \beta_w \cdot \gamma_{M2}} a \cdot L \quad (2.10)$$

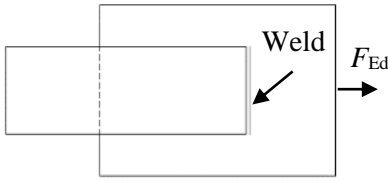
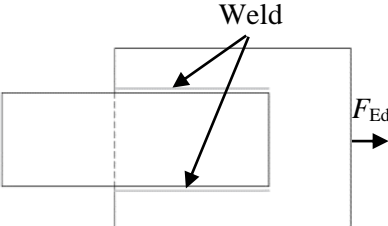
$$F_{w,Rd,L} = \frac{f_u}{\sqrt{3} \cdot \beta_w \cdot \gamma_{M2}} a \cdot L \quad (2.11)$$

Where a is the throat thickness of the weld and L is the length of the weld. In lap joint longer than 150 a , the weld resistance should be multiplied by reduction factor β_{Lw} to allow for the effect of non-uniform distribution of stress along its length and is given by [2]:

$$\beta_{Lw} = 1.2 - \frac{0.2L_j}{150a} \text{ but } \beta_{Lw} \leq 1.0 \quad (2.12)$$

Where L_j is the overall length of the weld in the direction of the force transfer.

Table 6 Design strength of transverse and longitudinal fillet welds according to EN 1993-1-8:2006 [2].

Sample	Description	Details
	Normal and Shear stress perpendicular to the direction of force:	$\sigma_{\perp} = \tau_{\perp} = \frac{F_{Ed}}{\sqrt{2} A_w}$
	Directional Method	$\sqrt{\sigma_{\perp}^2 + 3\tau_{\perp}^2} \leq \frac{f_u}{\beta_w \cdot \gamma_{M2}}$ $\frac{F_{Ed}}{A_w} \leq \frac{f_u}{\sqrt{2} \cdot \beta_w \cdot \gamma_{M2}}$
	Simplified Method	$\frac{F_{Ed}}{A_w} \leq \frac{f_u}{\sqrt{3} \cdot \beta_w \cdot \gamma_{M2}}$
	Comparison	Directional Method gives 22% more durable results than that of simplified method.
Sample	Description	Details
	Shear stress parallel to the direction of force:	$\tau_{\parallel} = \frac{F_{Ed}}{A_w}$
	Directional Method	$\sqrt{3\tau_{\parallel}^2} \leq \frac{f_u}{\beta_w \cdot \gamma_{M2}}$ $\frac{F_{Ed}}{A_w} \leq \frac{f_u}{\sqrt{3} \cdot \beta_w \cdot \gamma_{M2}}$
	Simplified Method	$\frac{F_{Ed}}{A_w} \leq \frac{f_u}{\sqrt{3} \cdot \beta_w \cdot \gamma_{M2}}$
	Comparison	Same strength from both method

According to Eurocode EN1993-1-8:2006 [2], the strength of the filler metal is not considered for the higher grade of steel than S460. However, the tensile strength of the base metal f_u should be replaced by the tensile strength of the filler metal if using under-matched electrodes in the case of higher-grade steel [26]. The Eurocode EN1993-1-8:2006 [2] and EN1993-1-12:2007 [26] do not provide the design guidelines for the use of matched or overmatched filler metal for welds of higher-grade steel S460 and S690. However, it can be possible to determine the design resistance of a fillet weld in connections of steel grades equal to or greater than S460 according to prEN 1993-1-8:2020 [27]. According to [27], for steel grades equal to or greater than S460, the filler metal may have lower strength than the base metal. The elongation at the fracture and minimum Charpy-V notch energy value of the filler metal should be equivalent to, or better than specified for the base metal, and with different base and filler metal strength, should be taken as sufficient if the following is satisfied:

$$\sqrt{\sigma_{\perp}^2 + 3 \cdot \tau_{\perp}^2 + 3 \cdot \tau_{\parallel}^2} \leq \frac{(0.25f_{u,PM} + 0.75f_{u,FM})}{\beta_{w,mod} \gamma_{M2}} \quad \text{and} \quad \sigma_{\perp} \leq \frac{0.9 \cdot f_u}{\gamma_{M2}} \quad (2.13)$$

where $f_{u,PM}$ is nominal ultimate tensile strength of the parent metal, which is of lower strength grade; $f_{u,FM}$ is nominal ultimate tensile strength of filler metal (see Table 7), and according to EN ISO 2560, EN ISO 14341, EN ISO 16834, EN ISO 17632, and EN 1876; $\beta_{w,mod}$ is modified correlation factor that depends on the filler metal strength (see Table 7).

Table 7 Ultimate strength of filler metals $f_{u,FM}$ and modified correlation factor $\beta_{w,mod}$ [27].

Filler metal strength class	42	46	69	89
Ultimate strength $f_{u,FM}$ [N/mm ²]	500	530	770	940
Correlation factor $\beta_{w,mod}$ [-]	0.89	0.85	1.09	1.19
For filler metals different to those given in Table 6.2 the correlation factor should be taken conservatively according to the given values.				

In the case of a simplified method of determination of the design resistance of fillet weld, the design shear strength of a weld in connections of steel grade equal to or greater than S460 should be determined from the following equations [27]:

$$f_{vw,d} = \frac{(0.25f_{u,PM} + 0.75f_{u,FM})/\sqrt{3}}{\beta_{w,mod} \gamma_{M2}} \quad (2.14)$$

where $f_{u,PM}$, $f_{u,FM}$, and $\beta_{w,mod}$ are defined in Equation 2.13.

Table 8 Design resistance of fillet welds based on prEN 1993-1-8:2020 [27].

Description	Combination of base metal & filler metal		
	S700 MC-G42	S700 MC-G46	S700 MC-G69
Base Metal (f_y) [N/mm ²]	700	700	700
Base Metal ($f_{u,PM}$) [N/mm ²]	750	750	750
Filler Metal (f_y) [N/mm ²]	420	460	690
Filler Metal ($f_{u,FM}$) [N/mm ²]	500	530	770
$\beta_{w,mod}$	0.89	0.85	1.09
γ_{M2}	1.25	1.25	1.25
$f_{vw,d} = \frac{(0.25f_{u,PM} + 0.75f_{u,FM})/\sqrt{3}}{\beta_{w,mod} \gamma_{M2}}$	291.92	317.88	324.16

From the above calculation examples (see Table 8) of the design resistance of fillet welds connection, it can be seen that the influence of the quality of the electrode on the shear design resistance of the weld connection. As the strength of the electrode increased, the design shear strength of the weld also increased as there is a 75% contribution of the filler metal on the strength of the weld connection, according to prEN1993-1-8:2020 [27].

2.2.2 US standard AISC 360-16

In the US, load and resistance factor design (LRFD) and allowable strength design (ASD) methods are used to compute the design strength of weld according to ANSI/AISC 360-16 [28]. In this study, the weld is designed by LRED and is designed to be the weakest component in the joint. The fillet weld is the only component examined in the study. The design strength of the fillet weld is determined using section J2.4 in ANSI/AISC 360-16 [28]. The available calculation methods for checking the strength of fillet welds are based upon simplifying the assumption that a fillet weld always fails in shear, and the failure occurs along a plane through the throat section of a fillet weld. According to ANSI/AISC 360-16 [28], the directional strength of fillet welds loaded perpendicular to the weld axis is increased by 50%. However, smaller transverse-to-longitudinal weld strength ratios result from theoretical analyses using various methods [29].

The design strength ϕR_n of welded joints shall be the lower of the base material strength and the weld metal strength. The weld metal strength is determined according to the limit state of rupture, and base material strength is determined according to the limit states of tensile rupture and shear rupture as follows:

For the base metal. However, the base metal check is not required for matching electrodes.

$$\phi R_n = \phi F_{nBM} A_{BM} \quad (2.15)$$

For the filler metal

$$\phi R_n = \phi F_{nw} A_{we} \quad (2.16)$$

Where A_{BM} is the cross-sectional area of the base metal, A_{we} is the effective area of the weld, F_{nBM} is the nominal stress of the base metal, and F_{nw} is the nominal stress of the weld metal. The values of ϕ , Ω , F_{nBM} , and F_{nw} and limitations thereon are given in Table J2.5 of ANSI/AISC 360-16 [28].

For a linear weld group loaded through the center of gravity having a uniform leg size, the design strength is determined as follows:

$$\phi R_n = \phi * 0.60 F_{EXX} * (1.0 + 0.50 * \sin^{1.5}(\theta)) * A_{we} \quad (2.17)$$

Where F_{EXX} is the filler metal classification strength, and θ is the angle between the direction of the force and the weld axis. In the case of fillet weld groups concentrically loaded and consisting of elements with a uniform leg size that are oriented both longitudinally and transversely to the direction of applied load, the combined strength R_n , of the fillet weld group shall be determined as the greater of the following:

$$R_n = R_{nwl} + R_{nwt} \quad \text{Or} \quad R_n = 0.85 R_{nwl} + 1.5 R_{nwt} \quad (2.18)$$

Where R_{nwl} is the total nominal strength of longitudinally loaded fillet welds, as determined in accordance with table J2.5, and R_{nwt} is total nominal strength of transversely loaded fillet welds, as determined in accordance with table J2.5 without the increase in section J2.4 (b) [28].

If the length of a fillet weld is longer than $100w$, the reduction factor, β , is given by:

$$\beta = 1.2 - 0.002 \left(\frac{L}{w} \right) \leq 1.0 \quad (2.19)$$

where L is actual weld length, and w is the size of the weld leg. When the length of the weld exceeds 300 times the leg size, w , the effective length shall be taken as $180w$.

The example of the minimum tensile strength of the filler metal F_{EXX} is given in Table 9. The load-bearing capacity of the welded connection is calculated as a function of the filler metal, and it is necessary to specify the steels belonging to the filler metals to be able to compare them with the other standards. The selection of the possible combinations of steel and welding consumables is given in Table 5.3 of AWS D1.1/D1.1M:2020 [30]. Table 10 presents the design resistance of fillet welds according to US standards with two different types of electrodes.

Table 9 Strength of steels with associated welding consumables according to AISC 360-16 [28] (AWS D1.1/D1.1M:2020 [30]).

Steel	f_y [N/mm ²]	f_u [N/mm ²]	F_{EXX}
A36 (≤ 20 mm)	250	400-550	60 ksi/70 ksi (414/483 N/mm ²)
A913 (Size 50)	345	Min. 455	70 ksi (483 N/mm ²)

Table 10 Design resistance of fillet welds according to AISC 360-16 [28], (AWS D1.1, 2020 [30]).

Description	Electrode	
	60 ksi	70 ksi
f_y [ksi/ N/mm ²]	48/331	57/393
f_u [ksi/ N/mm ²]	60/414	70/483
F_{EXX} [N/mm ²]	414	483
ϕ [-]	0.75	
$\phi * 0.60 * F_{EXX}$	186.3	217.35
$\phi * 0.60 * F_{EXX} (1.0 + 0.50 * \sin^{1.5}(\theta))$		
$\theta = 0^\circ$ (Welds parallel to the direction of force)	186.3	217.35
$\theta = 90^\circ$ (Welds perpendicular to the direction of force)	279.45	326.03

US Standards ANSI/AISC 360-16 [28] also allows the steel grade of yield strength up to 690 MPa, but there are no design provisions for steel grades higher than these values, which reflects the current state of research on the structural application of HSS [31]. According to AWS D1.1/D1.1M:2020 [30], filler metal with a strength level equal to or less than the base metal strength can be used. The design strength of the weld can be determined by using the equations discussed above.

2.3 Experimental research

In recent years, many steel industries have been working to develop light and slender constructions of steel structures having good welding characteristics and high ductility [5]. According to Barsoum et al. [10], the speed of developing the new steels is much higher than the speed of developing new filler materials of higher strength. HSSs have a lower deformation capacity, and with increasing the strength of steel, the loads that have to be transferred by the welded connections increase similarly [32]. Due to the absence of a well-defined strength function for welds in a higher steel grade, many researchers are involved in finding the behavior of matching or overmatching filler metal for mixed connections. Many researchers are working on the ultimate strength of welded connections made up of high-grade steels, and here only present the experimental knowledge of different researchers regarding the HSS welded connection with consideration of strength, quality of electrode, and welding process.

Collin and Johansson

Collin and Johansson [11] published experiments to determine the load-bearing capacity of filler welds in HSSs. Two specimens were considered to find the weld material strength and effective stress in the weld on both longitudinal and transverse fillet weld connection directions (see Fig. 2). Two combinations, Weldox 700 E with Electrode OK 75.75 and Domex 650 MC with OK 48.00 electrodes were used for the test specimens.

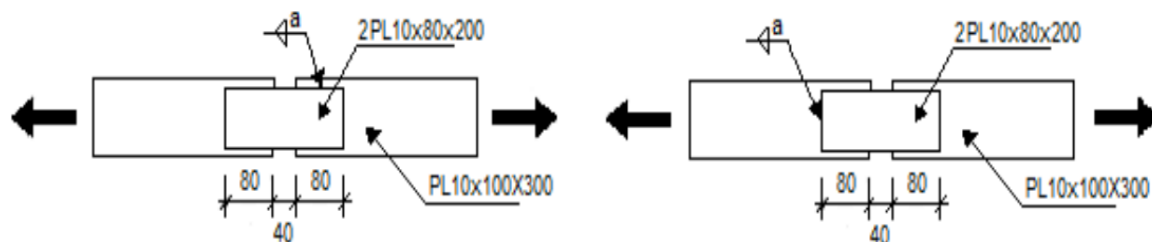


Fig. 2. Test specimens for longitudinal welds (left) and transverse welds (right) [11].

According to the experimental results, it shows that the weld strength seems to be closer to the strength of the stronger material, between the ultimate tensile strength of base material (f_u) and electrode materials (f_{eu}). The average of the electrode strength and the base material can be used as a conservative expression of weld strength, and the new thing is that this formula works for both under and overmatching electrodes, which is more rational than the method in Eurocode 1993-1-8:2006 [2].

$$f_w = \frac{f_u + f_{eu}}{2} \quad (2.20)$$

According to the stress component method for fillet welds in Eurocode 1993-1-8:2006 [2], it tends to underestimate the strength of transverse welds compared to the longitudinal one. In connection with this, the authors proposed the following modification of the assessment of the load-bearing capacity of fillet welds:

$$\sigma_{\text{eff}} = \sqrt{\sigma_{\perp}^2 + 2 \cdot \tau_{\perp}^2 + 3 \cdot \tau_{\parallel}^2} \quad (2.21)$$

Then, from the expression (2.20) and (2.21), the bearing capacity of fillet welds can be derived depending on the direction of the applied load:

$$F_{R\parallel} = \frac{f_w A_w}{\sqrt{3}} \approx 0.58 f_w A_w \quad (2.22)$$

$$F_{R\perp} = \frac{f_w A_w}{\sqrt{1.5}} \approx 0.82 f_w A_w \quad (2.23)$$

Expression 2.23 would give a 15% increase in the resistance compared to Eurocode 1993-1-8:2006 [2] if f_w was taken as same.

Khulmann et al. and Gunther et al.

To overcome the absence of well-defined strength functions for welds of high steel grade and to investigate the strength and ductility of welded HSS connections by means of experimental and numerical studies, Khulmann et al. [32] and Gunther et al. [6] published experiments within the research program P 652. To find out the strength function of welds, two types of joints were tested: lap joints with longitudinal fillet welds and cruciform joints with transverse fillet welds (see Fig. 3). In most of the tests, strength, and ductility of joints with fillet welds and partial penetration welds of HSSs, S460 M & S690 Q have been examined.

According to Kuhlmann et al. [32], most of the test specimens were fabricated using MAG welding, and the welding parameters, cooling rate, etc., were chosen based on the recommendation for welding of metallic materials according to EN 1011-2 [25]. The grade of base metal filler metals was considered according to EN 10025-1[22] and EN ISO 14341[33], and EN ISO 16834 [34], respectively.

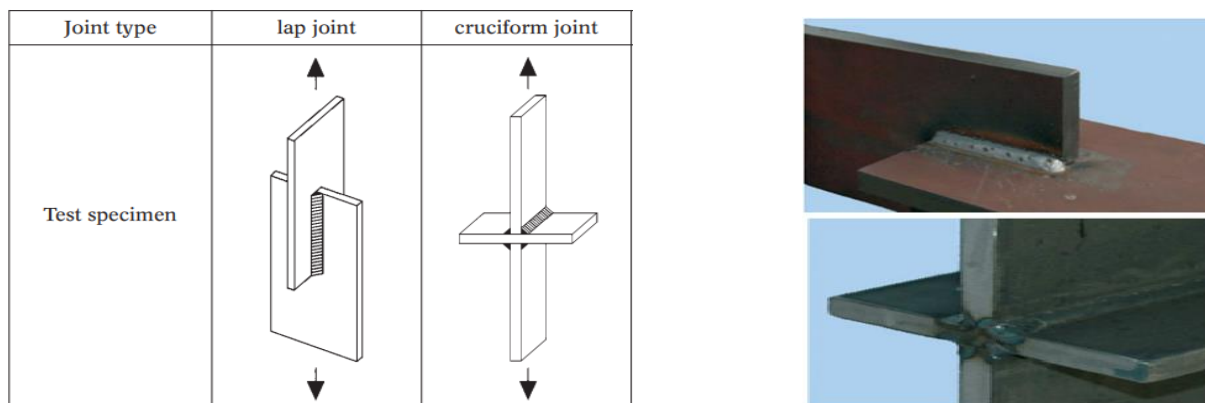


Fig. 3. Typical drawing of lap and cruciform joint (left) [6] and the picture of respective joints (right) [32].

For lap joints with longitudinal weld direction, Kuhlmann et al. [32] also choose all the test specimens for the matching conditions of all steel grades (S355J2, S460M, and S690Q), which means the same nominal strength of base and filler metal. The comparison of ultimate shear stress reveals that connections made of steel grade S460M are significantly stronger than those formed of steel grade S355J2, however for steel grade S690Q, only a little stronger comparison to S460M can be obtained (see Fig. 4a).

Test specimens with different base metal combinations of mild and HSS in combination with different filler metals have been examined on mismatched conditions (see Fig. 4b). There is a tendency that with increasing the strength of the filler metal, the load-bearing capacity also increased.

Similarly, to determine the influence of filler metal's strength on load-bearing capacity, Gunther et al. [6] investigated the behavior of different base materials (see Fig. 5a) on mismatched conditions. Filler metals with undermatching (G42), matching (G46), and overmatching (G69) conditions were studied for the base metal S460. Moreover, tests for matching (G69) and undermatching (G46) for the base metal S690 were conducted. Higher filler metal strength tends to correspond with increased load-carrying capacity.

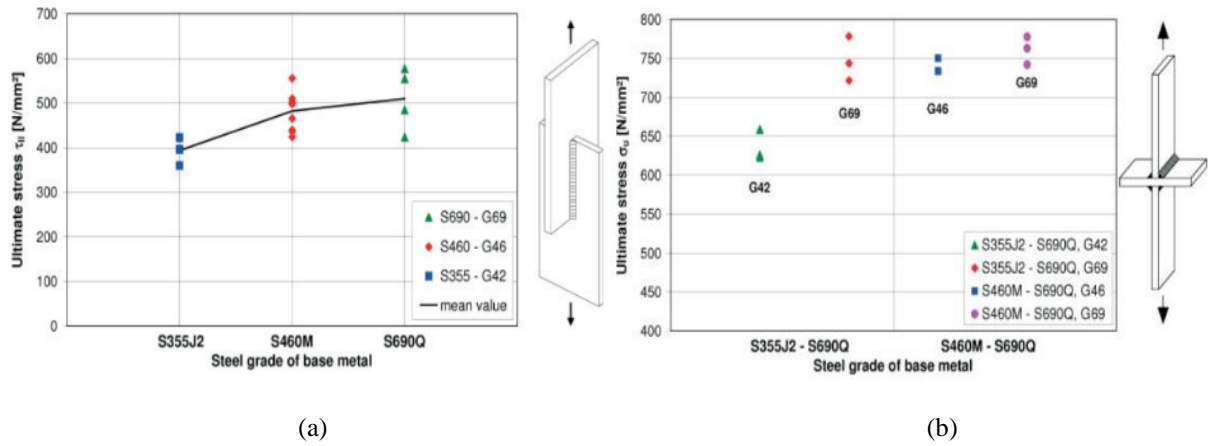


Fig. 4. (a) Comparison of ultimate stresses of lap joints of S355J2, S460M, and S690Q, matching condition [32], (b) Comparison of ultimate stresses of cruciform joints with mismatching conditions [32].

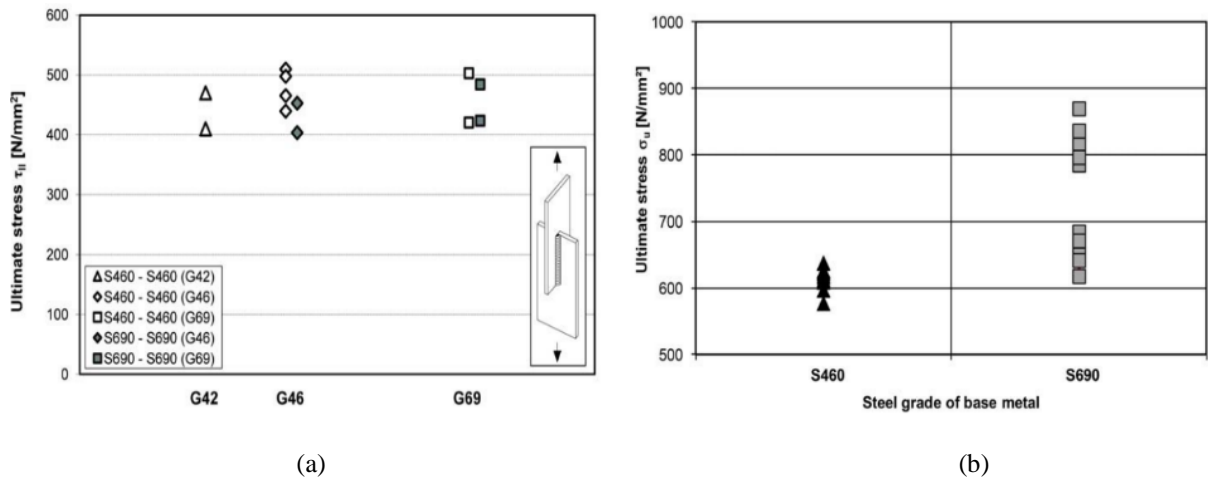


Fig. 5. a) Comparison of ultimate stress of lap joints with different filler metals [6], b) Comparison of ultimate stresses of cruciform joints S460M and S690Q, matching condition [6].

Gunther et al. [6] illustrated a comparison of the test result for steel grades S460M and S690Q in terms of the ultimate strength for cruciform joints with transverse fillet welds where ultimate strength is determined based on the maximum load measured during the test divided by the effective weld area (see Fig. 5b). For all the tests matching conditions were chosen, which means the same nominal strength of base and filler metal. The results of the cruciform joints with steel grade S690Q reveal higher load-bearing capability when compared to measurements of welded connections with base material S460M [6].

Björk, J. Toivonen and T. Nykänen

The main aim of the investigation was to find out the ultimate load-bearing capacity of typical fillet welded joints made of ultra-high-strength steel (UHSS) S960 [35]. To determine the capacity of fillet welded joints, nonlinear finite element analysis (FEA) and experimental testing were used. Table 11 presents the mechanical properties of the base and filler materials. They conducted different joint configurations of fillet welds for the investigation (see Fig. 6 and Fig. 7).

The joint behavior was assessed using the nonlinear FEA, and the outcomes were contrasted with experimental tests. In finite element (FE) calculation, the material properties of the base and filler materials were presented using bilinear true stress-strain curves. When the true stress governs the critical plane of weld throat thickness along the whole weld length, the joint is assumed to have reached its

ultimate capacity. This concept presents the ultimate load-carrying capabilities (F_u) and deformations [35]. Ultimately, they concluded that ductile rupture was the failure mode for all joints tested at room temperature. FEA accurately predicted the ultimate capacity and failure path but not the ultimate deformation capacity.

Table 11 Mechanical properties of materials [35].

Group	Material code		f_y [MPa]	f_u [MPa]	A_5 [%]	KV [J]
Base material (BM)	S960	Nominal	960	1000	7.0	50 (-40 °C)
		Measured	1014	1076	12.5	
Filler metal = weld metal (WM)	X96	Nominal	930	980	14.0	40 (-40 °C)
		Measured	990	1245		
	12.64	Nominal	470	500	26.0	70 (-30 °C)
		Measured	580	690		
	13.31	Nominal	850	890	18.0	50 (-30 °C)
		Measured	790	915		

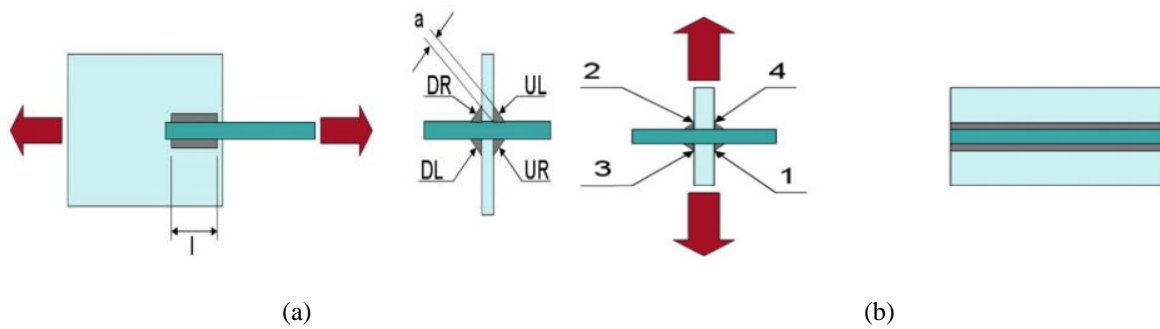


Fig. 6. a) Longitudinal cruciform joint (L-series), b) Load-carrying transverse cruciform joint (X-series) [35].

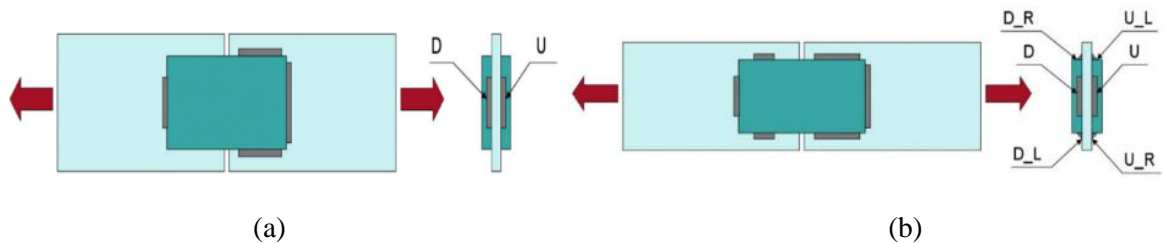


Fig. 7. a) Transverse load-carrying lap joint (T-series), b) Transverse and longitudinal load-carrying lap joint (LT-series) [35].

Christina Rasche

Christina Rasche [21] revised the correlation coefficient for the existing design model in EN 1993-1-8:2006 [2] and developed a new design approach that allows an economical design of fillet welds in HSSs. Based on the test results of 103 own tests on fillet welds from the research project FOSTA P652, the additional experiments, and FOSTA P812 with a further 160 investigations from the literature by previous research, Rasche was able to develop a modified design approach for fillet weld connections, which also considers the influence of the filler metal on the load-bearing capacity. The new design proposal considers the strength of the base metal at 25% and the strength of the filler metal at 75%. The design resistance is shown in the equation:

$$\sigma_{w,Rd} = \frac{0.25 \cdot f_{u,PM} + 0.75 \cdot f_{u,FM}}{\beta_{w,mod} \cdot \gamma_{M2}} \quad (2.24)$$

where $f_{u,PM}$ is nominal ultimate tensile strength of the parent metal; $f_{u,FM}$ is nominal ultimate tensile strength of filler metal; and $\beta_{w,mod}$ is modified correlation factor that depends on the filler metal strength.

Correlation coefficients for the Rasche design approach should not be selected depending on the base material but on the filler metal used. Rasche also proposed the new correlation coefficients based on a statistical evaluation of all experiments, tabulated below; see Tables 12 and 13.

Table 12 Proposal for the correlation coefficient for fillet weld connections S460 and S690 according to EN 1993-1-8:2006 [2] and 1993-1-12:2007 [26] from Rasche [21].

Steel grade	Correlation coefficient
S460 N/NL; M/ML	0.85
S690 Q/QL/QL1	1.10

Table 13 Proposal for the correlation coefficients according to EN 1993-1-8:2006 [2] and 1993-1-12:2007 [26] from Rasche [21].

Filler metal	Correlation coefficient
G42/E42	0.89
G46/E46/T46	0.85
G69/T69	1.09
G89	1.19

According to Rasche [21], one advantage of the modified design approach is that different strengths can be considered for the base and filler metal. When using the higher-strength welding filler metals, higher design limit stresses can be claimed than according to the design concept according to EN 1993-1-8:2006 [2] and EN 1993-1-12:2007 [26].

Barsoum and Khurshid, and Khurshid et al.

To investigate the impact of the penetration ratio on its ultimate strength capacity, Barsoum and Khurshid [10] published an experiment using specimens of fillet welds-cruciform joints on which the lower weld in the joint is always fully penetrated. In contrast, the upper weld has different penetration levels, i.e., complete 100%, partially, 50%, and 75%. The flange in these joints is made of S690 QL HSS, whereas the web plates are built of S600 MC HSS; see Table 14 for the mechanical properties. Three strength mismatch cases—under-matched, matched, and over-matched—were chosen as the filler materials. Fig. 8 illustrates the dimensions and geometry of the cruciform joints.

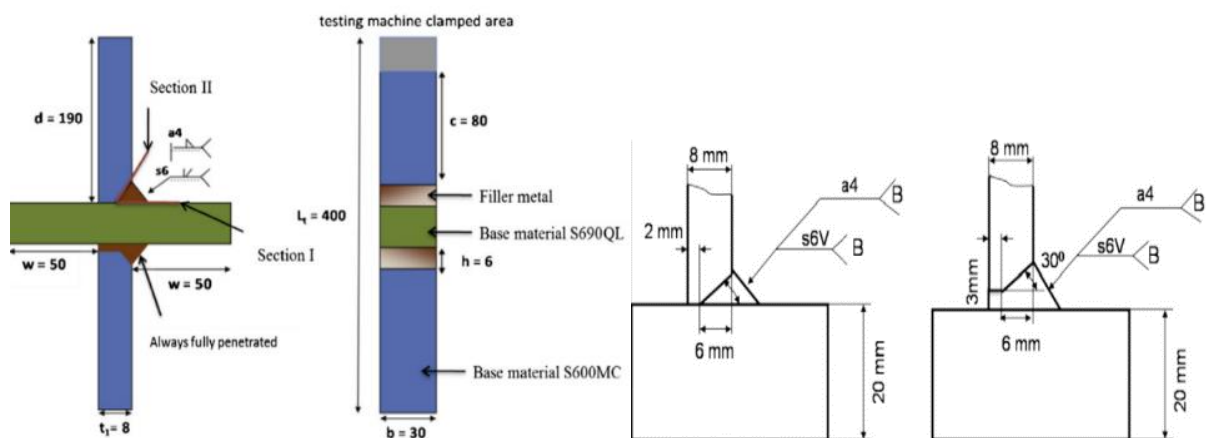


Fig. 8. Geometry and dimension of cruciform specimen [10].

Table 14 Mechanical properties of base and filler materials [36].

Material	Electrode standard	Symbol	Yield strength (MPa)	Ultimate tensile strength (MPa)	Strength mismatch (%)
Under-matching filler material	SS-SN ISO 17632:2008	42	420	500-640	20
Matching filler material	SS-EN ISO 17632:2008	50	500	560-720	0
Over-matching filler material	SS-EN ISO 18276:2006	69	690	770-940	26
Base material webs	EN 10149-2	S600MC	600	650-820	Nil
Base material flanges	EN 10025	S690QL	700	770-940	Nil

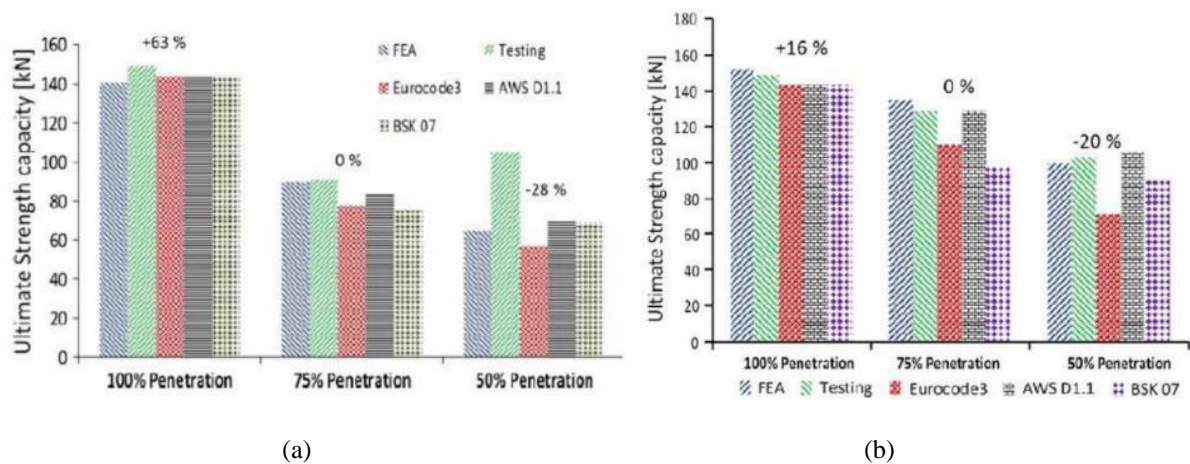


Fig. 9. Comparison of the ultimate strength capacity for filler welds based on penetration (a) Under-matching (b) Over-matching filler material [10].

Fig. 9. represents the maximum strength capacity for fillet welds in various penetration ratios with different filler materials assessed by FEA. The testing results and several design codes (including Eurocode, Swedish Standard BSK 07, and American Welding Society Code AWS D1.1) are similar when the penetration ratio at 75% as a reference, the weld metal penetration ratio has more influence on under-matched filler materials than over-matched filler materials on the ultimate strength capacity of the joint.

Spiegler and Kuhlmann

Spiegler et al. [5] published an experiment on the mixed fillet weld connection from HSS. As the exact procedure for the determination of the load-bearing capacity of a mixed connection is insufficient in EN 1993-1-8:2006 [2], they experimented based on a new design resistance proposal by Rasche [21] with considering the influence of the filler metal on the design resistance of fillet welded connections. In contrast to the current design rules, the correlation factor depends on the strength of the filler metal. New correlation factors were determined for the mixed connections depending on the strength of the filler metal using statistical evaluation.

Although there is a negligible difference between the correlation factors obtained by Rasche [21], see Table 15, Spiegler et al. [5] stated that the modified design resistance using the correlation factors according to Rasche might also be used for the mixed connection, and using the prescribed throat thickness according to EN 1993-1-8:2006 [2].

Table 15 Comparisons of correlation factors $\beta_{w,mod}$ according to Rasche [21] and $\beta_{w,mod,mix}$ for mixed connections.

Filler metal	$\beta_{w,mod}$ according to Rasche (2012) [21]	$\beta_{w,mod,mix}$	
		Longitudinal fillet welds	Cruciform joints with fillet welds
G46/T46/E46	0.85	0.87	0.74
G69/T69	1.09	1.07	1.08
G89/T89	1.19	1.19	1.02

According to Spiegler and Kuhlmann [5], there is a considerable influence of the strength of the filler metal on the load-carrying capacities of fillet welded cruciform joint and longitudinal fillet welds depending on the combination of base metals and with increasing strength of filler metals. An increase in the nominal strength of filler metals leads to an increase in the load-carrying capacity of the joint and an increase in the strength of the base metals in comparison (see Fig. 10. and Fig. 11.).

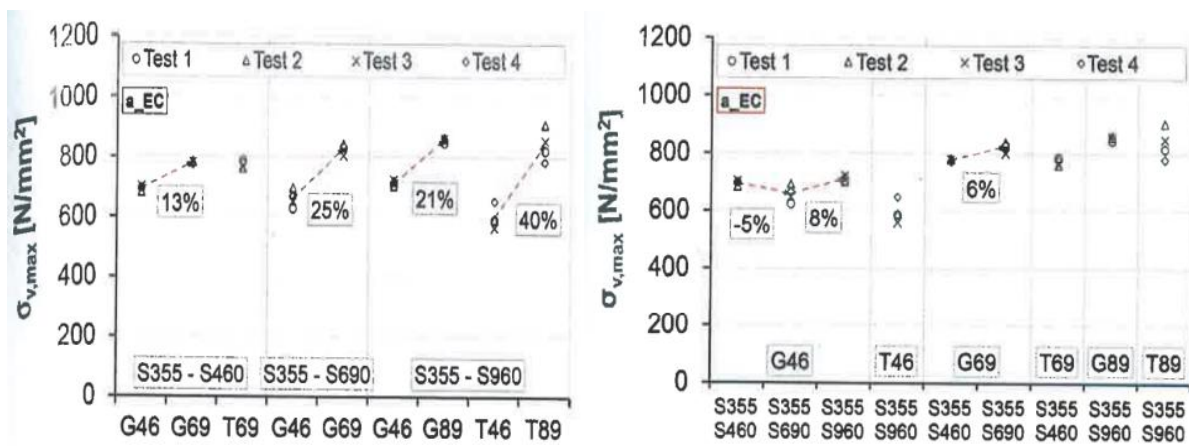


Fig. 10. The influence of filler and base metal strength on the load carrying capacities $\sigma_{v,max}$ of fillet-welded cruciform joints [5].

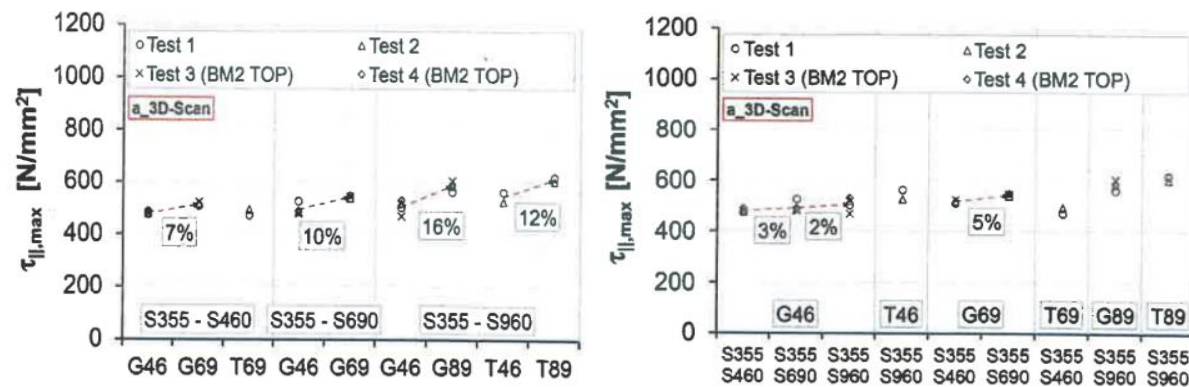


Fig. 11. The influence of filler and base metal strength on the load carrying capacities $\tau_{||,max}$ of longitudinal fillet-welded [5].

Andreas Kleiner

In 2018, Andreas Kleiner [13] published his dissertation on fillet weld connections from HSSs. The primary goal of the work was to verify and advance both the applicability of the existing and newly developed design rule for determining the load-bearing capacity of fillet welds made of normal and HSS based on experimental investigations. Three different steel grades of base metals (S355, S460, S690) were selected to examine the behavior of the filler metal concerning the base metal of the fillet

weld connection (see Fig. 12). The mechanical properties of base and filler materials are presented in Table 16 and Table 17 respectively.

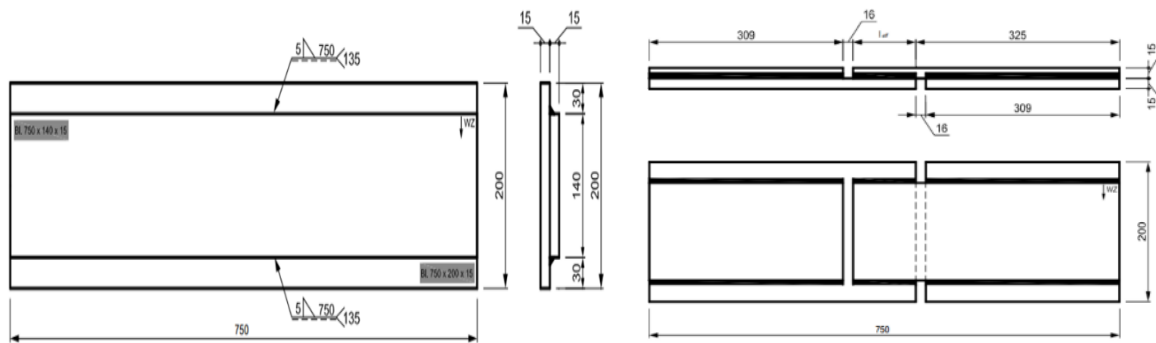


Fig. 12. Geometry of the lap joint [13].

Table 16 Mechanical properties of base materials [13].

Mechanical characteristics			S355 J2+N	S460 ML	S690 QL
$R_{eH}/R_{p0.2}$	[N/mm ²]	Nominal	355	460	690
		Experiment	425	512	824
R_m	[N/mm ²]	Nominal	470-630	540-720	770-940
		Experiment	545.7	575.0	873.7
A	[N/mm ²]	Nominal	22	17	14
		Experiment	26.92	25.20	14.75

Table 17 Mechanical properties of filler materials [13].

Mechanical characteristics			G46	G69	G89
$R_{eH}/R_{p0.2}$	[N/mm ²]	Nominal	460	690	890
		Experiment	519.0	646.3	729.3
R_m	[N/mm ²]	Nominal	530-680	770-940	940-1180
		Experiment	606.3	774.0	939.3
A	[N/mm ²]	Nominal	20	17	15
		Experiment	28.10	20.84	18.75

In addition, the deformation capacity of fillet weld connections was determined based on the tested results of fillet welded connections. The elastic deformation capacity of the fillet welded connection between the same base metals, S355 and S690, tends to increase with filler metal strength, except for S460, which exhibits an almost constant elastic deformation capacity of about three filler metals. However, the plastic deformation capacity of the same base metals, except S460, tends to decrease with the filler metals' strength.

Fei-Fei Sun et al.

Fei-Fei Sun et al. [37] [38] investigated the mechanical behavior of 24 lap-welded fillet joints, 20 cruciform fillet joints, and 28 longitudinal lap-welded joints (see Fig. 13 and Fig. 14) made of S690 HSSs under tension load with four different classifications of fillet metal, namely ER50-6, ER59-G, ER76-G, and ER96-G. The measured mechanical properties of steel plates and fillet metals are presented in Table 18.

Table 18 Measured average mechanical properties of steel plates and all-weld coupons.

No.	f_y^b or f_y^w [MPa]	f_u^b or f_u^w [MPa]	H_b or H_w [Hv0.1]	A_b or A_w [%]	ϵ_p^u
C1	807	856	270	11.3	0.035
C2	807	832	286	20.3	0.074
F1	547	627	192	23.3	0.133
F2	641	727	249	23.2	0.133
F3	688	771	265	21.0	0.091
F4	886	956	311	22.1	0.107

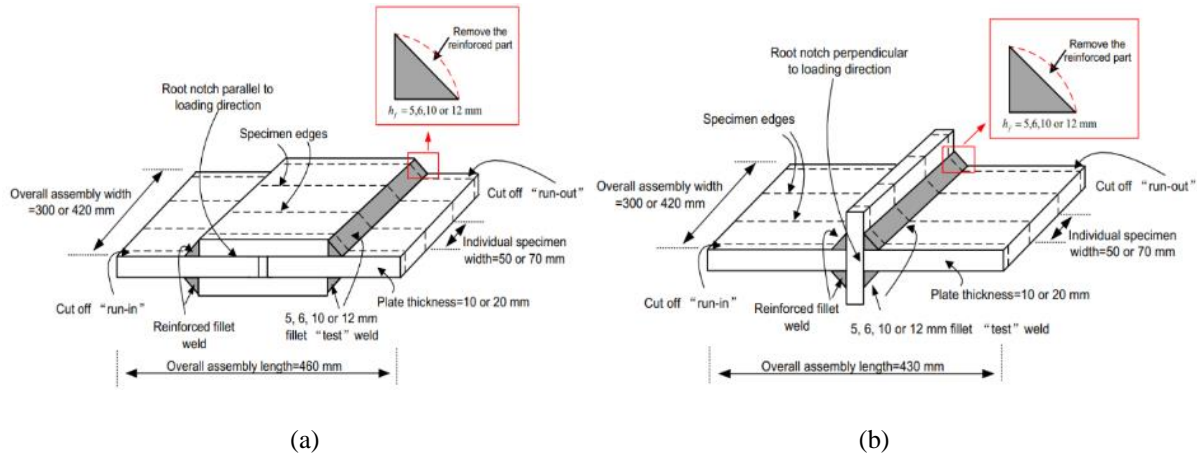


Fig. 13. (a) Transverse lap-welded fillet joint (b) cruciform fillet joints [37].

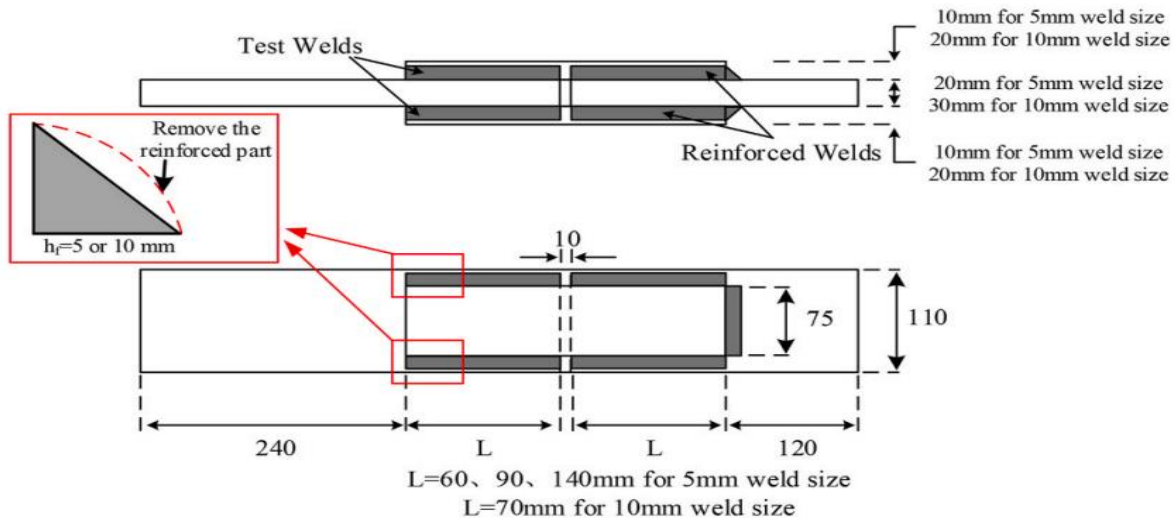


Fig. 14. Longitudinal lap-welded fillet joint [38].

Researchers measured the deformation capacity of welded connections using digital image correlation techniques (DIC), which have more advantages than traditional deformation measurements. The experimental investigation concluded that the mean strength of lap-welded specimens is higher than that of cruciform-type specimens. The ductility of a transverse fillet weld is small, and the total deformation is always less than 1 mm. Similarly, the deformation capacity of longitudinal filler welded joints is larger than transverse filler welded joints. Furthermore, the ultimate strength of longitudinal fillet welded joints is around 0.58 times that of transverse fillet welded joints.

2.4 Numerical modeling of welds

The finite element models are usually based on the idealized geometry neglecting the possible misalignments [39]. If the weld connections are modelled without considering the FEA, high stresses are observed near the connection, leading to overdesign. At the same time, if the predicted stresses in the weld region are less than the actual, it will be risky to rely on these estimations [40]. According to Weaver [41], to predict stresses and deflection for the loaded structures, FEA has become a practical method due to its nature of precisely identifying the load path, which using classical analysis with complex structures can be challenging.

The following paragraphs present the most frequently used weld modeling techniques in FEA. The geometry and stiffness of the welds can be easily modelled in the solid model using solid elements. In contrast, in shell element modeling techniques, the stress value at welded regions can be dependent on the modeling techniques [9]. Echer and Marczak [42] prefer shell elements in structural analysis due to the high computational time required to simulate solid models. It is necessary to do extrapolation at the intersection point when the weld is not modelled during shell modeling [43].

There are various weld modeling techniques used in shell models to represent the geometry and rigidity of welds. Most approaches were developed to compute structural hot spot stresses in fatigue: rigid links, increased thickness techniques, and inclined shell elements.

A few methods of modeling the welds in shell elements are as follows:

- Weld modeling uses rigid links linking the corresponding nodes on the two joined plates.
- Weld modeling by increasing the thickness of the shell elements in the weld region.
- Weld modeling using oblique shell elements.

Weld modeling using the rigid link.

Weld modeling using rigid links is the most straightforward representation in FEA models. Fayard et al. [44] suggested for fatigue to predict the hot spot stress at the weld toes (see Fig. 15a). In this modeling technique, the weld stress can be directly evaluated at the shell element's center of gravity, which implies that there is no need for any surface stress extrapolation [45]. Generally, the weld leg length and the sheet thickness are considered during the shell elements' size and positioning; typically, the element size is roughly equal to the weld leg length [43]. According to [9], it is essential to notice that the plates at the intersection are not connected in the joint, and 4-node shell elements are recommended for this technique.

Weld modeling using increased thickness.

The stiffness of the welds in the welded joints can be determined by increasing the thickness in the intersection region of welded connections [46]. In this method, the thickness of the shell element is increased to the thickness of the plate and weld (see Fig. 15b). In the case of cover plate connections; the rigid elements are used to join the attached plate to the parent plate [9].

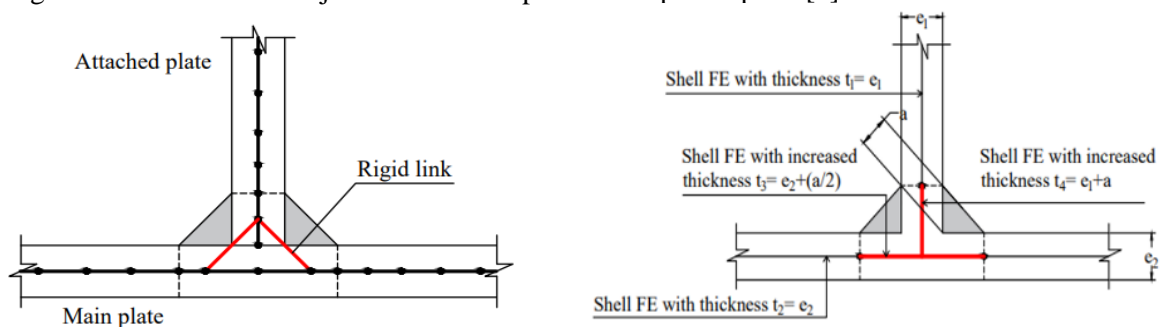


Fig. 15. Fillet welds modelled in T-joints, (a) Rigid links [44], and (b) Increased thickness method.

Weld modeling using oblique shell element.

According to Niemi et al. [46], welds represent by using inclined elements, which correctly represent both stiffness and geometry of the welds. The thickness of the inclined shell element is defined as the same as the throat thickness of the weld, and for the rest of the structural part, the shell element thickness is equal to the plate thickness of the respective plate [9], [42], [46], see Fig. 16a and 16b. Turilier et al. [47] proposed other possibilities to use inclined elements to represent the fillet weld. The rigid links were used to connect inclined shell elements with the mid-plane of the respective plates (see Fig. 16b).

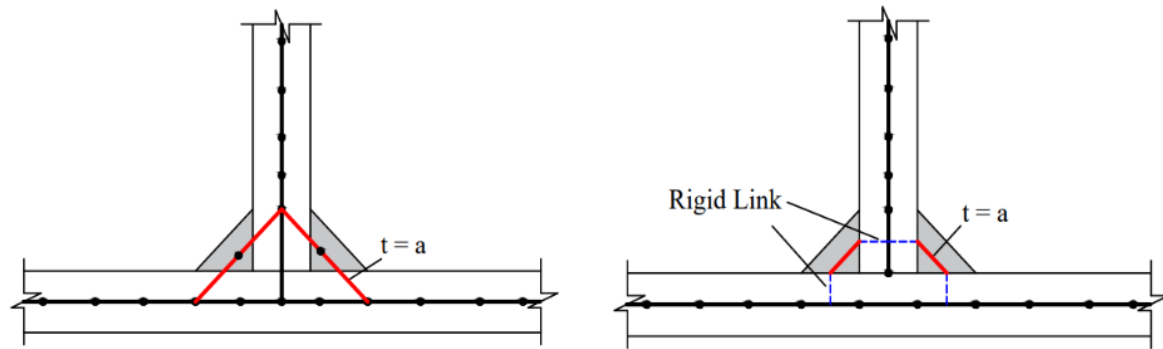


Fig. 16. Fillet welds modelled in T-joints, (a) Inclined elements having mid-side nodes and Inclined elements connections with rigid links [46].

2.5 Basic concepts of digital image correlation techniques

The core theory of digital image correlation (DIC) techniques is an image identification method that compares digital images taken before and after object deformation [48]. A correlation study is done on the optical instrument pictures taken before and after deformation. This method of inspecting the total displacement and strain field is non-destructive [49]. A single camera is used in classical DIC, and this method can only give in-plane displacement/strain fields on planar objects. However, using two cameras (stereovision), measured displacement and surface strain field of any 3-D object [50]. The shape of an object can be determined by comparing the corresponding subsets of surface images captured by the two cameras.

Additionally, three-dimensional displacement can be calculated by comparing the differences between a set of initial photos and a collection of images obtained after the load is applied [51]. Fig. 17 represents a typical diagram of a complete three-dimensional measurement system in DIC-3D.

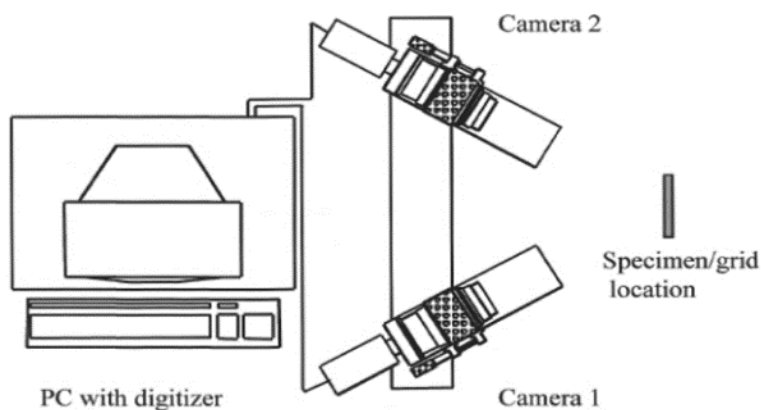


Fig. 17. Three-dimensional measurement system using DIC technique [51].

2.6 Strain limit

FEA approaches for joints have been used in research from the 1970s into the last century. They are a legitimate substitute for testing, the traditional but expensive method of learning about the behavior of joints, because they can accurately represent that behavior. The true stress-strain diagram used in the material model for FEM is derived from experimental data from coupon tests, considering the contraction of the specimen during the inelastic test phase. Today, computational analysis - particularly computational mechanics and fluid dynamics - is widely used as an essential design tool and a driving force in many relevant research areas. In Annex C of EN 1993-1-5:2006[52], the design recommendation using advanced structural steel modeling is ready for use. The notion of an ultimate strain limit for FE design is covered in Annex C of EN 1993-1-5:2006 [52] and by Wald et al. [53]. The limit is recommended to have a maximum principal strain of 5%. However, the complete load determines whether it occurs before the deformation limit. The clause Cl. C.9 (2) of EN 1993-1-5:2006 [52] summarizes incorporating safety into advanced design models under ultimate limit state design. The standard technique may be used with a partial safety factor for the material or connections. Structural connections can be solved more accurately and economically with a more sophisticated and precise solution that considers the precision of a model and material individually [54].

CHAPTER 3: OBJECTIVES

The use of high strength steels (HSS) in the steel market is growing due to their superior performance in tensile strength, toughness and weldability compared to traditional steel grades. In addition to their attractive appearance, these steels have the potential to reduce material and weight, making them attractive to the construction industry to create lightweight and slender structures. Structural integrity is critical in industries where welding is a primary technique, and the strength of welded joints can be determined by classical or finite element analysis (FEA) based on design guidelines. Numerical modeling provides reliable results on the proposed system and its components and has become a valuable tool in design practice. Recently developed welding modeling techniques can significantly reduce the time and effort required for fatigue design. However, there is currently a need for well-established methods to determine the resistance of welds in structural steels using numerical design models.

The objective of this study is to investigate the determination of the weld strength of HSS welds using the Finite Element Method (FEM) to develop a realistic and economical design model for the assessment of the strength of fillet welds of high strength structural steels for use in the design of steel structures.

The stresses acting on the weld profile are the most sensitive components of a welded joint, and the design model corresponds to them through FEM. The proposed numerical design calculation philosophy can be used in the complex geometry and loading conditions. To summarize, the main objectives of this work are to:

Create a numerical design model that calculates the strength of the high-strength steel (HSS) transverse fillet lap welds.

1. Test and validate the design model using experimental, analytical, and finite element results.
2. Investigate the deformation capacity of HSS transverse fillet lap welds.

In addition, the secondary objectives of the task are to:

1. Determine the strain limit for the HSS transverse and longitudinal fillet lap welds.
2. Present benchmark examples of NDC for the HSS transverse and longitudinal fillet welds.

CHAPTER 4: EXPERIMENT

This chapter presents the experimental investigation carried out as part of the TAČR Merlion III FW01010392 research project at the Department of Steel and Timber Structure at Czech Technical University in Prague. The resistance and deformation capacity of the transverse fillet lap-welded connections from high-strength steels (HSS) were analyzed at room temperature. The transverse fillet weld connections are used under matched welding consumables, which means that the ultimate tensile strength of filler metal is less than that of the base plate. The following sections present the base and welding consumables' properties. In addition to this, the welding parameters are also described in detail. The test results and their interpretation are present in the respective sections.

4.1 Material information

Steel plates 12 mm thick made from S700 MC Plus HSS and AristoRod 13.12 grade electrodes to create transverse fillet lap-welded connections. To analyze the properties of materials, conducted tests on three base metal tension coupons and three weld metal tension coupons following European Standards.

4.1.1 Base metal

Strenx 700 MC Plus is a high-strength structural steel with excellent formability. The low carbon contents characterize the chemical composition, see Table 19, to ensure good weldability and precisely added small amounts of elements such as Niobium, Titanium, and Vanadium to ensure the grain refinement of the final steel. According to EN-10149-2 [55], S700 MC Plus steels rank in the category of extra HSSs used for various applications, such as truck frames, cranes, and mining machines.

Three tension coupon tests were performed according to Eurocode to characterize the base plate's material properties. Tension coupon specimens were prepared with a nominal gauge length of 50 mm and diameter of 11 mm. Fig. 18 represents the typical geometric configuration of tension coupon specimens. The tensile test was performed in the UTS 100 KN testing machine, see Fig. 19. The elongation of the material is measured using extensometers and strain gauges. According to the Eurocode, the loading speed of the machine is 0.17 mm/min. The Annex 2-Material Properties section contains details of the tensile test data. Tables 20 and 21 show base metal's nominal and average measured mechanical characteristics. Fig. 20 presents the tensile coupon specimens before and after the tensile test. The Strenx 700 MC Plus steel plate's nominal mechanical characteristics are found in the product manual, and the measured stress-strain curve is present in Fig. 21.

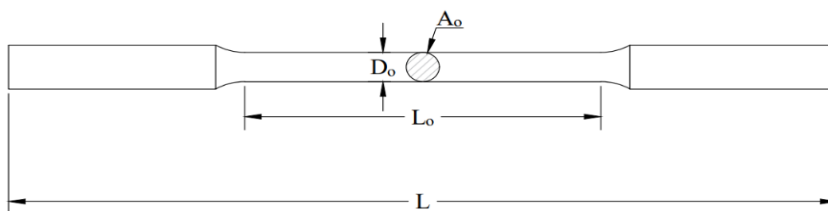


Fig. 18. Typical geometry of the coupon test specimen.

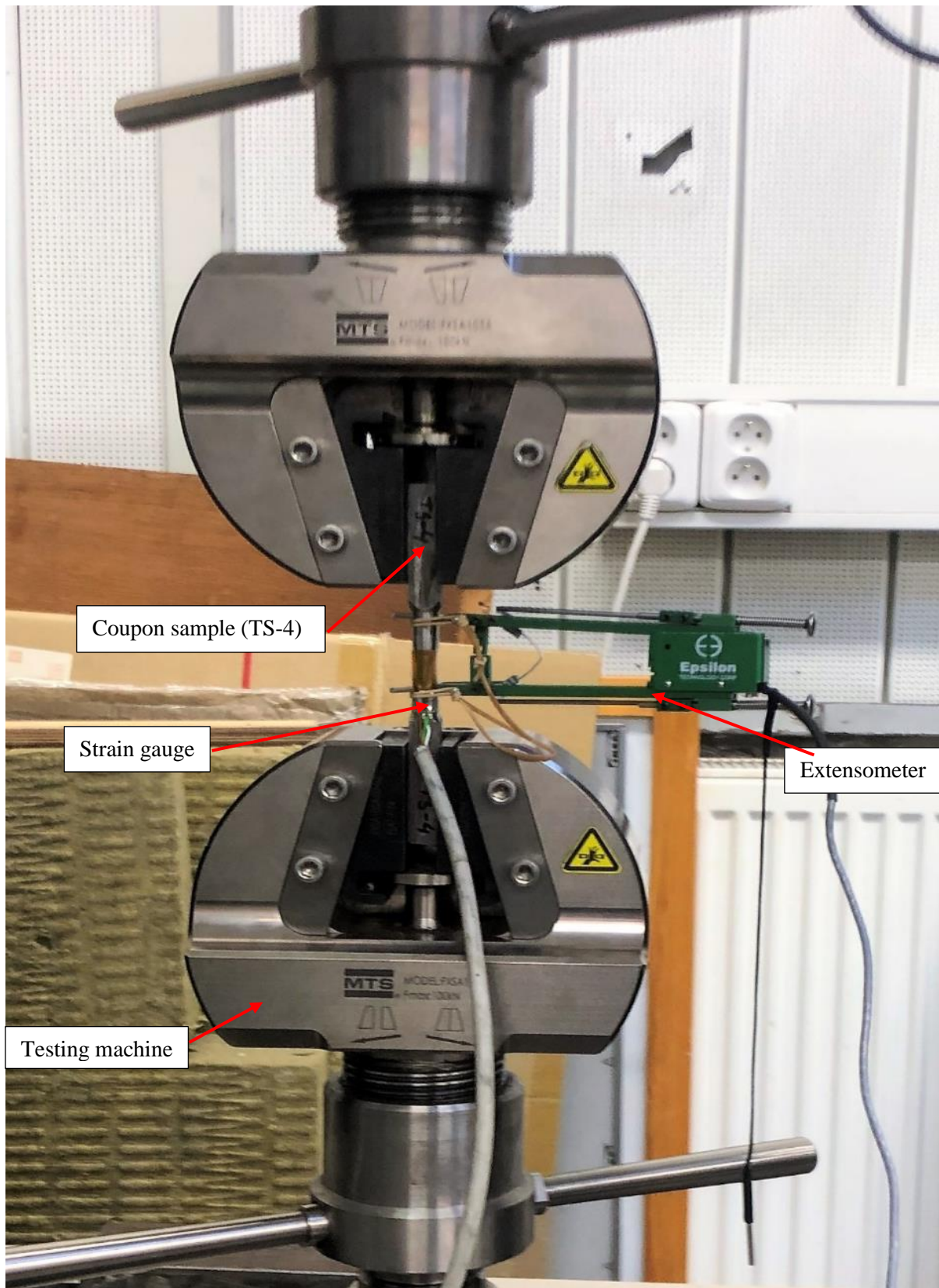


Fig. 19. Specimen ready for tensile testing.

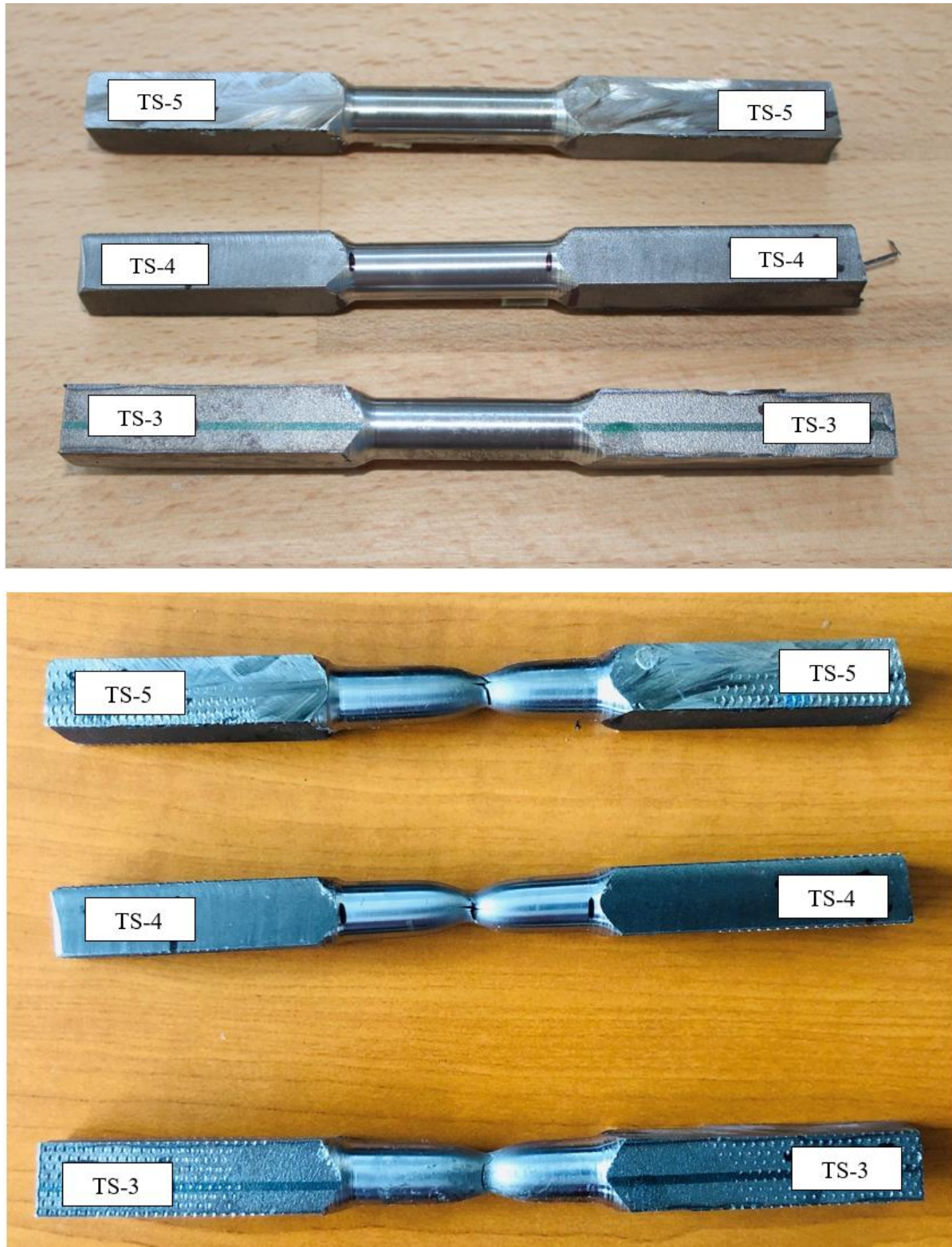


Fig. 20. Specimens before (Top) and after (Bottom) the tensile test.

Table 19 Chemical composition

C	Si	Mn	P	S	Al _{tot}	Nb ¹⁾	V ¹⁾	Ti ¹⁾
max %	max %	max %	max %	max %	max %	max %	max %	max %
0.12	0.25	2.10	0.020	0.010	0.015	0.09	0.20	0.15

Table 20 Nominal mechanical properties

Material	Yield Strength	Tensile strength	Elongation
	[min MPa]	[MPa]	[min %]
Strenx 700 MC Plus	700	750-950	13

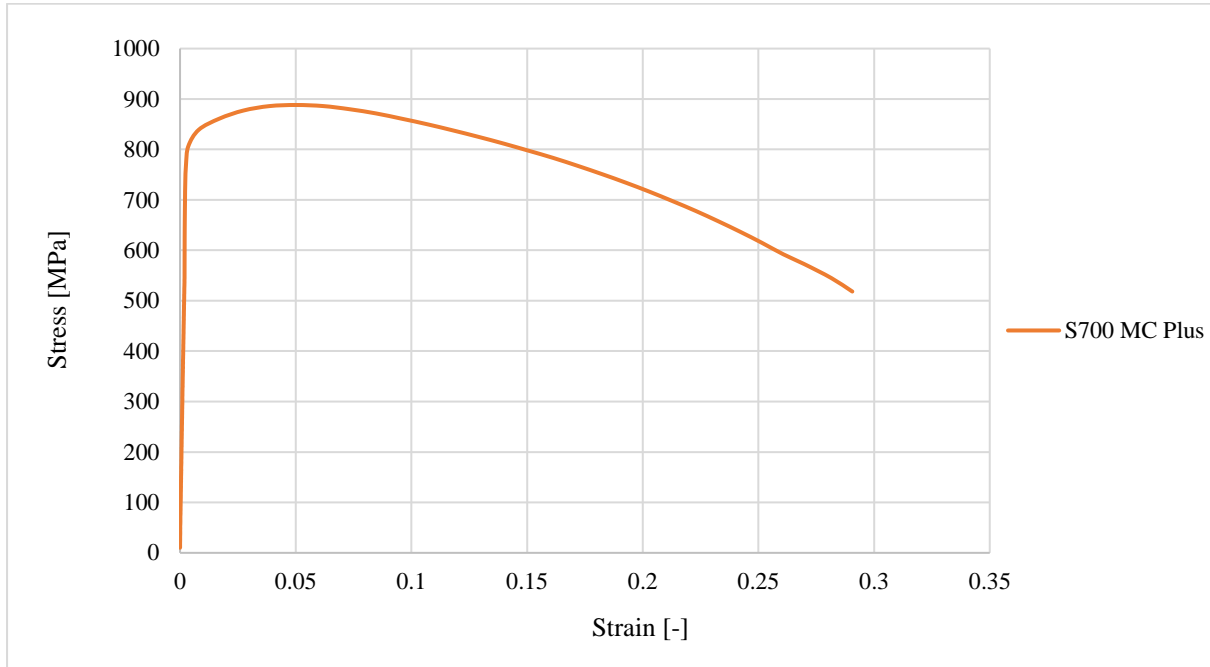


Fig. 21. Stress-strain curve of Strenx S700 MC Plus.

Table 21 Measured average mechanical properties.

Material	Yield strength	Tensile strength	Elongation
	[MPa]	[MPa]	[%]
Strenx 700 MC Plus	811.55	888.16	29.06

4.1.2 Filler metal

The ESAB OK Aristorod 13.12 low alloy wires are used as a filler material. Table 22 presents its chemical composition according to the delivered material datasheet with the wire supply. Three tension coupon specimens were performed according to Eurocode to characterize the material properties of the filler metal. Tension coupon specimens were prepared with a nominal gauge length of 50 mm and diameter of 10 mm. Figure 18 shows the typical geometric configuration of tension coupon test specimens.

For the experimental works of tension coupon specimens, butt welded joints were manufactured by welding two 12 mm thick Strenx 700 MC Plus steel plates by the MAG procedure. Before the welding, the edges of the steel metals were machined in a bevel to create a 60 V shape channel. Fig. 22 and Fig. 23 illustrate the welding using four beads (one root, two filling, and one covering bead). The tensile test was performed in the UTS 100 KN testing machine (see Fig. 19). The elongation of the material is measured using extensometers and strain gauges. According to the Eurocode, the loading speed of the machine is 0.17 mm/min. The Annex 2-Material Properties section contains details of the tensile test data. Fig. 24 presents the tension coupon specimens before and after the test. The nominal and average

measured mechanical properties of base metal are shown in Table 23 and Table 24, respectively, and the measured stress-strain curve is present in Fig. 25.

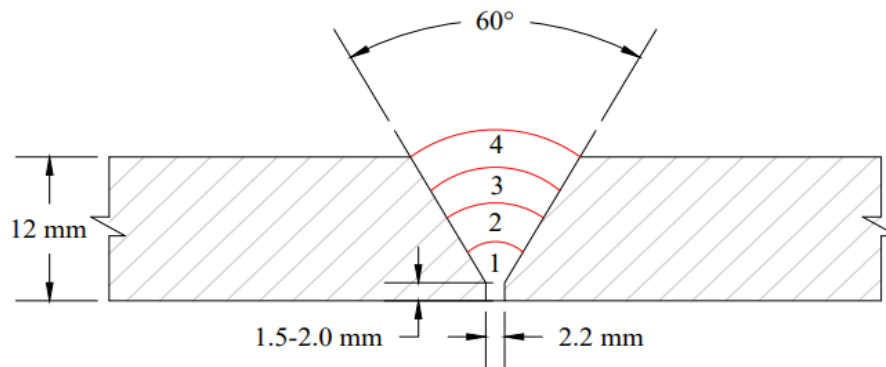


Fig. 22. Typical scheme for a sequence of the beads during the Strenx 700MC Plus steel welding process.

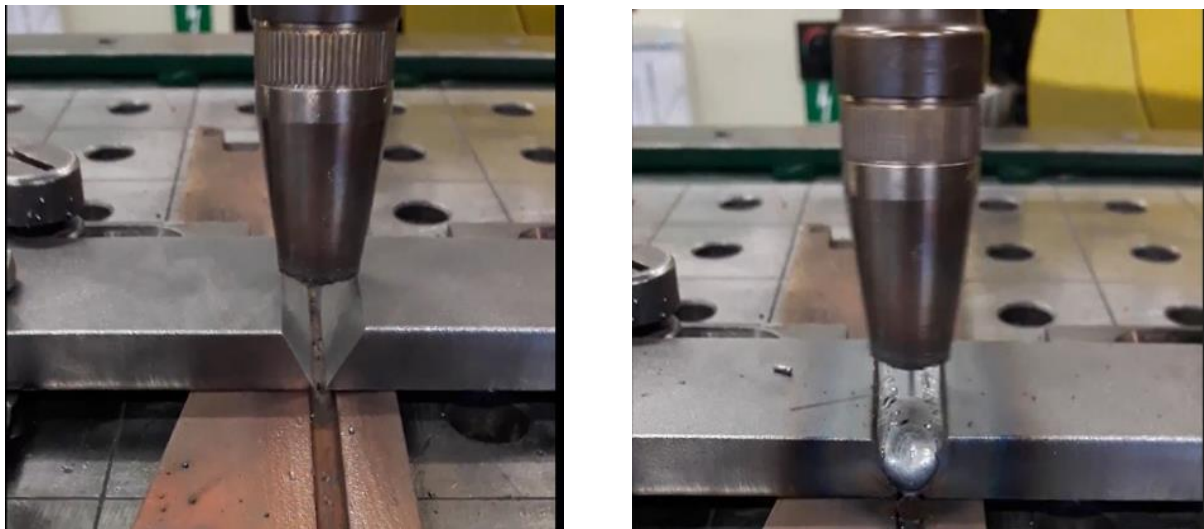


Fig. 23. Welding process of Strenx 700 MC Plus steel plates with a sequence of the beads.

Table 22 Chemical composition of wire (%).

	C	Si	Mn	N _i	M _o	C _r
OK Aristorod 13.12	0.110	0.65	1.00	0.02	0.42	1.18

Table 23 Nominal mechanical properties

Material	Yield Strength	Tensile strength	Elongation
	[min MPa]	[MPa]	[min %]
OK AristoRod 13.12	640	740	18

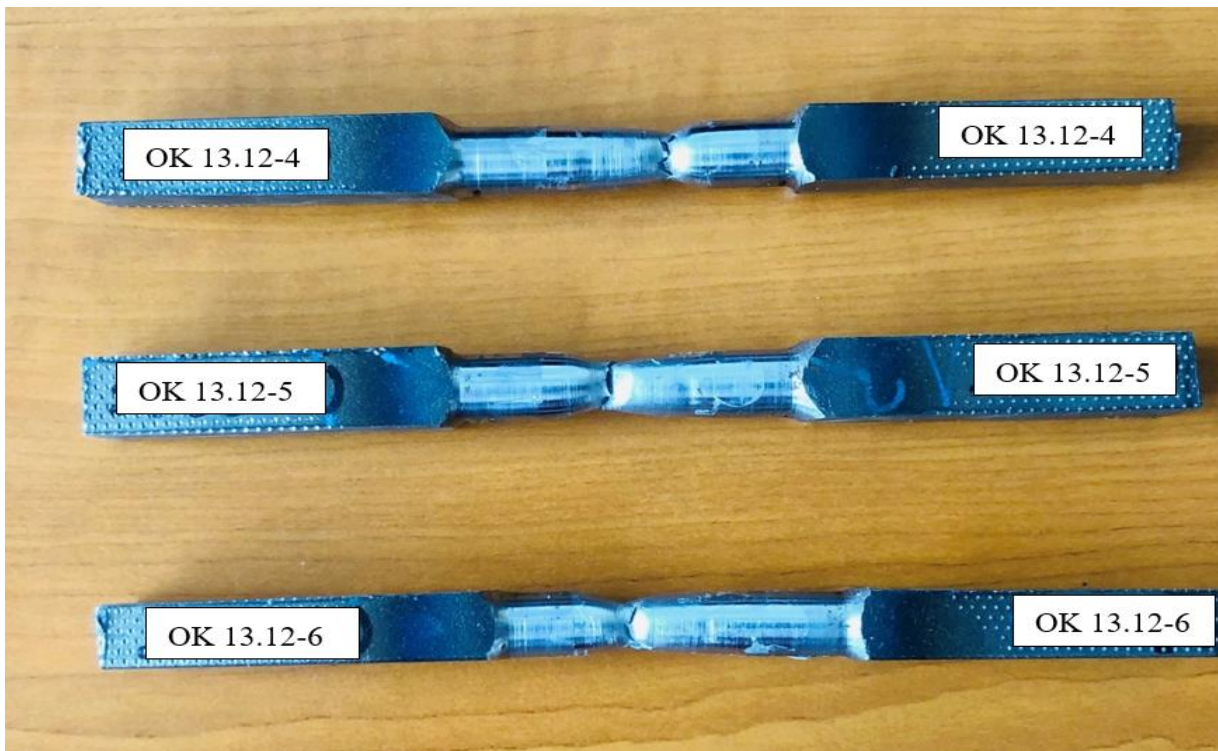
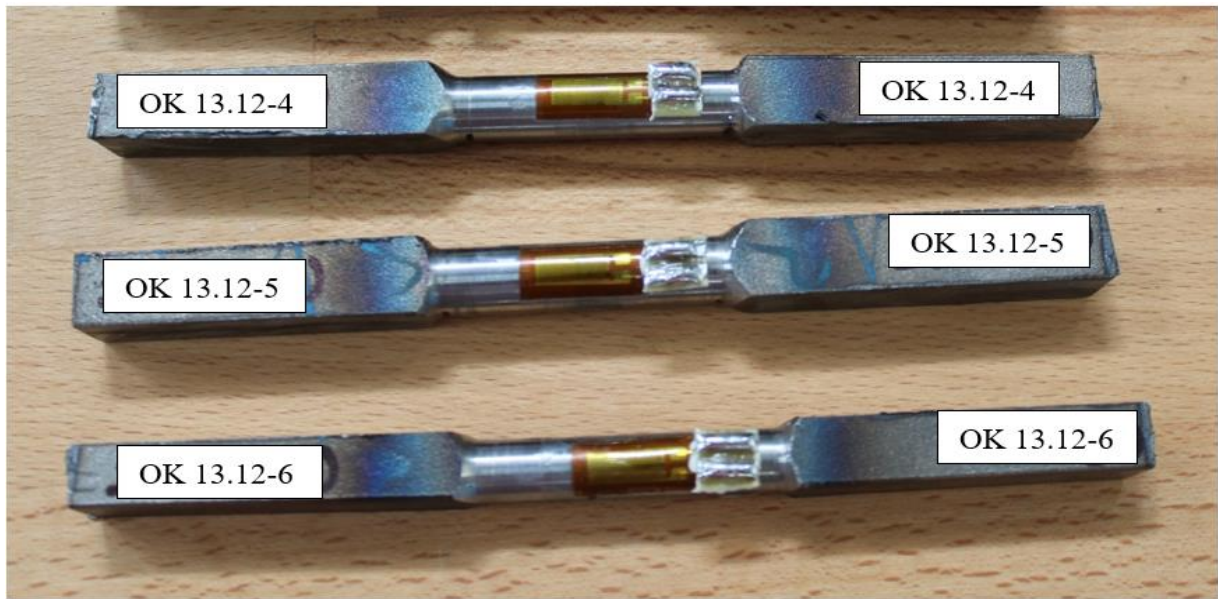


Fig. 24. Specimens before (Top) and after (Bottom) the tensile test.

Table 24 Measured average mechanical properties.

Material	Yield strength	Tensile strength	Elongation
	[MPa]	[MPa]	[%]
OK AristoRod 13.12	571.14	778.85	20.04

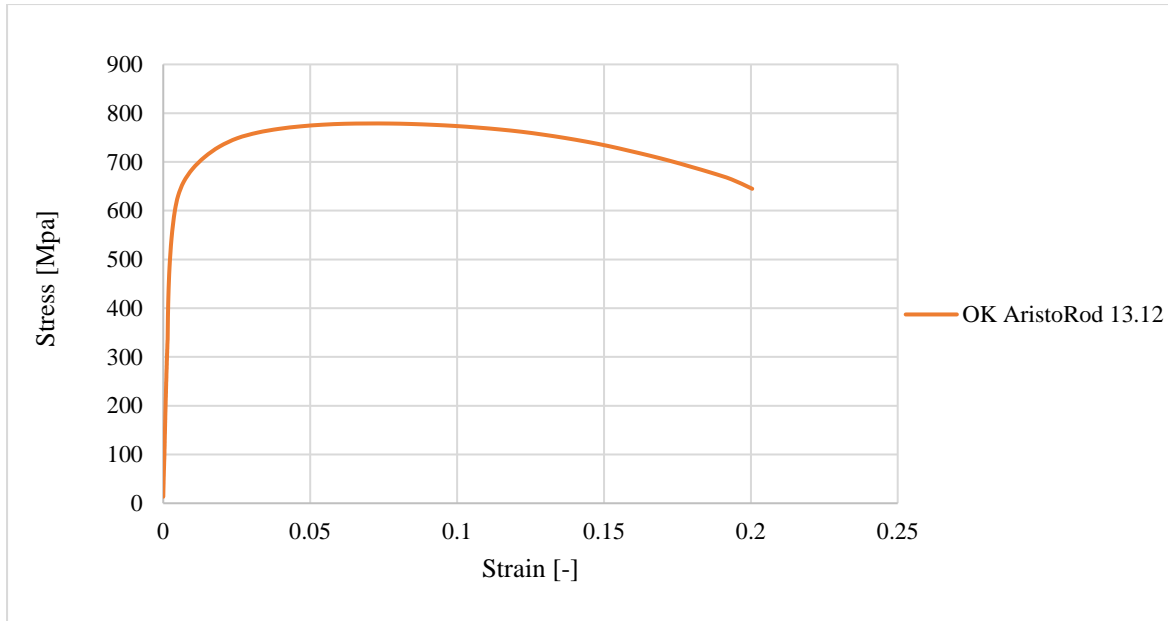


Fig. 25. Stress-strain curve of OK AristoRod 13.12 electrode.

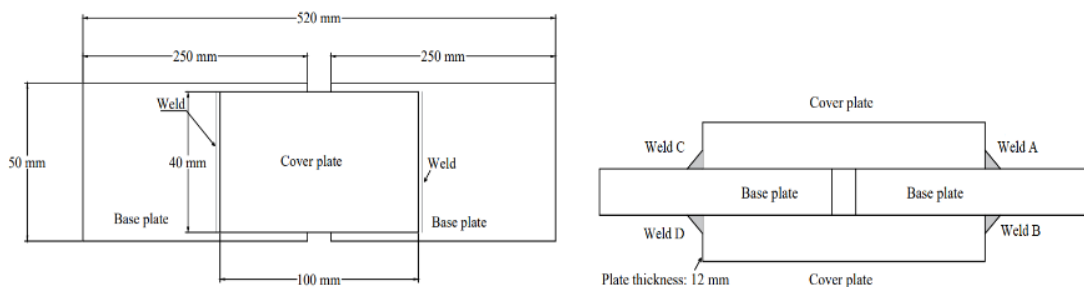
4.2 Specimen information

4.2.1 General

A total of six specimens of the transverse fillet lap-welded connections from HSS were prepared. The transverse fillet weld connection used under-matching welding consumables. All samples were used OK AristoRod 13.12. The main focus of the experimental investigations was the resistance and deformation capacity of transverse fillet lap-welded connections.

4.2.2 Geometry and Configuration

The typical geometry and configuration of a transverse fillet lap-welded connection are present in Fig. 26a. The measurements of the weld profile (such as tension leg, shear leg, and weld throat) and weld length were taken before testing, as illustrated in Fig. 26b, and summarized in Table 25. A vernier caliper was used to determine the dimensions of plates and weld profiles. Six specimens with a transverse fillet lap-welded connection were created (see Fig. 27), with "TS" denoting the transverse specimen.



(a)

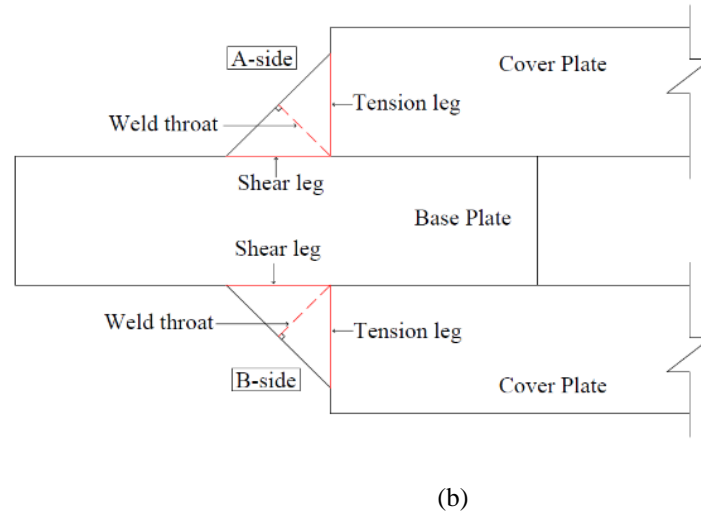


Fig. 26. (a) Layout and geometry of the transverse fillet lap-welded connection (b) weld measurements before fracture.

Table 25 Average dimension measurement for weld A and weld B before testing.

Specimen	Weld A				Weld B			
	Length	Tension leg	Shear leg	Weld's throat	Length	Tension leg	Shear leg	Weld's throat
	[mm]	[mm]	[mm]	[mm]	[mm]	[mm]	[mm]	[mm]
TS-1	45.0	5.43	5.88	4.00	45.0	5.45	7.70	4.65
TS-2	45.0	4.50	4.50	3.18	45.0	4.26	4.70	3.17
TS-3	44.0	4.70	5.09	3.46	44.0	4.19	4.29	3.00
TS-4	44.0	4.54	5.24	3.47	44.0	4.32	5.29	3.40
TS-5	45.0	5.20	5.40	3.75	45.0	5.73	4.87	3.75
TS-6	44.0	5.23	4.60	3.47	44.0	4.51	4.43	3.16

The table does not present the measurement of reinforced weld C and weld D. The detail of the size before and after fracture of each fillet welded connection is given in Annex 1.

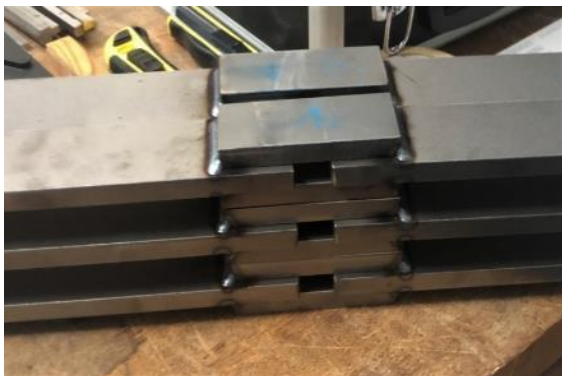


Fig. 27. Transverse fillet lap-welded connection

4.3 Test setup and the measurement

The test specimens underwent tensile loading with a maximum capacity of 1MN in the machine. A specimen was set up in the testing machine to carry out the test, as shown in Fig. 28. All tests are conducted with displacement control and a 1 mm/min loading rate. Displacement development and strain distribution during the loading process were measured using the digital image correlation (DIC) technique. Two cameras were used to capture measurements from both sides of the specimen's target surface area, which had speckle patterns. Speckle patterns significantly impact the precision of image correlation since the recorded speckle patterns before and after a surface movement are necessary for the analysis. If necessary, a light projector facilitated lighting on the surface, as shown in Fig. 28. The recorded measurements assessed the displacement and strain distribution of the transverse fillet weld.

The core theory of DIC techniques is an image identification method that compares digital images taken before and after object deformation [48]. Correlation analysis is performed on the photos taken using an optical instrument before and after deformation. This method of inspecting the total displacement and strain field is non-destructive [49].

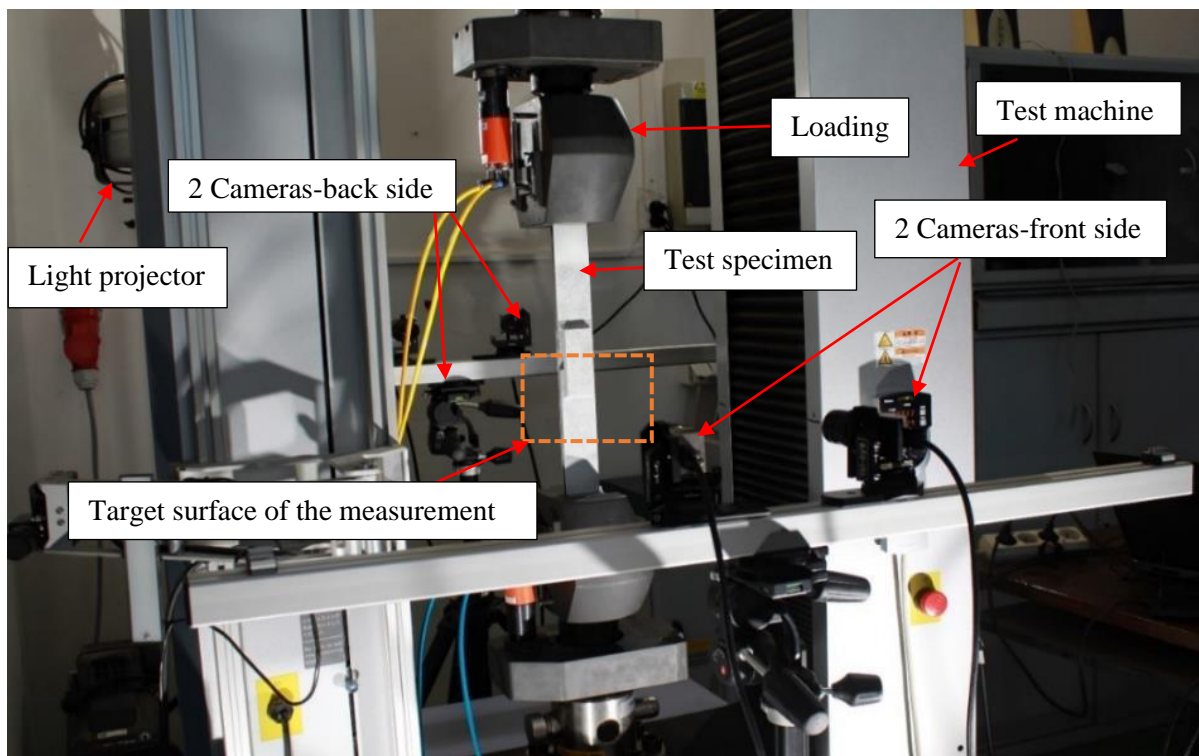


Fig. 28. Setting of specimens on a test machine.

4.3.1 Measurement of force and displacement

The force was measured using a load cell integrated with the testing machine. The recorded measurement was used to evaluate displacement and strain distribution on the transverse fillet weld. The general steps applied for the measurement using the DIC techniques are below.

General steps for measurement using the DIC technique.

- Ensure the measuring objects fit into the selected measuring volume in all its deformation stages.
- Prepare the specimen's surface and make speckle patterns on the target measurement area of the specimens, as shown in Fig. 29. The surface of the measuring object must have a pattern to allocate

the pixels in the camera images (facets). The surface patterns must be able to follow the deformation of the specimens. The surface patterns must stay intact. The pattern on the object should show a good contrast because otherwise, such an allocation (matching) does not work.

- Set up the samples in the machine and fixed the cameras for the measurement (see Fig. 28).
- Adjust brightness and focus on the target area of measurement.
- Calibrate the target measuring surface area by calibration plate before loading.
- Define a starting point for the computation process and record the image during loading.
- Compute the results with the help of images taken before and during the loading process.

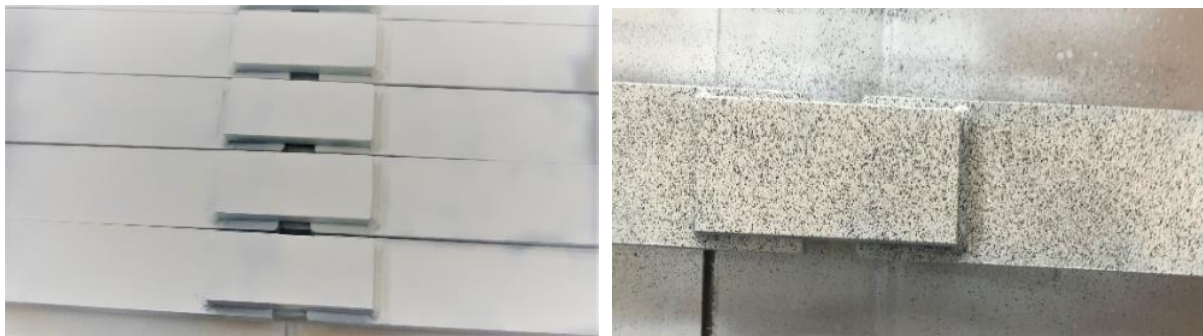


Fig. 29. Preparation of the surface (Left) and speckle pattern on the target measurement surface (Right).

4.3.2 Measurement of fracture surface area

All transverse fillet lap-welded connections failed in the weld from both sides, see Fig. 30. The fracture surface area of the weld was measured by the photogrammetry method. In this process, the photos of the specimens were taken, and created a 3D model of it. The target surface area of the weld was extracted from the 3D scanning analysis, see Fig. 31. The measured fracture surface area of the weld is present in Table 26.

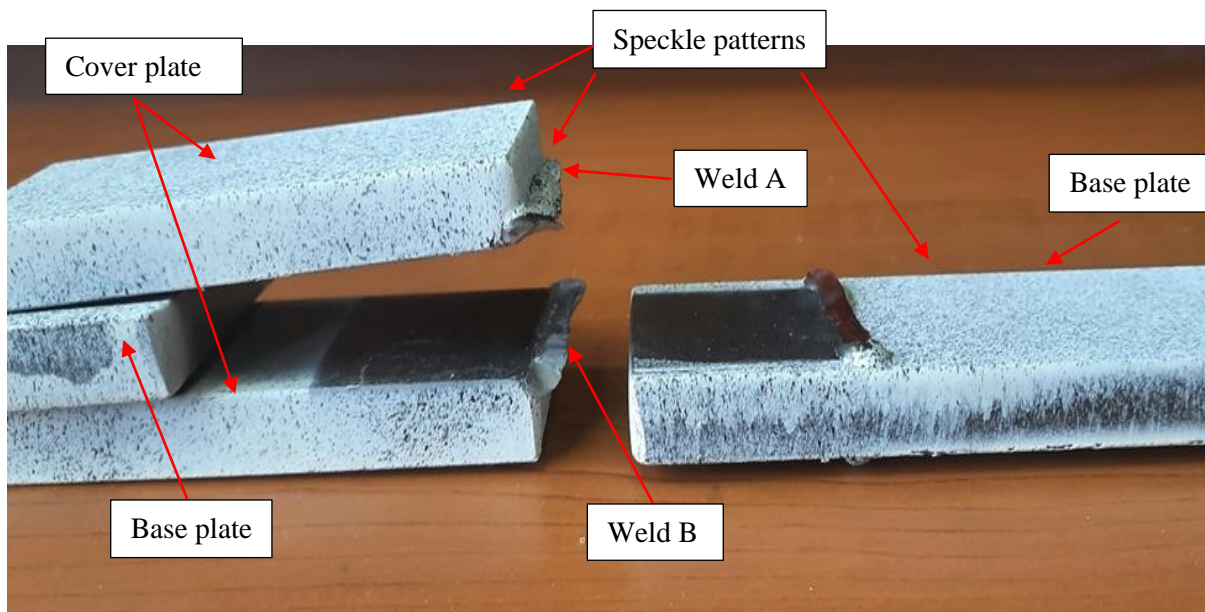


Fig. 30. Transverse fillet lap-welded connection after experiment.

Table 26 Average measurement of the fracture surface area after an experiment

Specimen	Weld		Total fracture surface area of the weld
	A [mm ²]	B [mm ²]	A_{fr} [mm ²]
TS-1	312	208	520
TS-2	178	160	338
TS-3	167	261	428
TS-4	179	219	398
TS-5	252	227	479
TS-6	225	248	473

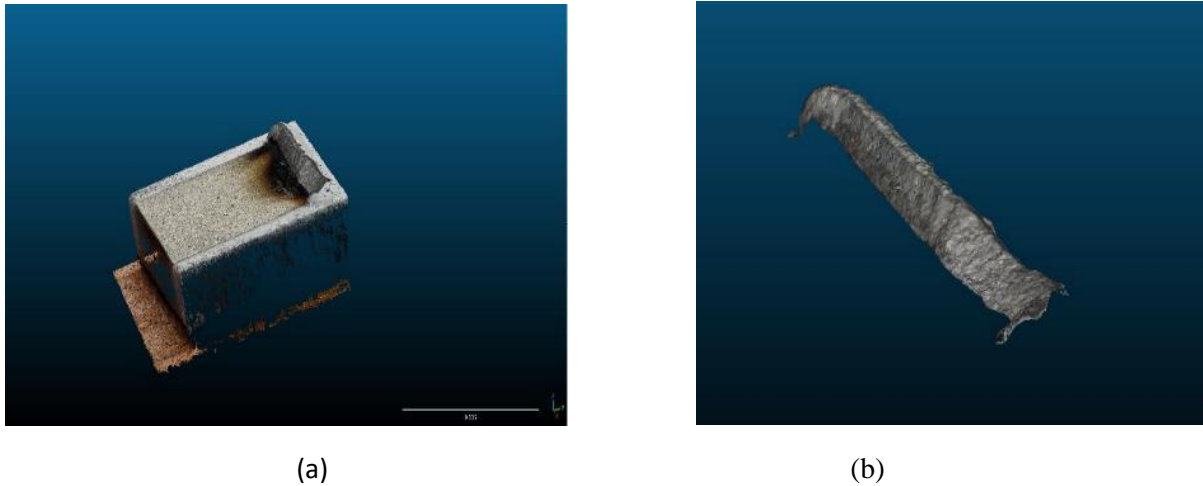


Fig. 31. Typical example of (a) 3D specimen model and (b) Extracted weld surface area.

Table 27 summarizes the average measurement of the weld profile and the weld area before and after the experiment.

Table 27 Summary of the mean measurement before and after an experiment.

Specimen	Weld			Total surface area	
	Length	Throat thickness	shear leg	Theoretical	Fracture
	L	a	w	A_{th}	A_{fr}
	[mm]	[mm]	[mm]	[mm ²]	[mm ²]
TS-1	90	4.30	6.80	387.0	520.0
TS-2	90	3.15	4.60	283.5	338.0
TS-3	88	3.25	4.70	286.0	428.0
TS-4	88	3.45	5.25	303.6	398.0
TS-5	90	3.75	5.15	337.5	479.0
TS-6	88	3.30	4.50	290.4	473.0

4.4 Results: Strength

Experiments were conducted to determine the strength of transverse fillet welds by measuring their ultimate load capacity F_u . Two welds are made on opposite sides of the base plate in a test specimen and are expected to share the ultimate load equally. The ultimate strength of the weld is calculated based on its failure surface area using theoretical throat area A_{th} and fracture surface area A_{fr} . A_{th} is calculated by multiplying the length and throat thickness of the weld, while A_{fr} is the entire fracture surface area of the specimen after the test. The computed ultimate strength of the transverse weld F_u / A_{th} is based

on the initial measurement of the weld profile, while the ultimate strength F_u / A_{fr} provides a real strength of the entire fracture surface.

The effect of weld size on the ultimate strength of transverse fillet weld is presented graphically in Fig. 32. There is no identical relationship between weld leg length and weld strength. However, the ultimate strength computed from the fracture surface area is less than that of using the theoretical area of the weld. This is because the fracture surface area is always higher than the theoretical area, and in most cases, the failure planes did not lie on the theoretical throat surface. Fig. 33a and Fig. 33b present the effect of the strength of weld metal and weld size on the ultimate strength of transverse fillet weld. The effect of different weld sizes is irregular for both ultimate strengths calculated by F_u / A_{th} and F_u / A_{fr} . However, the strength calculated for the maximum load divided by the theoretical throat area of the weld is always higher than that of the maximum load divided by the fracture surface area.

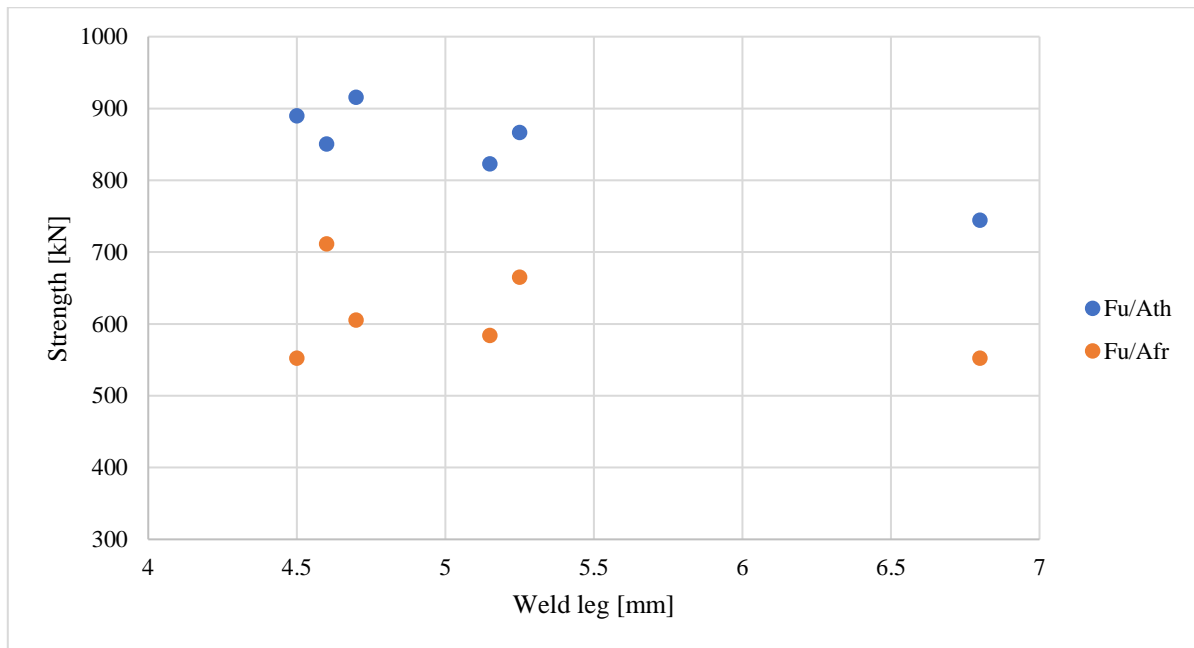
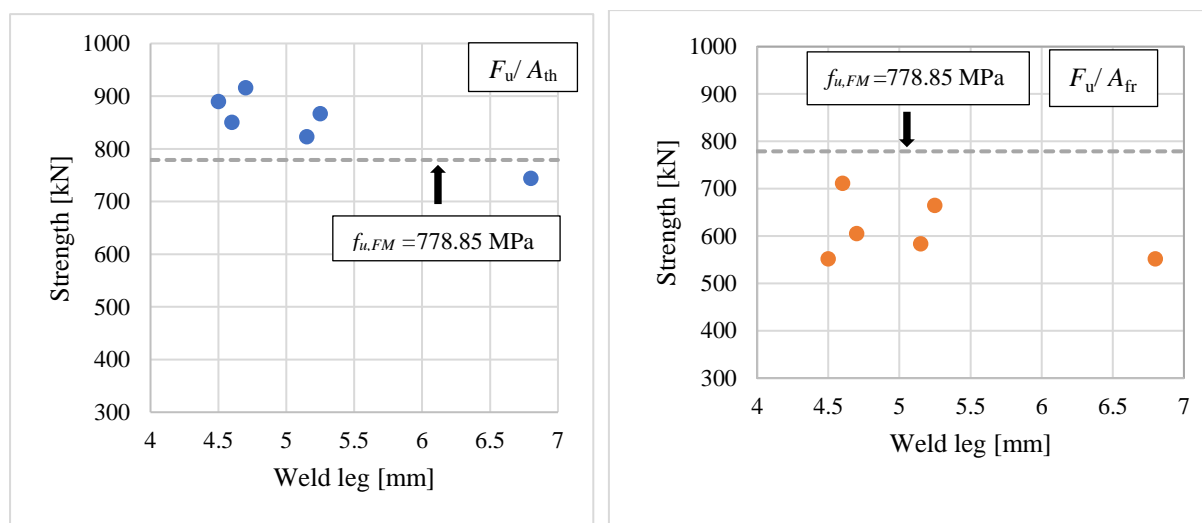


Fig. 32. The effect of the weld leg on the strength of transverse fillet lap-welded specimen.



(a)

(b)

Fig. 33. Comparison between the ultimate tensile strength of weld 13.12 concerning ultimate strength calculated by (a) F_u/A_{th} and (b) F_u/A_{fr} .

The weld strength of the transverse fillet lap-welded connection in Table 28 and Fig. 34 compares with the test strength and the predicted strength by the analytical model of European [27] and US standards [28]. During the calculation of weld strength, the ultimate strength of the filler and base materials was taken from the coupon test, and a safety factor of 1.0 was implemented to ensure an objective comparison.

Table 28 Summary of the strength of transverse fillet weld made from HSS.

Sample	Ultimate Load	Effective area		Strength		Test-to-predicted ratio	
	F_u [kN]	A_{th} [mm ²]	A_{fr} [mm ²]	F_u/A_{th} [N/mm ²]	F_u/A_{fr} [N/mm ²]	EC3 [-]	AISC [-]
TS-1	287.11	387.0	520	742.0	552.0	1.42	1.06
TS-2	240.50	283.5	338	848.0	712.0	1.62	1.21
TS-3	259.00	286.0	428	906.0	605.0	1.73	1.29
TS-4	264.60	303.6	398	872.0	665.0	1.67	1.24
TS-5	279.00	337.5	479	827.0	582.0	1.58	1.18
TS-6	261.25	290.4	473	900.0	552.0	1.72	1.28

No matter the predicted value by Eurocode or AISC, the test-to-predicted ratios are always greater than 1.0 in all cases (see Table 28). Fig. 34 compares the test results and predicted values of Eurocode and AISC. To sum up, both indicated capacities by Eurocode and AISC tended to give conservative values. The test-to-predicted ratios by Eurocode vary from 1.42 to 1.73 (mean value is 1.62), while by AISC vary from 1.06 to 1.29 (mean value is 1.21). The predicted strength of the weld computed using AISC provides a better prediction value.

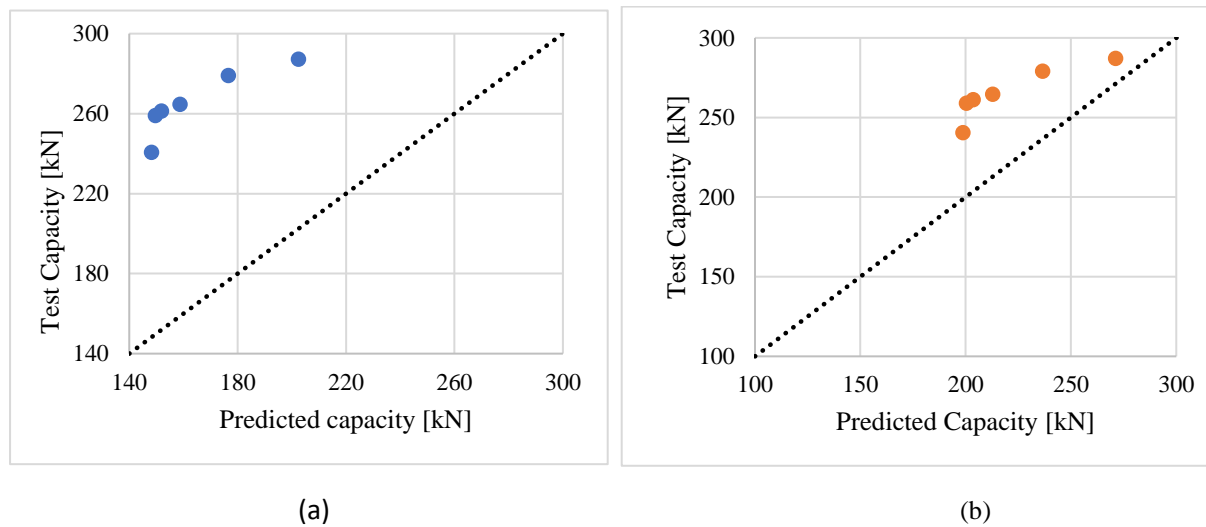


Fig. 34. Test vs. predicted capacity of transverse fillet weld according to (a) Eurocode and (b) AISC.

4.5 Results: Deformation capacity and ductility

Deformation capacity

This study defines the deformation capacity of welded connections as the deformation corresponding to the peak load. The deformation of the transverse fillet lap-welded connection was measured using DIC. The process involved recording the relative displacement of two points and determining the corresponding strain. Key points in the base plate, cover plate, and weld were assigned

and tracked over the loading process to show the displacement and strain development (see Fig. 36 and Fig. 37), with several key points highlighted in Fig. 35.

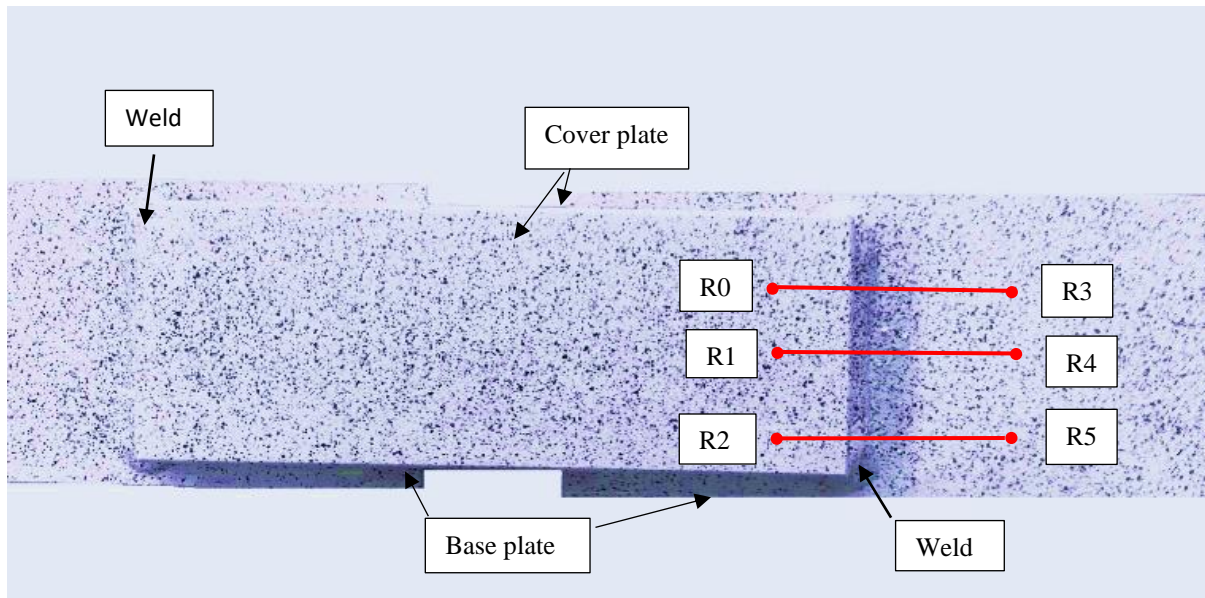


Fig. 35. The location of the measurement points on the transverse fillet lap-welded specimen at the initial state.

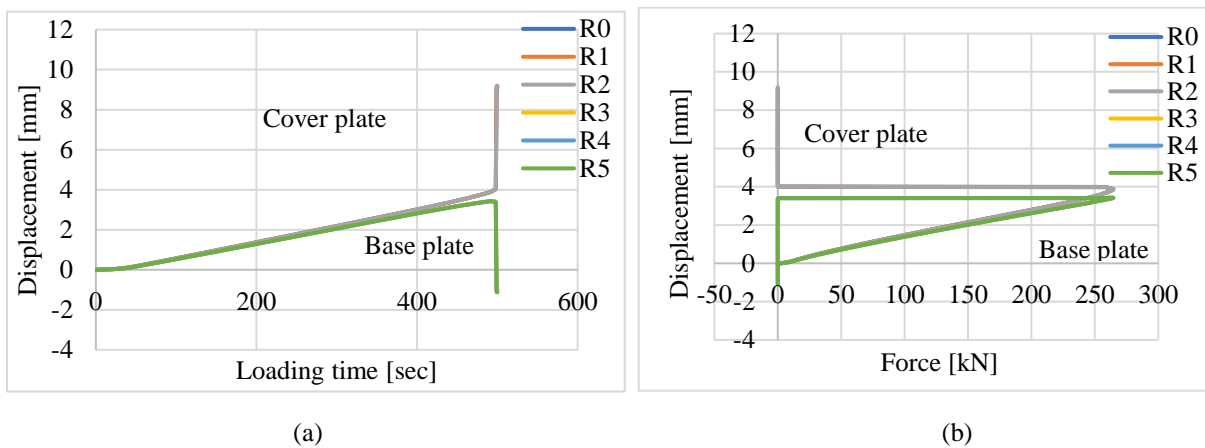


Fig. 36. Displacement developed along the measurement points, (a) Loading time and (b) Force (e.g., TS-4).

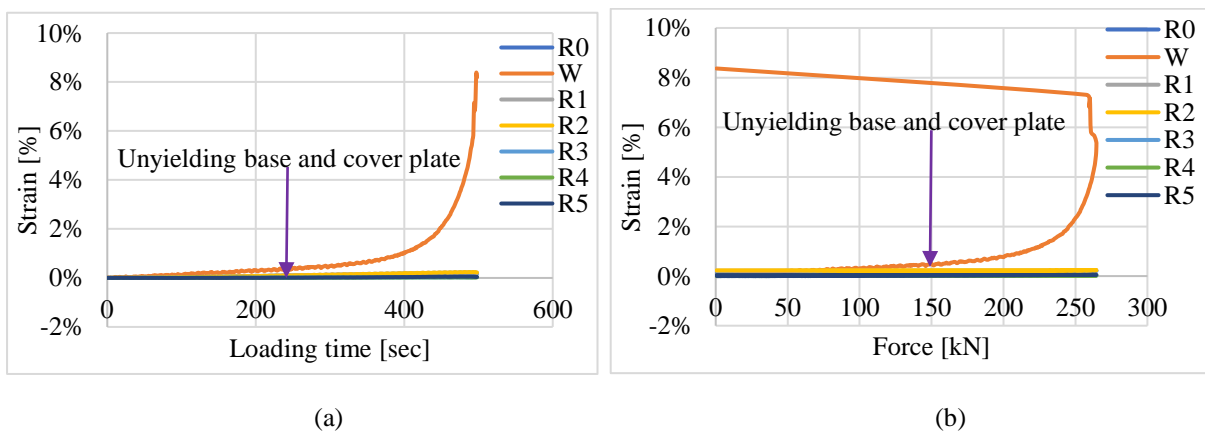


Fig. 37. Strain development along the measurement points, (a) Loading time and (b) Force (e.g., TS-4).

Fig. 36 shows that the critical points in the plate underwent the same displacement over time and force while being loaded. However, the base and cover plates experienced different displacements. Fig. 37. shows that the critical points in the base and cover plates remained unyielding throughout the loading process. This behavior suggests that the base and cover plate displacement is disregarded in transverse fillet lap-welded connections. Therefore, the deformation of the fillet weld can be depicted by the relative displacement of two arbitrary points between the base and cover plate [37].

The typical force-deformation diagram of the transverse fillet lap-welded connections includes the relative displacement of points R0R3, R1R4, and R2R5 and the average values of three points as recorded by DIC measurement (see Fig. 38a). This study utilized the average value of relative displacement of R0R3, R1R4, and R2R5 to measure the deformation of the specimens, as shown in Fig. 38b.

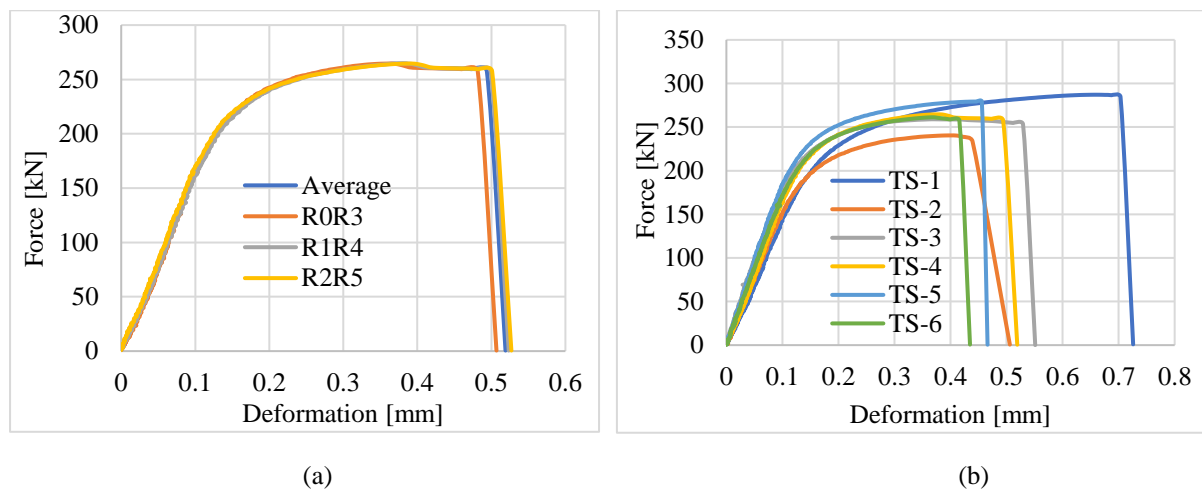


Fig. 38. Load-deformation curve of transverse fillet lap-welded specimen, (a) measurement of relative displacement of TS-14, and (b) average load-deformation curve of all specimens.

Ductility

Ductility is a material property that describes its ability to undergo plastic deformation or stretching without fracturing. It measures the material's ability to deform under stress and retain its load-carrying capacity even when subjected to significant strain.

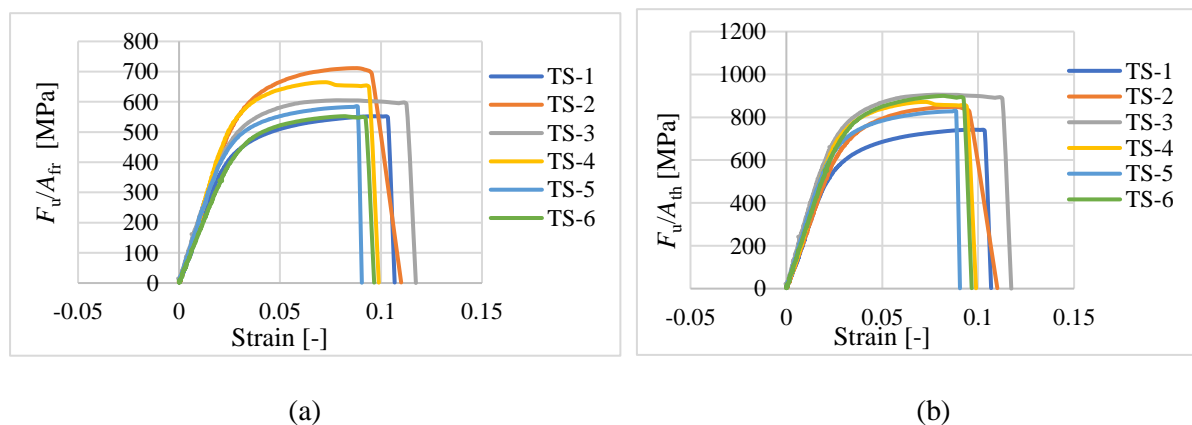


Fig. 39. Stress-strain diagram of the transverse fillet-lap welded connection (a) Stress corresponds to fracture surface area, (b) Stress corresponds to the theoretical effective area of the weld.

The stress-strain curve of each specimen is presented in Fig. 39. In the case of welded connections, ductility plays a crucial role in ensuring that the welded joint and the surrounding base material can

deform and absorb energy without catastrophic failure. To assess the ductility of a transverse welded connection, divide the measured deformation capacity by the measured shear leg of the fillet weld [37]. In this study, the mean values of the shear legs associated with fractured welds A and B and the deformation capacity δ_u of the transverse fillet lap-welded connection at ultimate load are used to calculate the mean ductility ϵ_u (see Fig. 40).

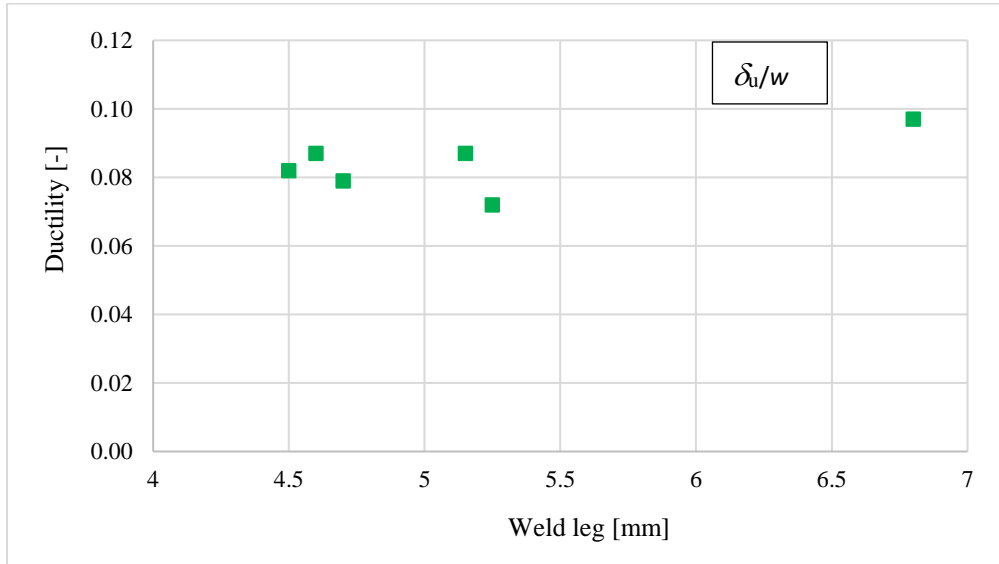


Fig. 40. Comparison of the weld leg's effect on the transverse fillet weld's ductility.

There is no definite relationship between weld leg length and ductility, see Fig. 40. However, the ductility of the transverse fillet lap-welded connection is small, and the total deformation capacity is always less than 1 mm for HSS. Table 29 summarizes the mean strength, deformation capacity, and ductility values of transverse fillet lap-welded connections from HSS specimens.

Table 29 Mean strength and ductility of the transverse weld from high-strength steel.

Sample	Ultimate Load	Strength		Mean deformation capacity	Mean shear leg	Mean ductility
	F_u	F_u/A_{th}	F_u/A_{fr}	δ_u	w	δ_u/w
	[kN]	[MPa]	[MPa]	[mm]	[mm]	[-]
TS-1	287.11	742.0	552.0	0.66	6.80	0.097
TS-2	240.50	848.0	712.0	0.40	4.60	0.087
TS-3	259.00	906.0	605.0	0.37	4.70	0.079
TS-4	264.60	872.0	665.0	0.38	5.25	0.072
TS-5	279.00	827.0	582.0	0.45	5.15	0.087
TS-6	261.25	900.0	552.0	0.37	4.50	0.082

CHAPTER 5: ANALYTICAL MODEL

5.1 Material information

The same thickness of 12 mm steel plates of S700 MC Plus HSS and AristoRod 13.12 electrode were used to fabricate different transverse welds. To characterize material properties, three base metal tension coupons and three weld metal tension coupons were tested per Eurocode; see sections 4.1.1 and 4.1.2 for more information. The measured and nominal material properties of base metal and filler metal are presented in Fig. 41 and Table 30.

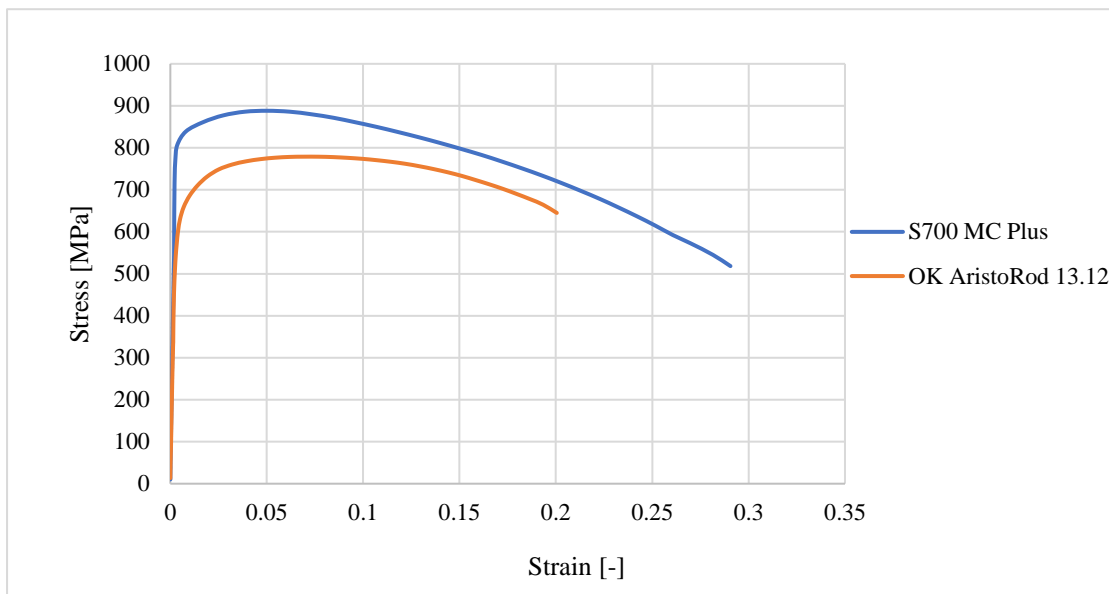


Fig. 41. Stress-strain curve of the material.

Table 30 Material properties of base and filler materials.

Material	Yield Strength	Tensile strength	Elongation
	[MPa]	[MPa]	[min %]
Strenx 700 MC Plus (Nominal)	700	750-950	13
Strenx 700 MC Plus (Measured)	811.55	888.16	29.06
OK AristoRod 13.12 (Nominal)	640	740	18
OK AristoRod 13.12 (Measured)	571.14	778.85	20.04

5.3 Specimen information

A total of six specimens of the transverse fillet lap-welded connections from HSSs were prepared. They used under-matching welding consumables. All specimens were used OK AristoRod 13.12. Fig. 42 presents the typical specimen geometry and configuration of the fillet weld. Table 31 summarizes the measurements of the weld throat, weld length, and the weld's theoretical and fracture surface area, where fracture surface area is calculated from the 3D scanning photogrammetry approach.

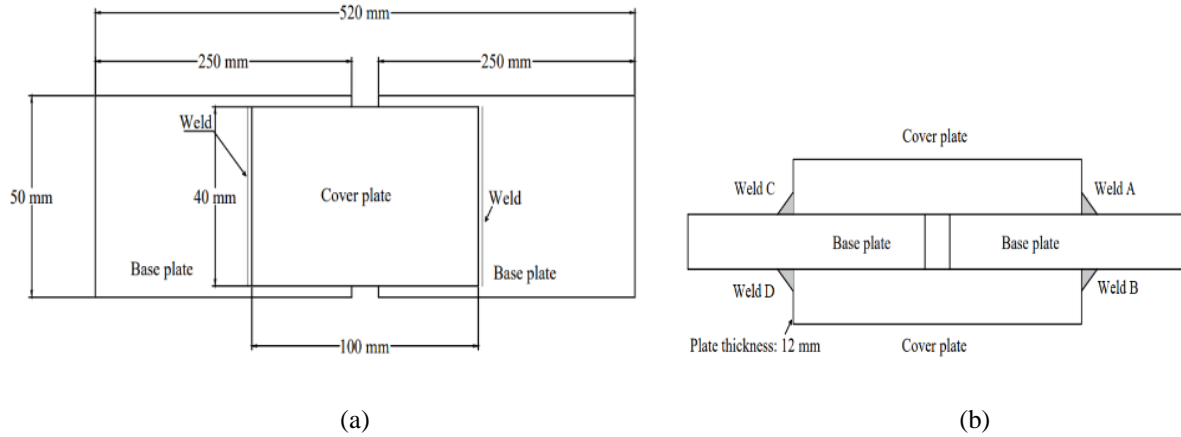


Fig. 42. Transverse fillet lap-welded specimen (a) Plan view, and (b) Section.

Table 31 Average measurement of weld profile and effective area of the weld.

Specimen	Weld profile		The effective area of the weld	
	a	L	A_{th}	A_{fr}
	[mm]	[mm]	[mm ²]	[mm ²]
TS-1	4.30	90	387.00	520.00
TS-2	3.15	90	283.50	338.00
TS-3	3.25	88	286.00	428.00
TS-4	3.45	88	303.60	398.00
TS-5	3.75	90	337.50	479.00
TS-6	3.30	88	290.40	473.00

5.4 Analytical calculation: Weld resistance

The directional method determines the resistance of welded connections made up of HSSs according to prEN1993-1-8:2020 [27]. The orientation of the weld profile influences the design weld resistance of a welded connection. In this study, a transverse fillet welded connection is taken into account for the evaluation of the resistance, which is the combination of S700 MC Plus base metal and OK AristoRod 13.12 filler metal having ultimate stress ($f_{u,PM}$) 888.16 MPa and ($f_{u,FM}$) 778.85 MPa respectively. The conservative value of the modified correlation factor ($\beta_{w,mod}$) 1.09 is taken according to table 6.2 in prEN 1993-1-8:2020 [27] for the calculation. The calculated weld resistance of transverse fillet lap-welded connections from HSSs is presented in Table 32 with the following function:

$$F_{w,Rd,T} = \frac{(0.25f_{u,PM}+0.75f_{u,FM})}{\sqrt{2}\beta_{w,mod}\gamma_{M2}} a \cdot L \quad (5.4)$$

Where a is the throat thickness of the weld and L is the effective length of the weld.

Table 32 Weld resistance by using the theoretical effective area of the weld.

Specimen	Weld profile		Weld resistance
	a	L	$F_{w,Rd,T}$
	[mm]	[mm]	[kN]
TS-1	4.30	90	162
TS-2	3.15	90	119
TS-3	3.25	88	120
TS-4	3.45	88	127
TS-5	3.75	90	141
TS-6	3.30	88	122

CHAPTER 6: FINITE ELEMENT MODEL

This chapter describes the finite element (FE) model of high-strength steel (HSS) welded connections. The solid model of transverse and longitudinal fillet lap-welded connections was prepared to validate it with the experiment results. Similarly, shell element models were also simulated to perform numerical design calculation for the prediction of the ultimate stress and deformation capacity of the welded connections. The verification of the shell element model with the solid element model and analytical model also explains in this chapter.

6.1 Specimen information

Six FE models of transverse fillet lap-welded connections from HSS were created using the commercial software ABAQUS. These models used OK AristoRod 13.12 as a weld metal and S700 MC Plus base plate. For detailed specimen information, please refer to Chapter 4.2.

Kleiner's thesis [13] examined the geometry configuration of longitudinal fillet lap-welded connections. During the study, Kleiner [13] conducted several experiments using the same materials and mixed materials combinations, and in this particular study, the S690-S355-G46 welded configuration was further examined. Figure 43 illustrates the fabrication of the longitudinal fillet lap-welded connection, which has a 100 mm weld length l and 5.96 mm throat thickness a . It is a combination of base metal S690 with cover plate S355.

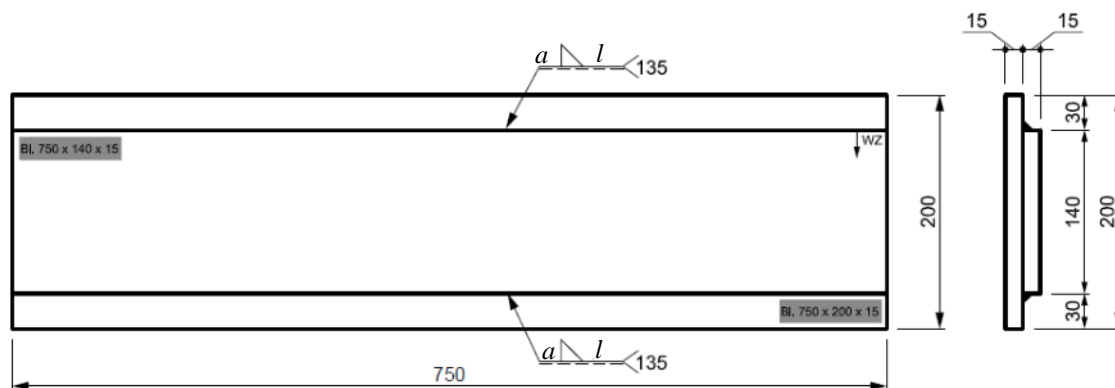


Fig. 43. Longitudinal fillet lap-welded connection [13].

6.2 Solid model

6.2.1 Material model

When creating FE models of structural steel, the most frequently used material diagrams are the ideal plastic, the elastic-plastic model with a small yielding plateau, the elastic model with strain hardening, and the stress-strain diagram that has been measured [56]. In solid models, material models for the base and filler metals are calculated by the material calibration process in Abaqus. This process involves adjusting the parameters of a constitutive model within Abaqus to match the real-world material behavior, as seen in the experimental stress-strain curve in section 4.1. The elastic-plastic isotropic behavior of the material is considered during the calibration to create precise mechanical properties that can be utilized for future simulations and analyses. Table 33 summarizes the material model parameters. The Poisson's ratio was taken as 0.3 for both materials. The true plastic stress at the

end of the yield plateau is represented by σ_0 , while the ultimate stress and true plastic strain of the material are represented by F_u and ϵ_p^u , respectively.

Table 33 Material properties of base and filler materials for solid finite element model.

Material	E	σ_0	F_u	ϵ_p^u
	[MPa]	[MPa]	[MPa]	[-]
Strenx 700 MC Plus	215200	781.17	930.21	0.046
OK AristoRod 13.12	203523	407.05	829.19	0.062
S690	199445	771.85	869.71	0.057
S355	233560	401.72	634.95	0.131
G46	252513	500	668.74	0.121

6.2.2 Finite element modelling

Solid finite element models are considered research-oriented models. In Abaqus, the plate and welds are represented by the solid element C3D8R, with six degrees of freedom in each node. The base and cover plates are the master surface, while the weld is the slave surface. These two surfaces are connected by a tie constraint, as illustrated in Fig. 44 and 45. The FE modeling involved analyzing material nonlinearity behavior using ABAQUS/CAE 6.14. The surface-to-surface contact type was used between the base and cover plate. The base plate was subjected to tensile load on one end, while the other had a fixed support boundary condition. The longitudinal edge of the base plate and cover plate were permitted to move only in the direction of the applied load, where it was clamped during the experiment, as shown in Fig. 44.

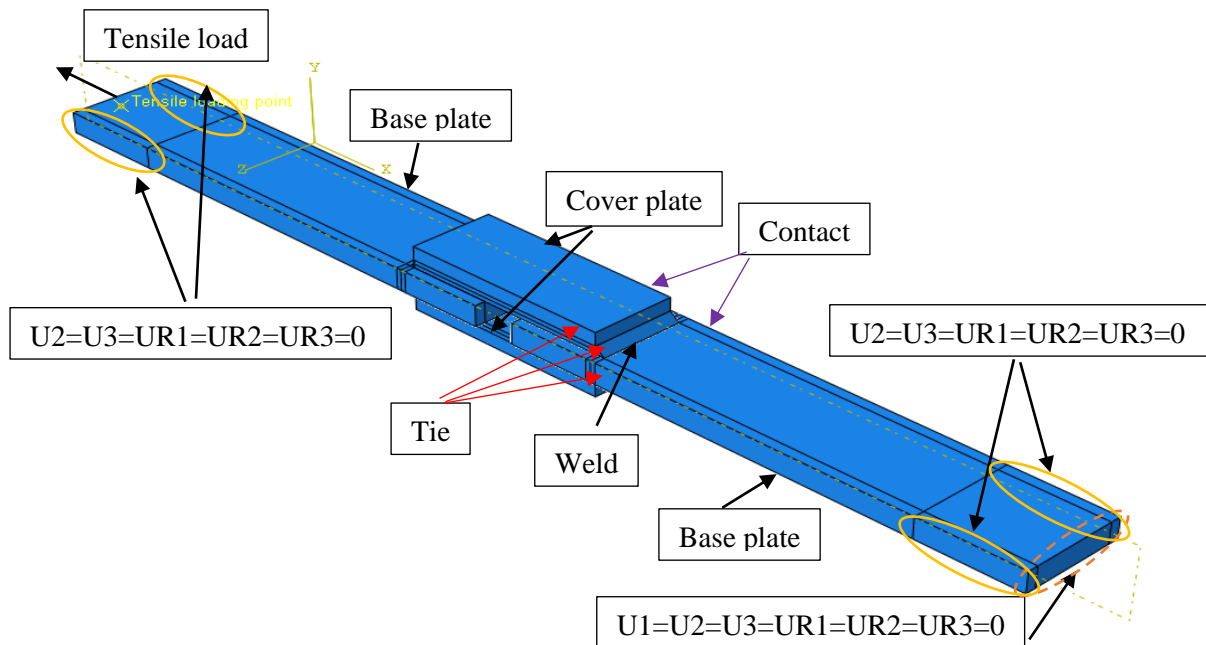


Fig. 44. Three-dimensional finite element model and boundary conditions for transverse fillet welded connection.

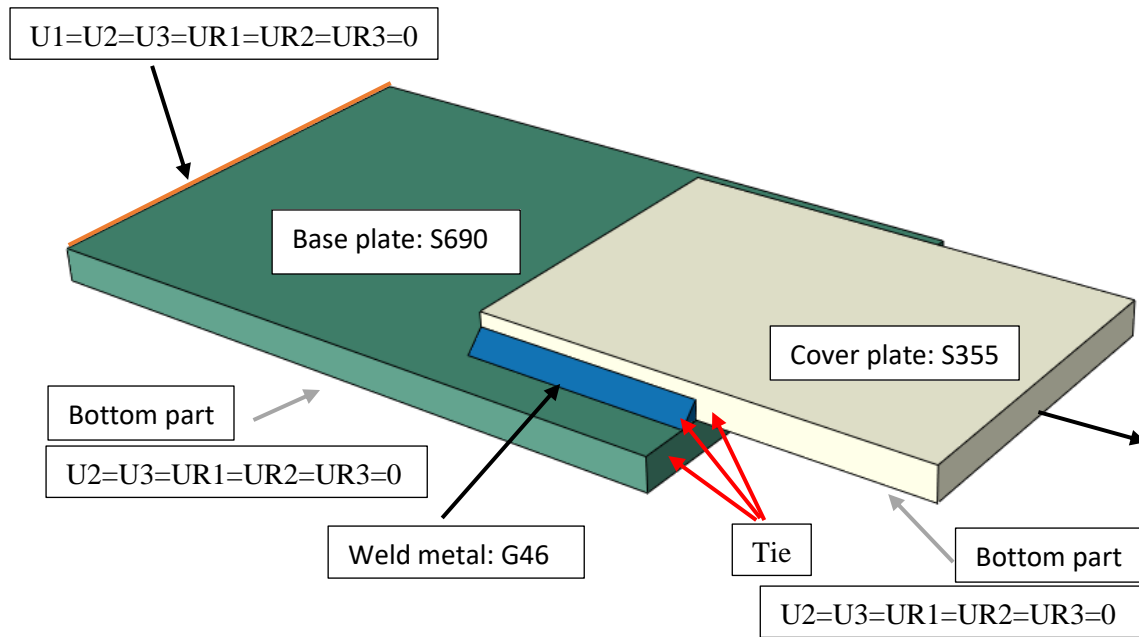


Fig. 45. Three-dimensional finite element model and boundary conditions for longitudinal fillet welded connection.

6.2.3 Mesh sensitivity study

A mesh sensitivity study involves using various grid resolutions in simulations to evaluate how the accuracy of solutions changes with each mesh. This study examines explicitly the welded section, which plays a critical role in determining the resistance of the welded connection and is considered as the failure criteria. The mesh size is notably finer in the weld than in the base and cover plate. The mesh size represents in terms of the weld's throat thickness a , which makes consistency to perform and comparison the results of all the specimens which have different throat thickness.

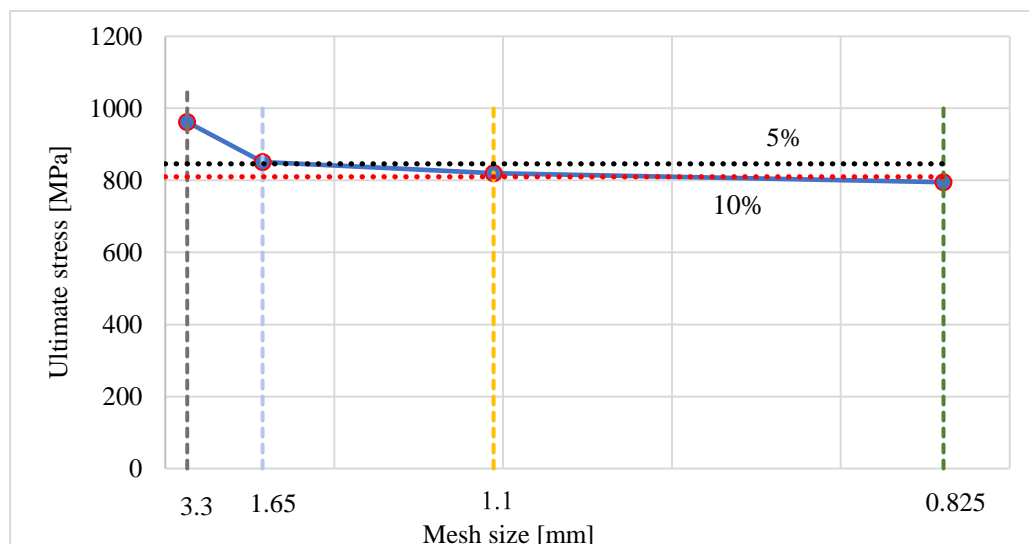


Fig. 46. Influence of mesh size on ultimate stress in the transverse fillet lap-welded connection.

In the case of transverse fillet welded connection, the mesh size varies from a , $\frac{a}{2}$, $\frac{a}{3}$, and $\frac{a}{4}$, which corresponds to mesh size (MS): 3.3 mm X 3.3 mm, 1.65 mm X 1.65 mm, 1.1 mm X 1.1 mm, 0.825 mm X 0.825 mm. The influence of the mesh sizes on weld ultimate stress is present in Fig. 46. The black

dashed line and red dashed line represent the 5% and 10% differences with respect to experimental results respectively. Although a mesh size of 1.1 mm X 1.1 mm to 0.825 mm X 0.825 mm provides more consistency results, for more accurate results comparable to the experimental results, it is advisable to utilize a mesh size of 1.65 mm X 1.65 mm in the weld. This mesh size should be the $\frac{a}{2}$, in the weld.

In a longitudinal fillet welded connection, the mesh size can vary from $\frac{a}{1.5}$, $\frac{a}{2}$, and $\frac{a}{3}$ corresponding to mesh size: 4 mm X 4 mm, 3 mm X 3 mm, and 2 mm X 2 mm. The impact of mesh sizes on the equivalent plastic strain at the weld failure stage is shown in Fig. 47. The mesh sizes between 2- and 3-mm yield more consistent results. As a result, for the simulation, a mesh size of $\frac{a}{2}$ was chosen for the inclined shell element.

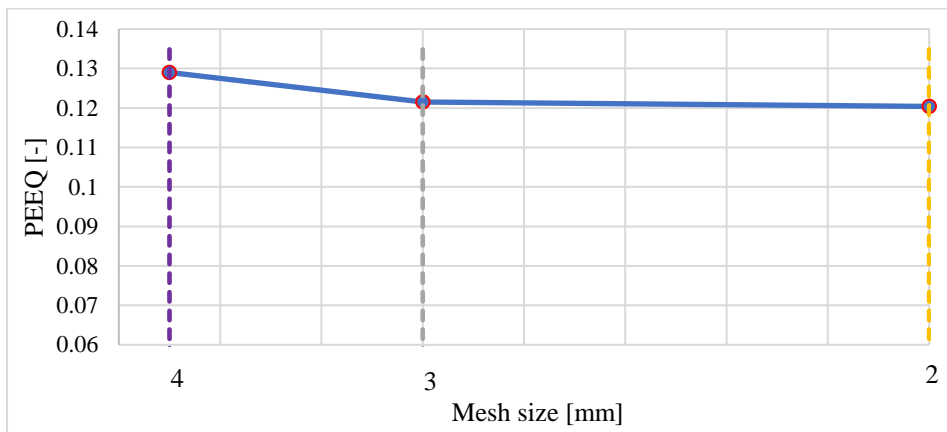
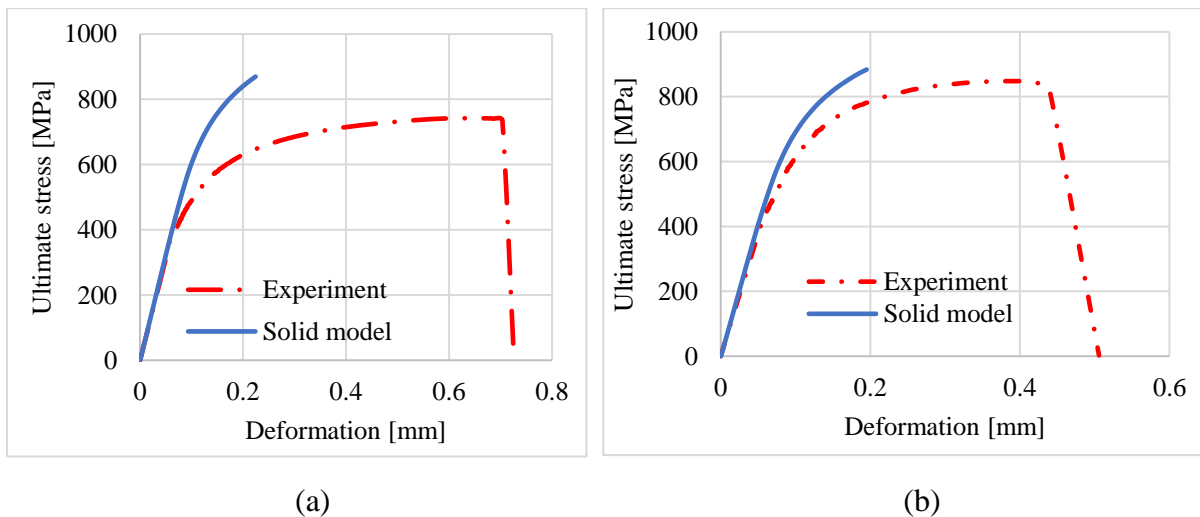


Fig. 47. Influence of mesh size on maximum equivalent plastic strain in the longitudinal fillet lap-welded connection.

6.2.4 Validation of solid model

The comparison of the strength-deformation curves between experiment and solid model was presented in Fig. 48 and 49. Experimental and numerical models have shown some differences in their results. Specifically, the strength-deformation curve from the finite element simulation did not have a falling branch in both welded configurations. This may have been because the simulation did not consider material damage and subsequent fracture in the welds. However, the predicted strength from the simulation was close to the peak strength and landed on the plastic-developed platform of the curves from the test in both transverse and longitudinal welded connection.



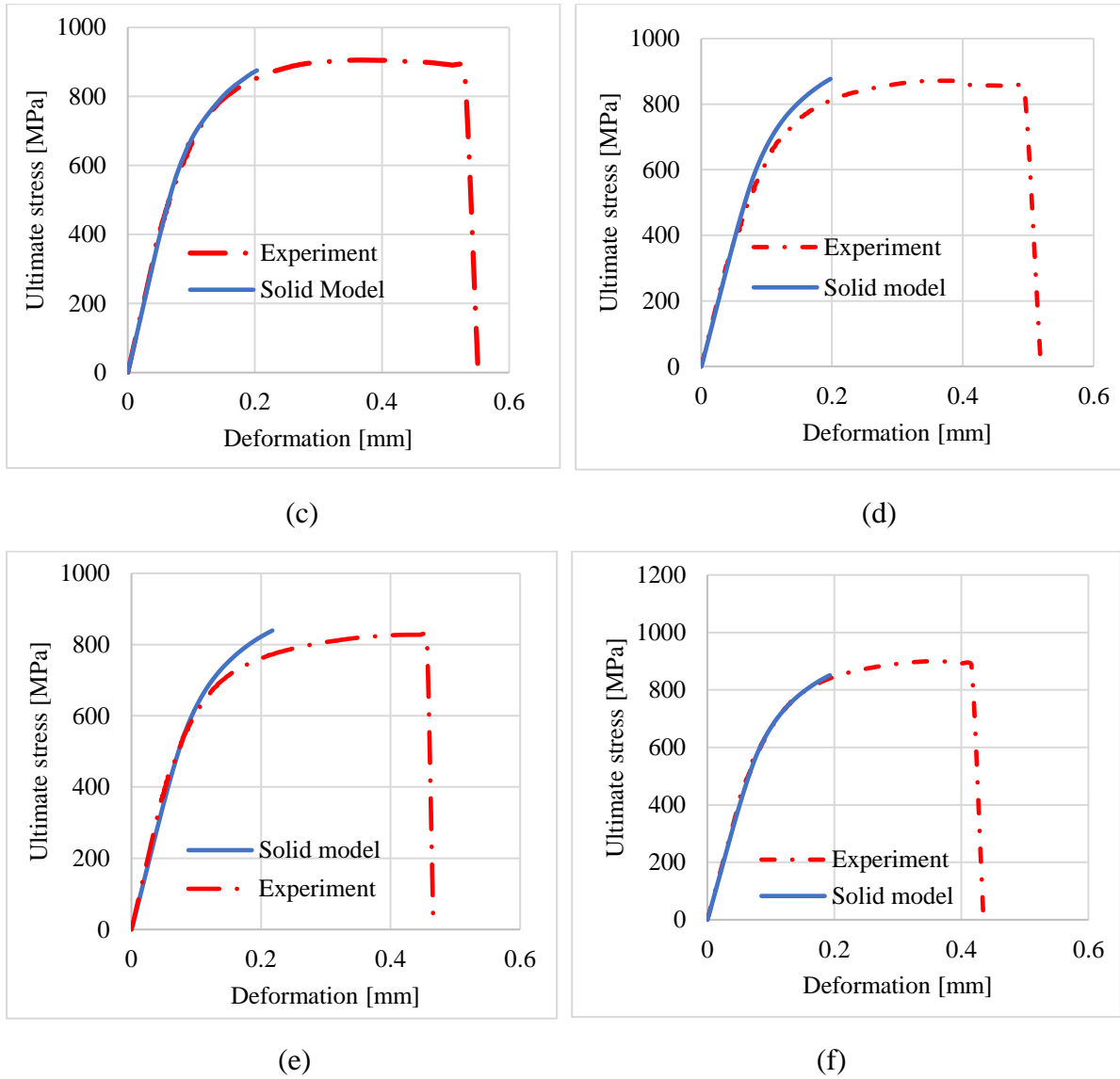


Fig. 48. Strength-deformation diagram of transverse fillet lap-welded connections; (a) TS-1, (b) TS-2, (c) TS-3, (d) TS-4, (e) TS-5, and (f) TS-6.

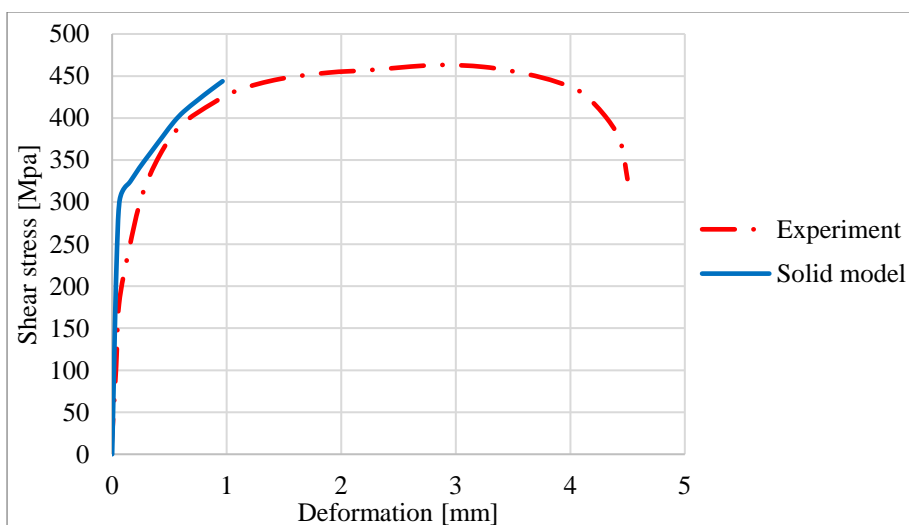


Fig. 49. Strength-deformation diagram of longitudinal fillet lap-welded connections.

Table 34 summarizes the comparison results, indicating that the predicted maximum stress from the FE simulation agreed well with the ultimate stress and shear stress from the experiment, with a deviation of the predicted value of less than $\pm 15\%$.

Table 34 Comparison on strength between experiment and solid finite element model.

Specimen	Experiment	FEM	Exp./FEM
	[MPa]	[MPa]	[-]
TS -1	742	869	0.85
TS -2	848	884	0.96
TS -3	906	875	1.04
TS -4	872	877	0.99
TS -5	827	839	0.99
TS -6	900	851	1.06
L100	463	444	1.04

6.3 Shell model

6.3.1 Material model

In shell models, material models for the base and filler metals are calculated by the material calibration process in Abaqus. This process involves adjusting the parameters of a constitutive model within Abaqus to match the real-world material behavior, as seen in the experimental stress-strain curve in section 4.1. The elastic-plastic isotropic behavior of the material is considered during the calibration to create precise mechanical properties that can be utilized for future simulations and analyses. Table 35 summarizes the material model parameters, and Fig. 43 shows nominal stress-plastic strain curves for each material. The Poisson's ratio was taken as 0.3 for both materials. The plastic strain and stress at the end of the yield plateau are represented by ϵ_p^o and σ_o , respectively, while the ultimate stress and plastic strain of the material are represented by F_u and ϵ_p^u , respectively.

Table 35 Material properties of base and filler materials for FEM.

Material	E	σ_o	F_u	ϵ_p^u
	[MPa]	[MPa]	[MPa]	[-]
Strenx 700 MC Plus	215200	781	888.16	0.047
OK AristoRod 13.12	203523	407	778.85	0.064
S690	199445	772	821.00	0.058
S355	233560	402	557.02	0.139
G46	252513	500	592.74	0.128

6.3.2 Finite element modelling

In Abaqus, the plate and welds are represented by the shell element S4R, with six degrees of freedom in each node. These elements are positioned at the mid-plane of the real structural component [57], as demonstrated in Fig. 50. In this model, the inclined shell element represents welds and has the same thickness as the throat thickness of the weld. The thickness of other structural parts is defined as plate thickness. The weld model aims to yield results like design codes with minimal computational requirements rather than simulating real-life behavior. The calculations do not consider the residual stresses and weld shrinkage. When analyzing fillet welds, an inclined shell element is utilized between

multi-point constraints to represent the weld. The element behaves according to the code's assumption that stresses are uniformly distributed in the weld throat, considering the thickness, location, and orientation of the weld throat. The base and cover plates are the master surface, while the inclined shell element is the slave surface. These two surfaces are connected by a multi-point constraint rigid link, as illustrated in Fig. 50. Using multi-point constraints has many advantages, such as allowing the connection of plates with different mesh densities and modeling plates with an offset, which considers the actual plate thicknesses and positions.

When choosing FE modeling techniques, the goal is to make it easier for engineers to speed up computation time and achieve accurate welding resistance results in larger structures. A scientific approach is taken to analyze, interpret, and select the best modeling technique compared to others. Three modeling approaches were considered to compare stress distribution in the inclined shell element and deflections on the cover plate during the loading process. In all cases, the plates and the weld are positioned at the mid-plane of the real structural components (see Fig. 50 a-d). The first option was to provide vertical restraint for the cover plate to prevent deflection after the weld failure (refer to Fig. 50 b). The second option was adding an MPC between the cover and base plates (refer to Fig. 50 c). The third option was without vertical restraint or additional MPC (refer to Fig. 50). When comparing the equivalent stresses acting on the inclined shell element, all three approaches showed only a 1-2% difference, even with increased weld length through a parametrical study. Due to the simplicity of the modeling, faster computation, and negligible displacement of the cover plate, the third approach (see Fig. 50 d) was chosen for further calculation.

However, it is essential to note that these types of weld modeling techniques are only suitable for simple welding configurations, such as transverse and longitudinal fillet lap-welded connections, with only a tangential load and deflection along the loading directions. Results may vary for longer welds or weld configurations with shear and bending moments, such as fin plate and connection to an unstiffened plate.

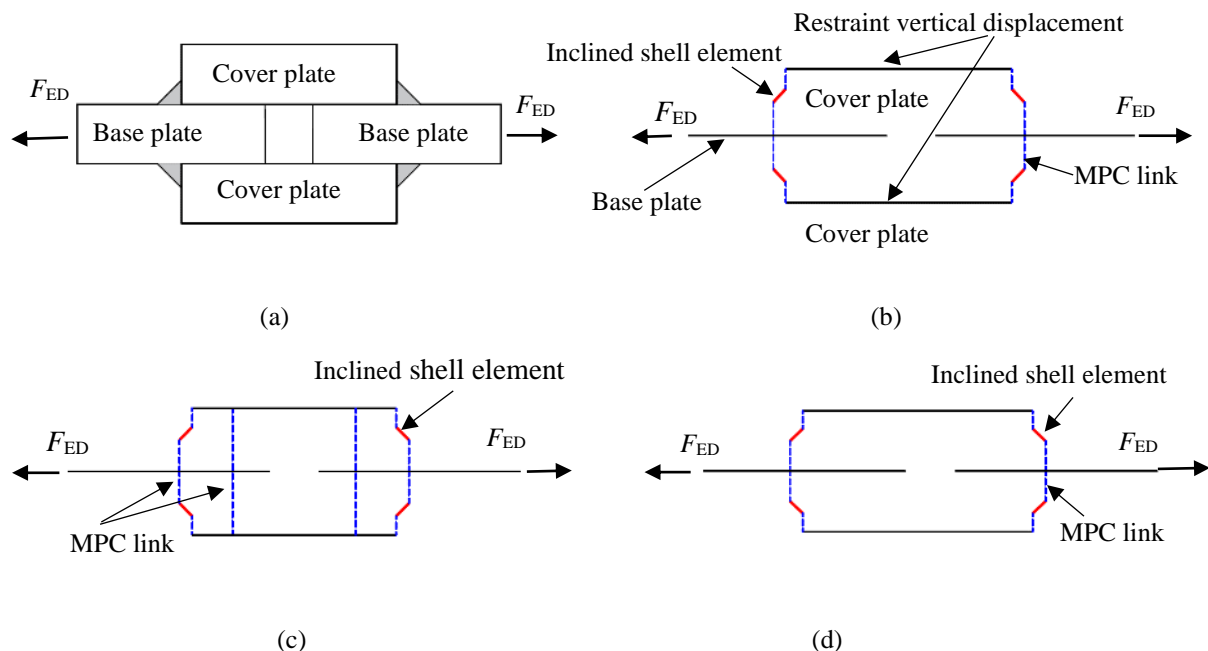


Fig. 50. Typical scheme used for NDC, (a) real structural parts, (b) option 1, (c) option 2, and (d) option 3.

The FE modeling involved analyzing the material nonlinear behavior using ABAQUS/CAE 6.14. The surface-to-surface interaction type and frictionless contact properties were used between the base and cover plate. The base plate was subjected to a tensile load at one end, whereas the other had a fixed support boundary condition. The longitudinal edge of the base plate was permitted to move only in the direction of the applied load, where it was clamped during the experiment, as shown in Fig. 51.

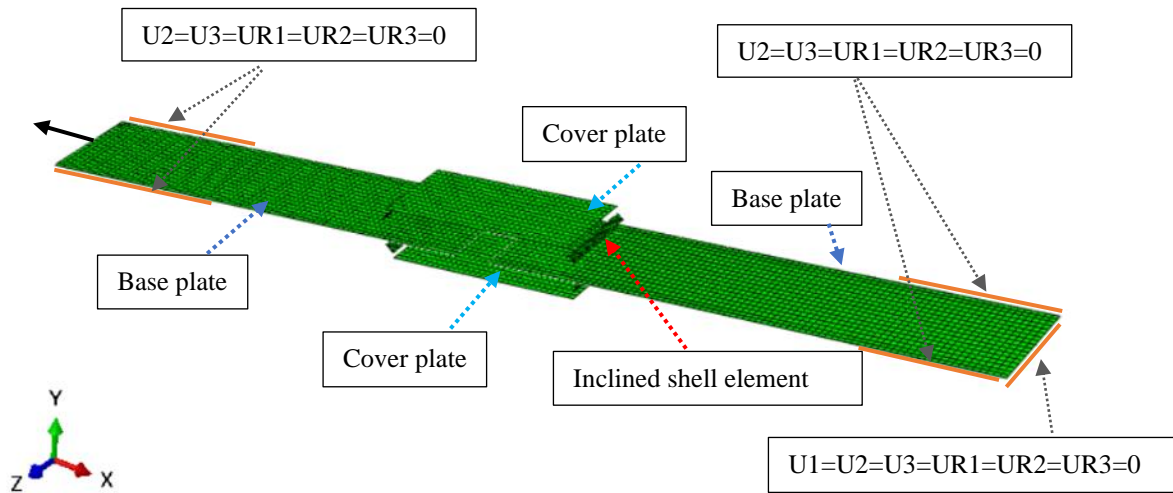


Fig. 51. Regular inclined shell element model (RISEM) with boundary conditions for transverse welded connections.

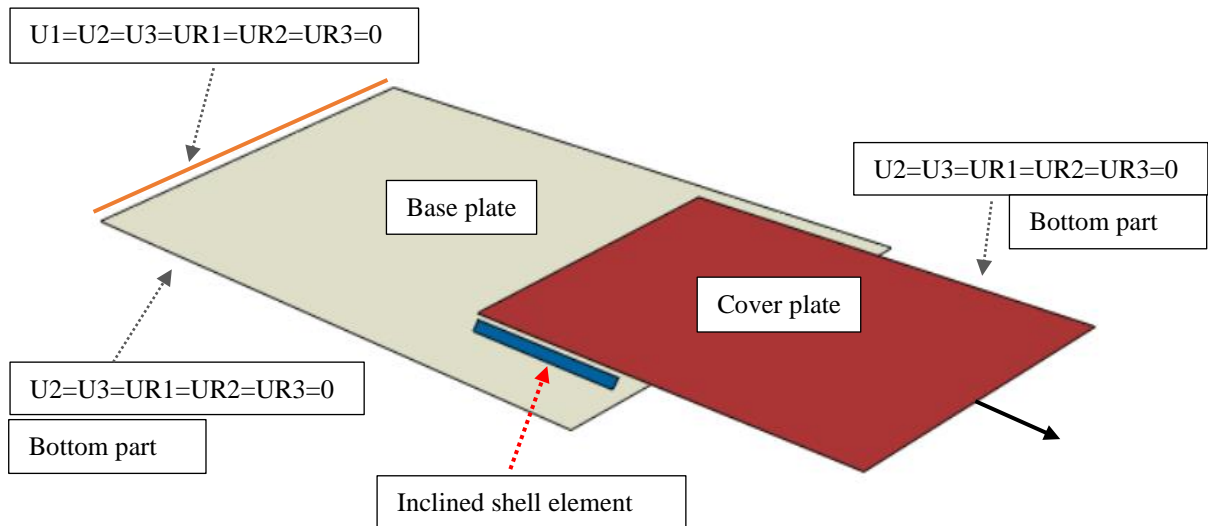


Fig. 52. Regular inclined shell element model (RISEM) with boundary conditions for longitudinal welded connections.

6.3.3 Mesh sensitivity study

A mesh sensitivity study involves using various grid resolutions in simulations to evaluate how the accuracy of solutions changes with each mesh. This study examines explicitly the inclined shell element, which plays a critical role in determining the design resistance of the welded connection. The mesh size is notably finer in the inclined shell element than in the base and cover plate. The mesh size is represented in terms of the weld's throat thickness a , making it consistent to perform and compare the results of all specimens with different throat thicknesses. The mesh size varies from a , $\frac{a}{1.43}$, $\frac{a}{1.5}$, $\frac{a}{1.75}$, $\frac{a}{2}$, $\frac{a}{5}$, and $\frac{a}{5.7}$, which corresponds to mesh size (MS): 4.3 mm X 4.3 mm, 3 mm X 3 mm, 2.87 mm X 2.87 mm, 2.45 mm X 2.45 mm, 2.15 mm X 2.15 mm, 0.86 mm X 0.86 mm, 0.75 mm X 0.75 mm respectively. The influence of the mesh sizes on the equivalent plastic strain in the inclined shell element is present in Fig. 53. The mesh size ranges from 0.86 mm to 2.45 mm, providing more consistent results

for more accurate results comparable to the analytical results. Utilizing a mesh size of inclined shell element within the range of $\frac{a}{1.75} - \frac{a}{5}$ is advisable.

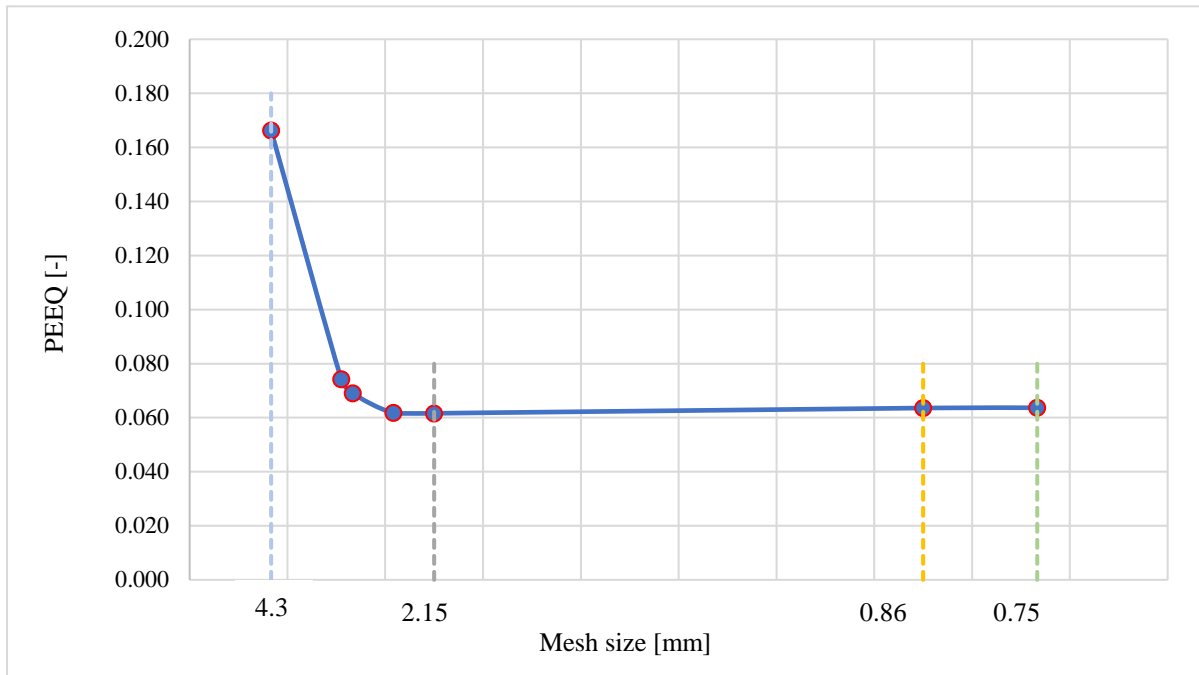


Fig. 53. Influence of mesh size on the equivalent plastic strain (PEEQ) of the inclined shell elements for transverse weld.

For longitudinally welded connections, mesh sizes ranging from 0.6 mm to 0.3 mm produce consistent PEEQ results (see Fig. 54). These mesh sizes correspond to $\frac{a}{10} - \frac{a}{20}$ in an inclined shell element. It is, therefore, advisable to use mesh sizes within this range to achieve the desired level of accuracy in the results.

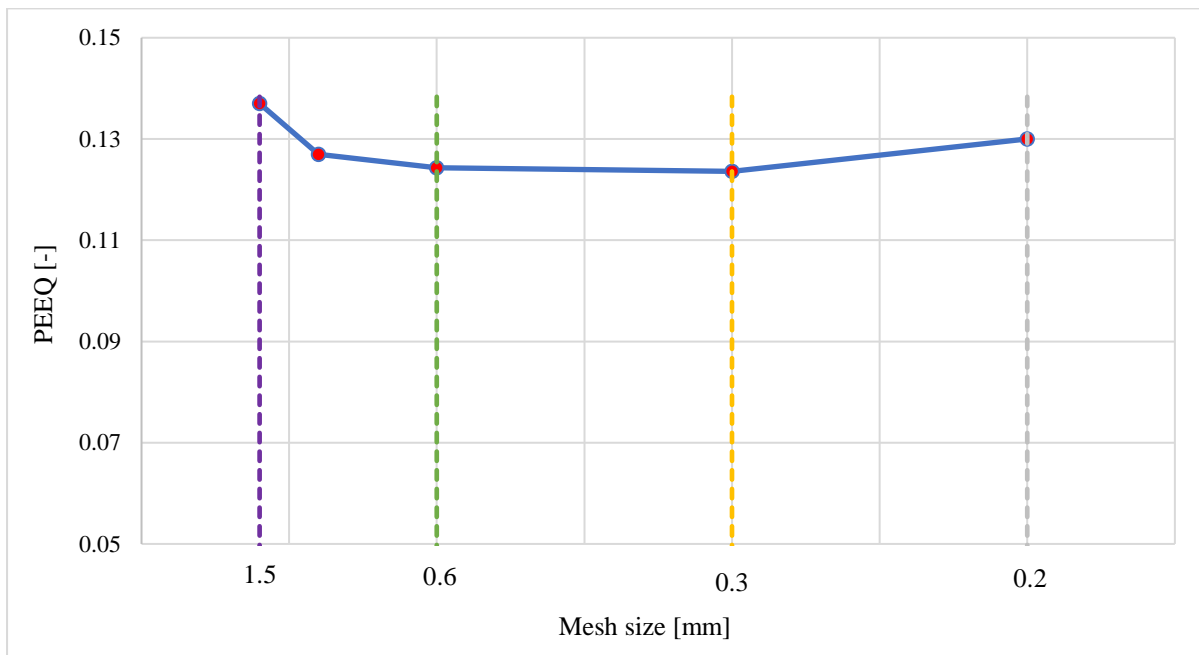
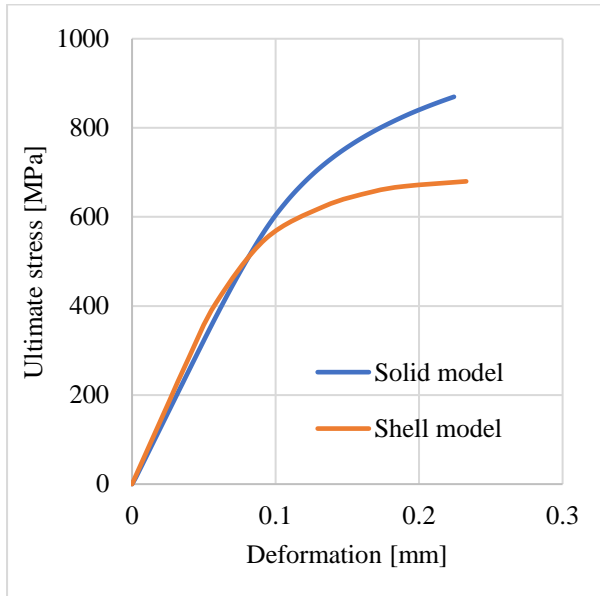


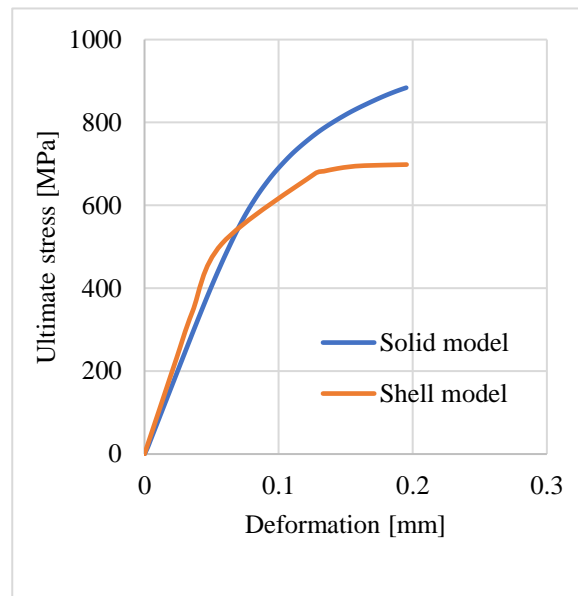
Fig. 54. Influence of mesh size on the equivalent plastic strain (PEEQ) of the inclined shell elements for longitudinal weld.

6.3.4 Verification of shell with solid model

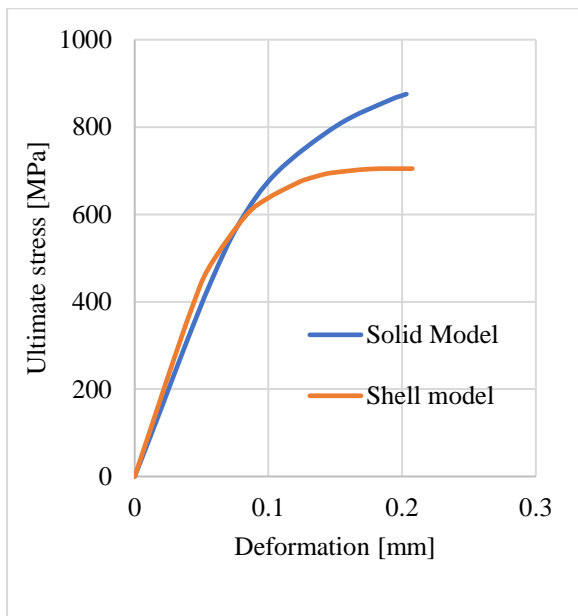
The comparison of the strength-deformation curve between the solid and shell models is presented in Fig 55 and 56. The volume and shell modes have shown some differences in their results. Specifically, the maximum strength of the welded connection significantly differs in weld failure criteria. This may have been because the volume model used the true material model, whereas the shell model used the engineering material model. However, the predicted deformation capacity from the simulation was close to each other at the stage of weld failure. Table 36 summarizes the comparison results, indicating that the predicted deformation capacity from the shell model agreed well with the deformation capacity of the volume model, with a deviation of the predicted value of less than $\pm 3\%$.



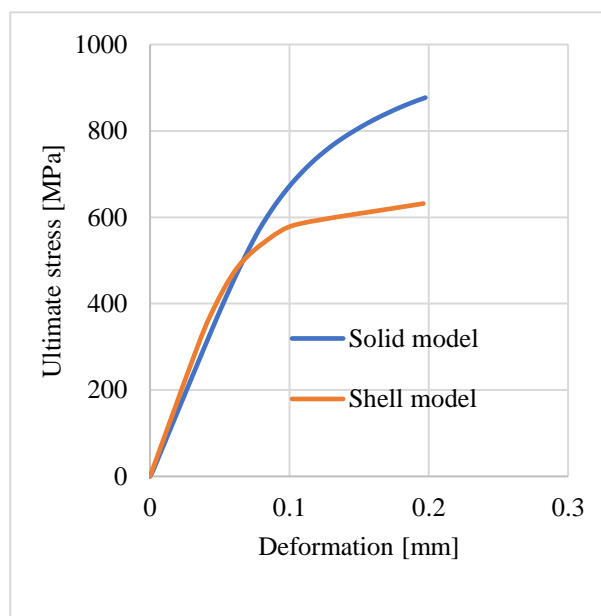
(a)



(b)



(c)



(d)

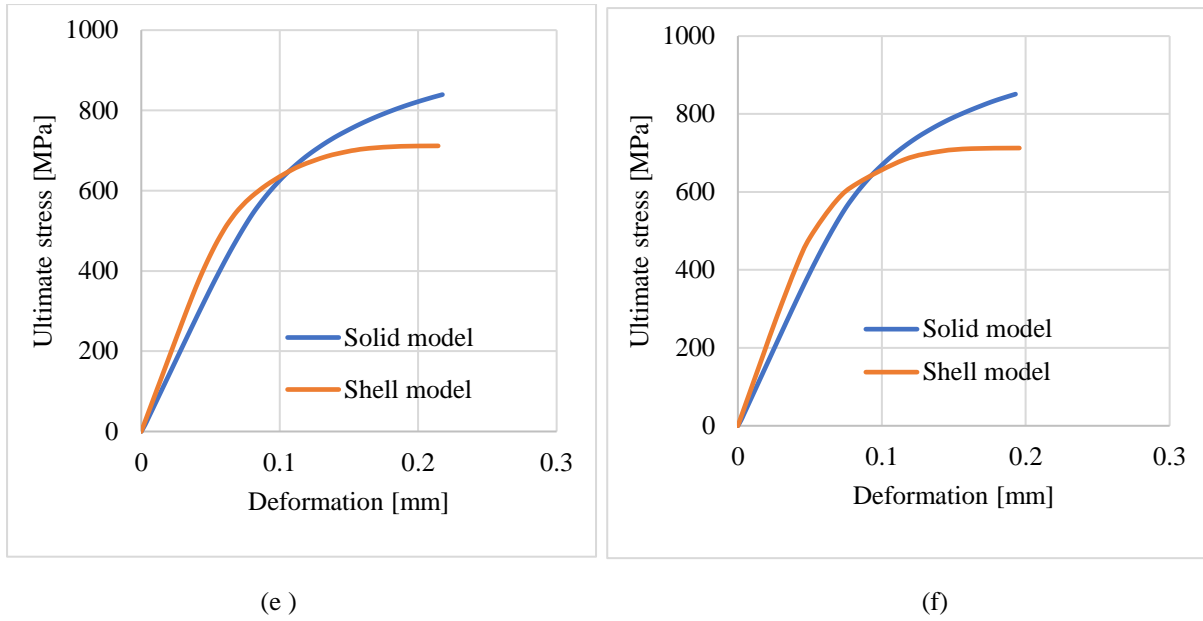


Fig. 55. Strength-deformation diagram of transverse fillet lap-welded connections; (a) TS-1, (b) TS-2, (c) TS-3, (d) TS-4, (e) TS-5, and (f) TS-6.

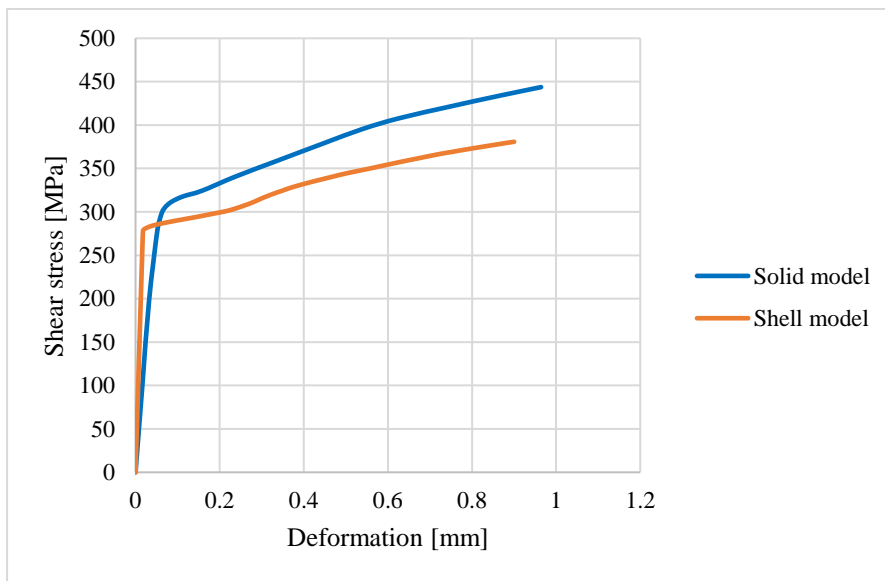


Fig. 56. Strength-deformation diagram of longitudinal fillet lap-welded connections.

Table 36 Comparison on deformation capacity between volume and shell finite element model.

Specimen	Volume model	Shell model	Volume/Shell
	[mm]	[mm]	[-]
TS -1	0.224	0.232	0.97
TS -2	0.195	0.195	1.00
TS -3	0.203	0.207	0.98
TS -4	0.198	0.196	1.01
TS -5	0.218	0.214	1.02
TS -6	0.193	0.195	0.99
L100	0.960	0.900	1.06

6.3.5 Verification of shell with analytical model

Figures 57 and 58 show that the results of analytical models show conservative with respect to the shell element model in both welded configurations.

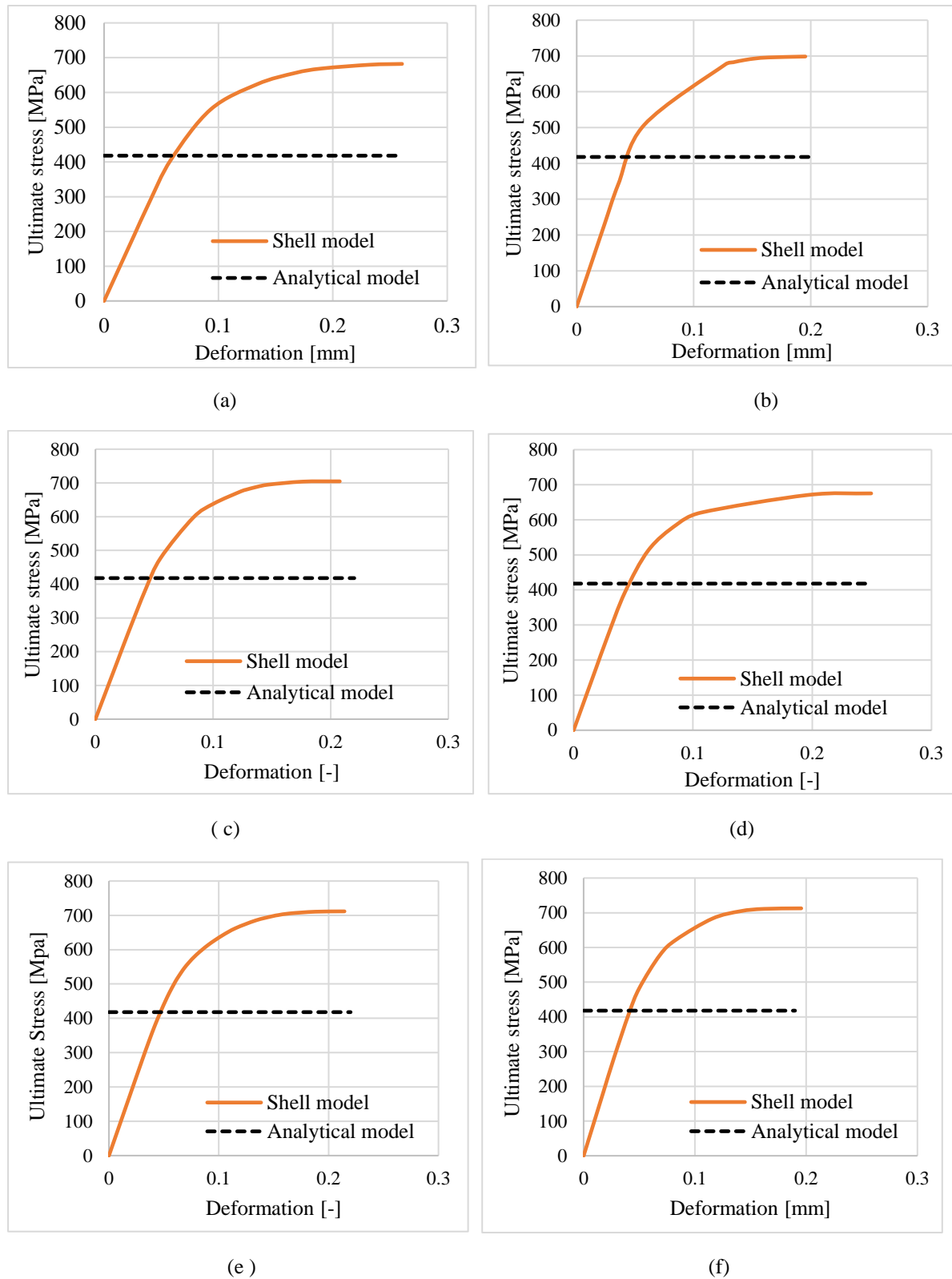


Fig. 57. Strength-deformation diagram of transverse fillet lap-welded connections: verification with analytical model.

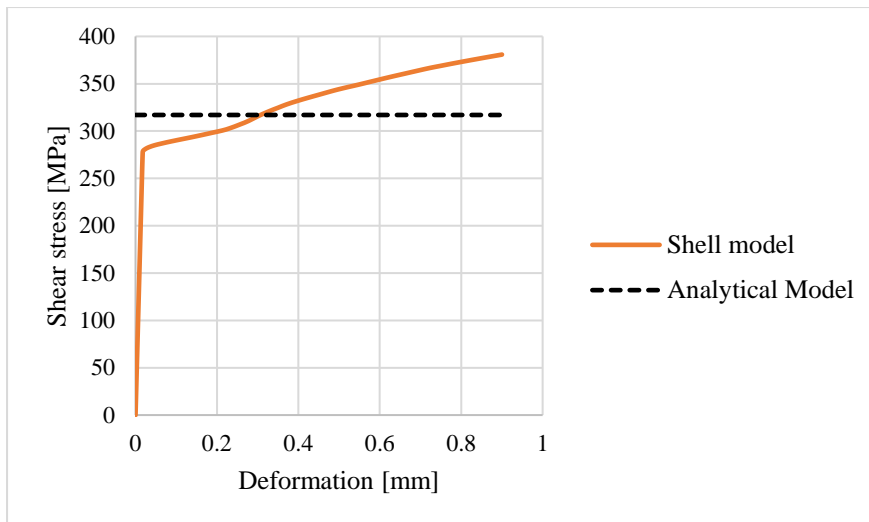


Fig. 58. Strength-deformation diagram of longitudinal fillet lap-welded connections: verification with analytical model.

CHAPTER 7: NUMERICAL DESIGN CALCULATION

Numerical models composed of finite shell elements are used to assess the strength of a structure or component during static design checks [56] in the numerical design calculation (NDC). This chapter focuses on creating models of fillet welded connections using common inclined shell elements, known as regular inclined shell element models (RISEM), to analyze their direct weld resistances. This section outlines the design approach for proposing a new strength criterion for transverse and longitudinal fillet lap-welded connections made from high-strength steel (HSS) welds.

7.1 Strength criterion of fillet welded connection

This section describes the development of a novel method for determining the load-carrying capacity of transverse and longitudinal lap-welded connections. RISEM determines the resistance of fillet welds by considering the equivalent stresses on the inclined shell element. These stresses are obtained from FE shell models in two different approaches: maximum equivalent stress method and stress integration method. Fig. 59 represents the inclined surface from the mid of the shear and tension leg of the weld and the corresponding stresses acting on the inclined surface with its inclination angle θ .

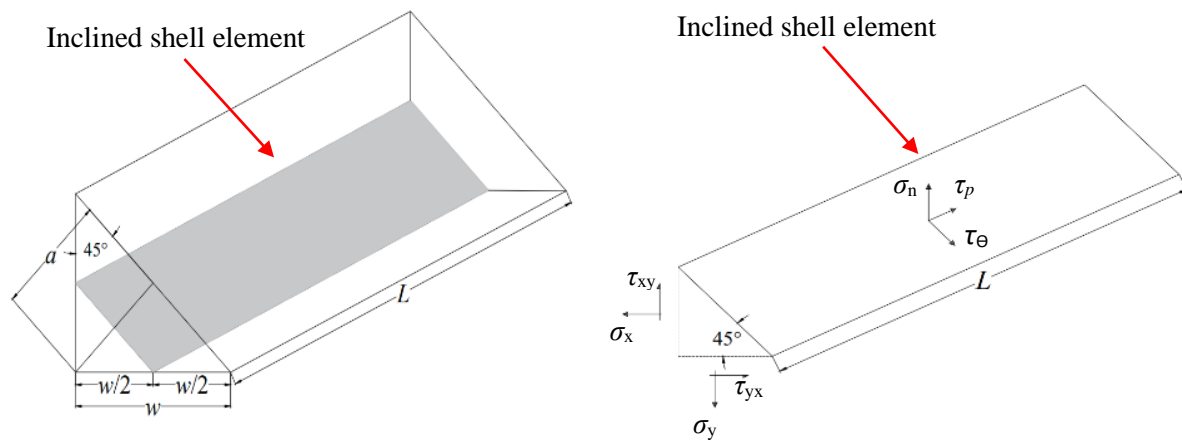


Fig. 59. Stresses acting on the inclined surface of the weld.

7.1.1 Maximum equivalent stress method

In this method, the maximum stresses acting on the inclined shell element are considered during the calculation of equivalent stress. The general principle of plane stress transformation equations in the inclined surface is applied to evaluate the equivalent stress [58] [59]. The theory of transformation of plane stress has been developed for a long time and is well explained in many material and mechanic textbooks [60]–[62]. The transformation equations determine the stress components acting on an inclined plane. These equations also find the plane's maximum and minimum stress values.

When the force is perpendicular to the weld direction, the maximum resultant equivalent stress is determined by calculating the resultant of normal and shear stress that acts on the inclined shell element using the following function.

$$\sigma_{\text{eqv,max}_T} = \sqrt{\sigma_n^2 + \tau_\theta^2} \quad (6.1)$$

Where $\sigma_{eqv,max,T}$ is the maximum resultant equivalent stress acting on inclined shell element in FE shell model when a line of action of the force is perpendicular to the weld direction, σ_n is the normal stress acting on inclined shell element, τ_θ is normal shear stress acting on inclined shell element.

$$\sigma_n = \frac{\sigma_x + \sigma_y}{2} - \left(\frac{\sigma_x - \sigma_y}{2} \right) \cos 2\theta - \tau_{yx} \sin 2\theta \quad (6.2)$$

$$\tau_\theta = \left(\frac{\sigma_x - \sigma_y}{2} \right) \sin 2\theta - \tau_{yx} \cos 2\theta \quad (6.3)$$

Similarly, suppose the line of action of the force is parallel to the weld direction. In that case, maximum resultant equivalent stress is calculated with the resultant of normal and parallel shear stress acting on the inclined surface from the following function:

$$\sigma_{eqv,max,L} = \sqrt{\tau_p^2 + \tau_\theta^2} \quad (6.4)$$

Where $\sigma_{eqv,max,L}$ is the maximum resultant equivalent stress acting on inclined shell element in FE shell model when a line of action of the force is parallel to the weld direction, τ_p is the shear stress acting parallel on an inclined plane, and τ_θ is the normal shear stress on an inclined plane.

$$\tau_p = \left(\frac{\sigma_x - \sigma_y}{2} \right) \sin 2\theta + \tau_{xy} \cos 2\theta \quad (6.5)$$

$$\tau_\theta = -\tau_{xy} \sin 2\theta \quad (6.6)$$

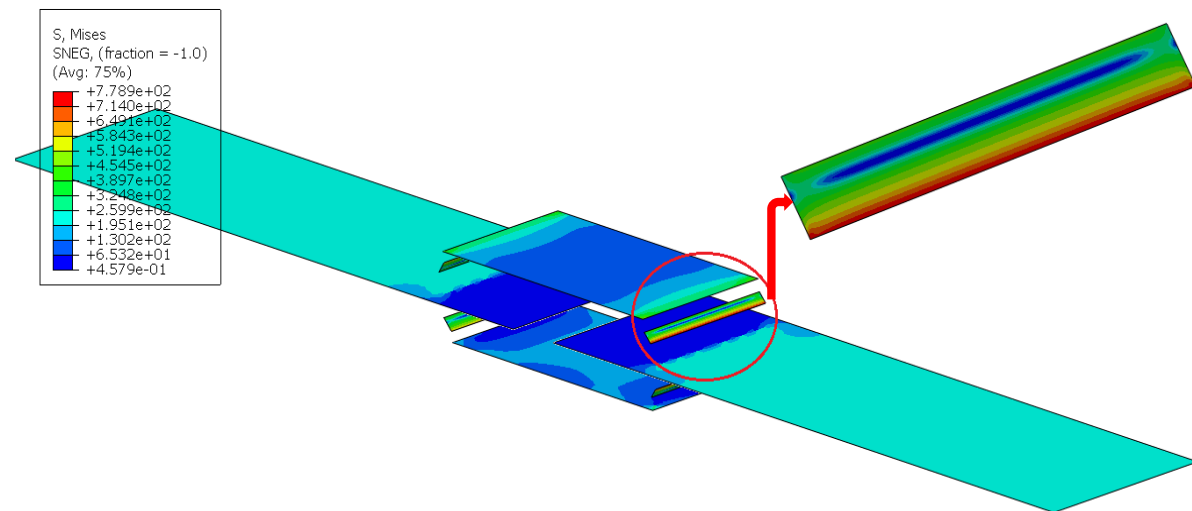


Fig. 60. Numerical model of the specimen TS-5.

All stress components σ_x , σ_y , τ_{xy} , and τ_{yx} , σ_x , σ_y , τ_{xy} , and τ_{yx} required for the normal stress, normal shear stress, and parallel shear stress on the inclined shell elements are computed from the RISEM in Abaqus (see Fig. 60). Similarly, the inclination of the inclined shell element θ is considered as per the modeling of the specimens. The values correspond to σ_x is marked as S11, σ_y as S22, $\tau_{xy} = \tau_{yx}$ as S12 in RISEM.

This work aims to develop numerical design calculations based on the principles outlined in the current analytical model of Eurocodes. The analytical model assumes uniform stress on the weld, but this method considers maximum values from the inclined shell element. Therefore, this method will not be taken into consideration further. However, this method provides good agreement results for both transverse and longitudinal welds, with an analytical model having only an 8% variance [58].

7.1.2 Stress integration method

In this method, the numerical calculation considers each stress component acting throughout the weld length. The maximum stress acting on the bottom path of an inclined shell element (see Fig.61) is considered an indicative path for the calculation. However, the stress distribution is not uniform throughout the inclined shell element, especially at the end, due to stress concentration (see Fig. 62 and 63). In order to assume a uniform stress distribution in the weld, it is necessary to calculate the average value of each stress component. There are several ways to calculate averages, and the integration procedure is considered one of the most reliable approaches. To obtain more reliable and accurate results, the length l of the inclined shell element is divided into small fragments n , and the average values of each component are calculated.

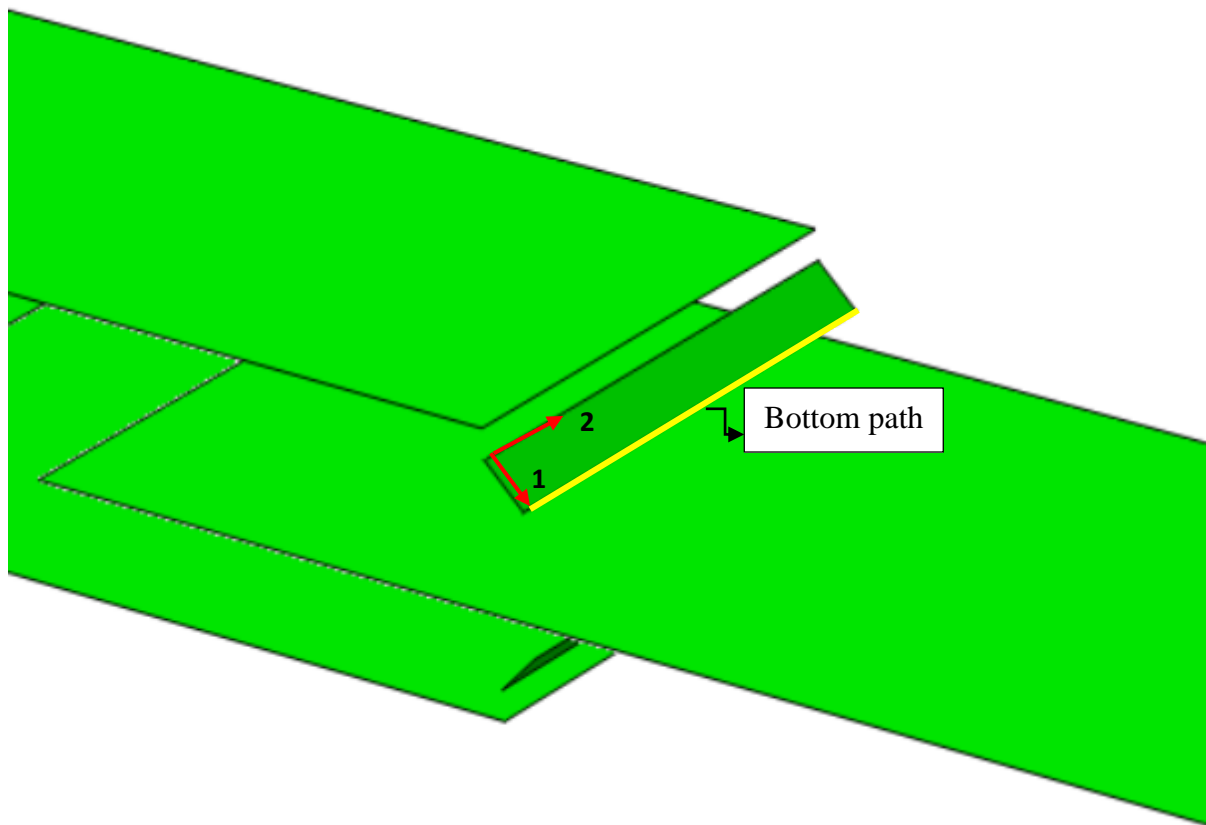


Fig. 61. Representation of stresses computation path along the length of the inclined shell element.

In the integration method if we denote the function as $f(x)$, then the integration of $f(x)$ over a given interval $[0, N]$ is represented by:

$$\int_0^N f(x) dx \quad (6.7)$$

To find the average value of $f(x)$ over the interval $[0, N]$, it is necessary to integrate $f(x)$ over the interval and then divide by the length of the interval:

$$\text{Average} = \frac{1}{N-0} \int_0^N f(x) dx \quad (6.8)$$

This mathematical equation represents the average value of the function $f(x)$ over the interval $[0, N]$.

When analyzing a two-dimensional (2D) system, the equivalent stress acting on an inclined surface can be determined using the von Mises equivalent stress formula [60]. This formula calculates an equivalent

uniform stress acting on an inclined shell element, which considers normal and shear components. if the line of action of force is perpendicular to the inclined shell element, then the equivalent uniform stress can be determined with following function:

$$\sigma_{eq_in_T} = \sqrt{\sigma_n^2 + 3\tau_\theta^2} \quad (6.9)$$

$$\sigma_n = \frac{S_{11}+S_{22}}{2} \text{ and } \tau_\theta = S_{12} \quad (6.10)$$

Similarly, if the line of action of force is parallel to the inclined shell element, then the equivalent uniform stress can be determined with following function:

$$\sigma_{eq_in_L} = \sqrt{\tau_\theta^2 + 3\tau_p^2} \quad (6.11)$$

$$\tau_p = \frac{S_{11}-S_{22}}{2} \text{ and } \tau_\theta = S_{12} \quad (6.12)$$

Let us consider an example of a TS-5 specimen to explain the concept better. Calculating the equivalent uniform stress acting on the inclined shell element's bottom path requires integrating the inclined shell element's length with an interval of 0.5 mm over a length of 40 mm. This integration will give us the average stresses acting on it, which can be determined for each component and presented in Fig.62.

$$\sum \sigma_{int.} = \frac{1}{l-0} * \int_0^l f(x)dx = \frac{1}{80-0} * \int[0, l] * f(x)dx$$

$$\sum \sigma_{int.} = \frac{1}{80} * \left[\frac{f(0)+f(80)}{2} + \sum [f(x_i)] \text{ for } i \text{ from } 1 \text{ to } 79 \right]$$

Once we have calculated the average stress components, we can use the following formula to compute the equivalent uniform stress acting in the inclined shell element.

$$\sigma_{eq_in_T} = \sqrt{\sigma_n^2 + 3\tau_\theta^2} = 671.74 \text{ MPa}$$

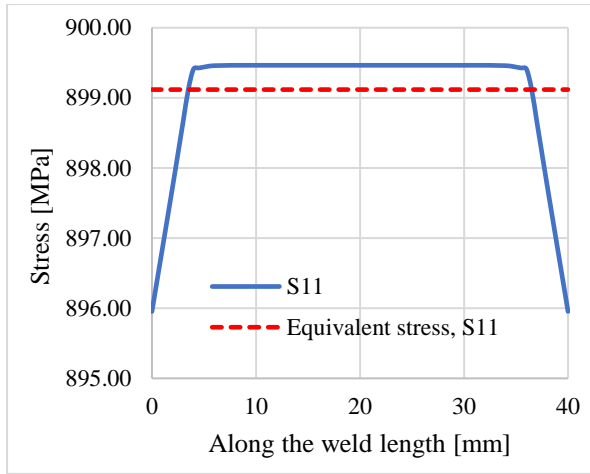
In order to ensure that the bottom path of the inclined shell element experiences uniform stress, the same principle was applied to the longitudinal fillet lap-welded connection. We integrated the length of the inclined shell element using a 1 mm interval over a length of 100 mm. This allowed us to calculate the average stresses acting on each component, which we presented in Fig. 63.

$$\sum \sigma_{int.} = \frac{1}{l-0} * \int_0^l f(x)dx = \frac{1}{100-0} * \int[0, l] * f(x)dx$$

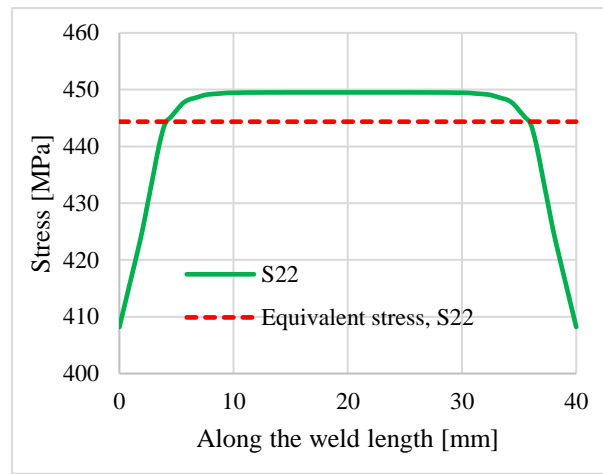
$$\sum \sigma_{int.} = \frac{1}{100} * \left[\frac{f(0)+f(100)}{2} + \sum [f(x_i)] \text{ for } i \text{ from } 1 \text{ to } 99 \right]$$

Using these integrated average stress components, we then calculated the equivalent uniform stress acting in the inclined shell element using a following function.

$$\sigma_{eq_in_L} = \sqrt{\tau_\theta^2 + 3\tau_p^2} = 314 \text{ MPa}$$



(a)



(b)

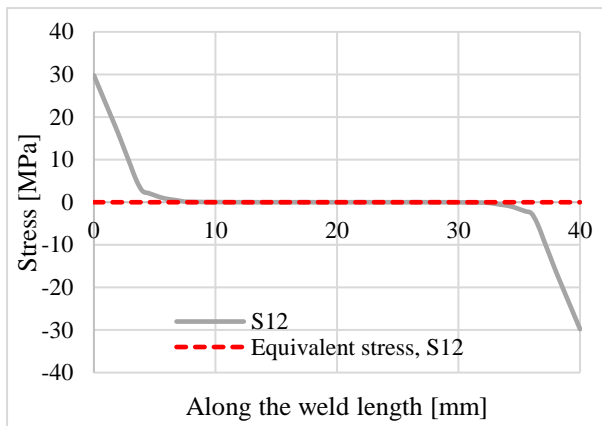


Fig. 62. Representation of converted equivalent uniform stresses along the length of the inclined shell element (transverse welded connection – TS5).

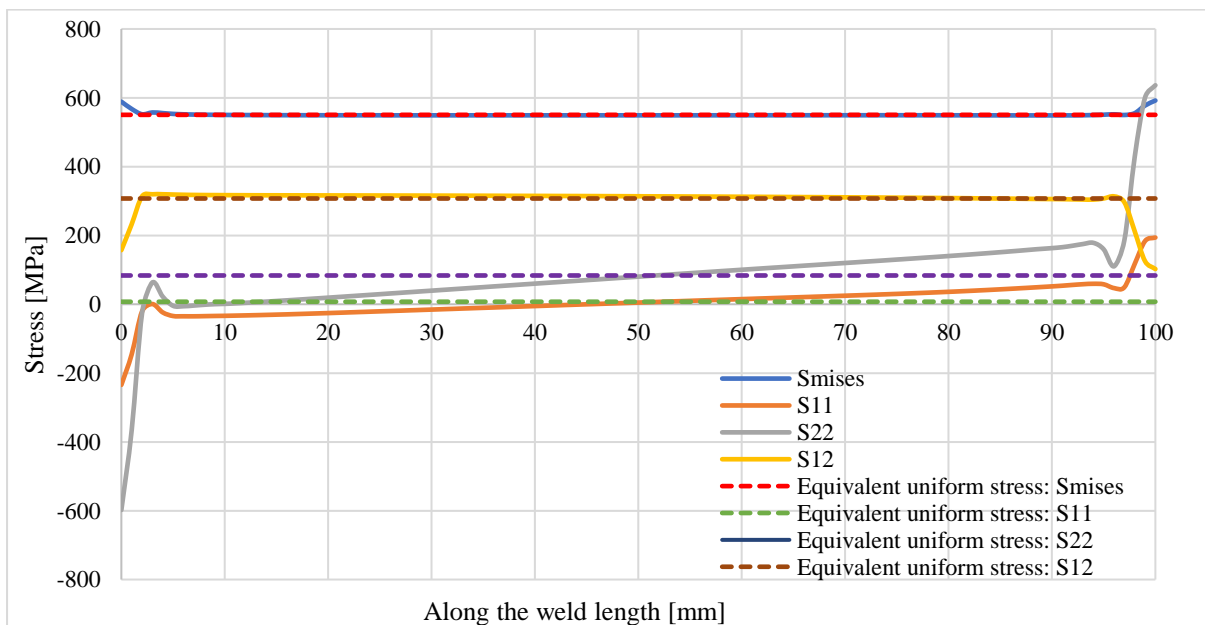


Fig. 63. Representation of converted equivalent uniform stresses along the length of the inclined shell element (longitudinal welded connection).

7.2 Results

Fig. 64 shows the typical numerical model of specimen TS-5. The equivalent uniform stresses acting on inclined shell elements evaluated with equations 6.9 (see section 7.1.2) are considered and limited as the maximum uniform stresses of the weld in RISEM (see Table 37). The RISEM stresses are verified against the weld stresses calculated by the European standards' analytical model (AM) [27]. The effective area of the weld is considered to calculate the weld resistance in both methods.

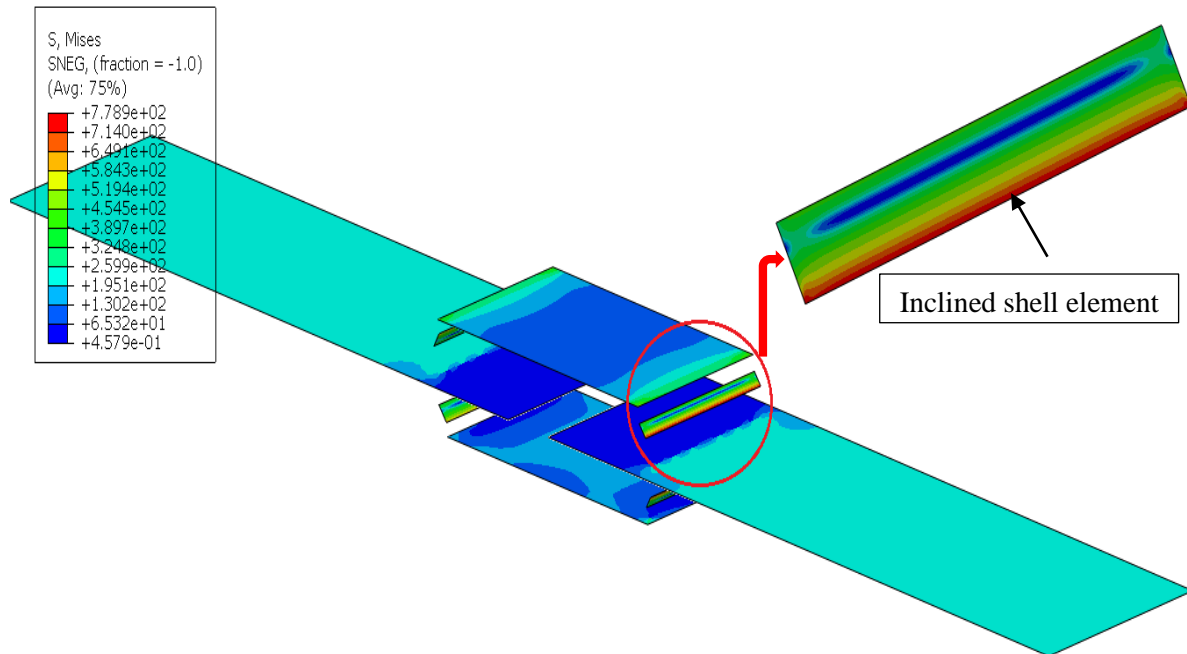
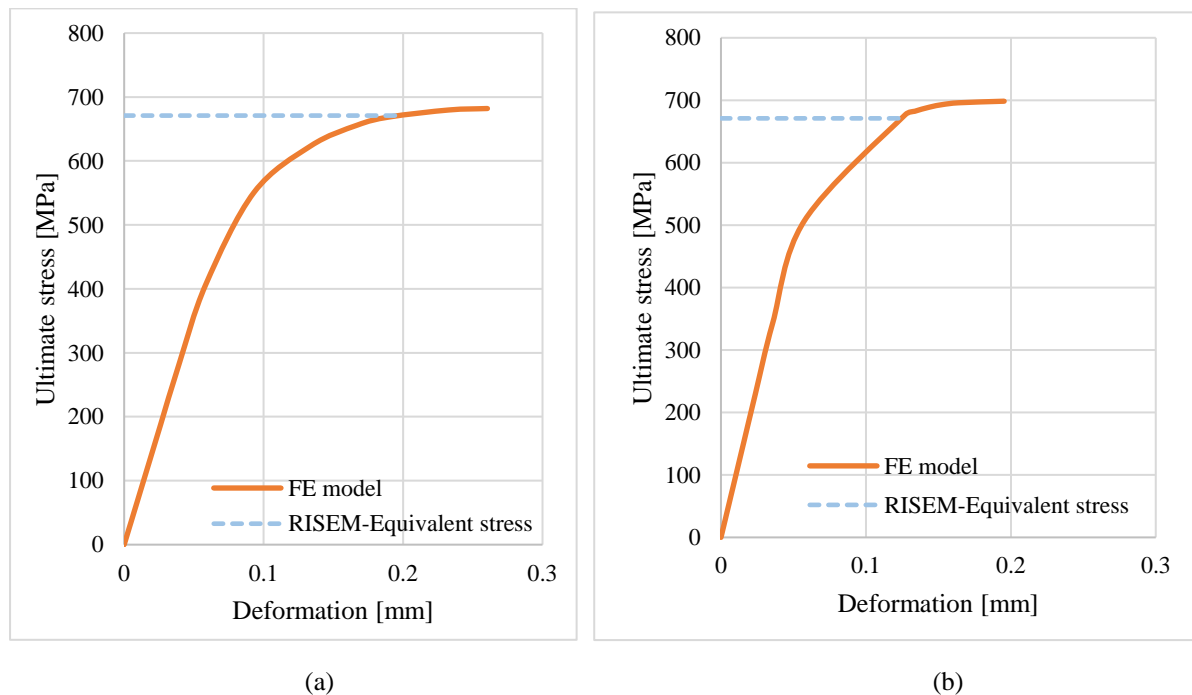


Fig. 64. Numerical model of the specimen TS-5.



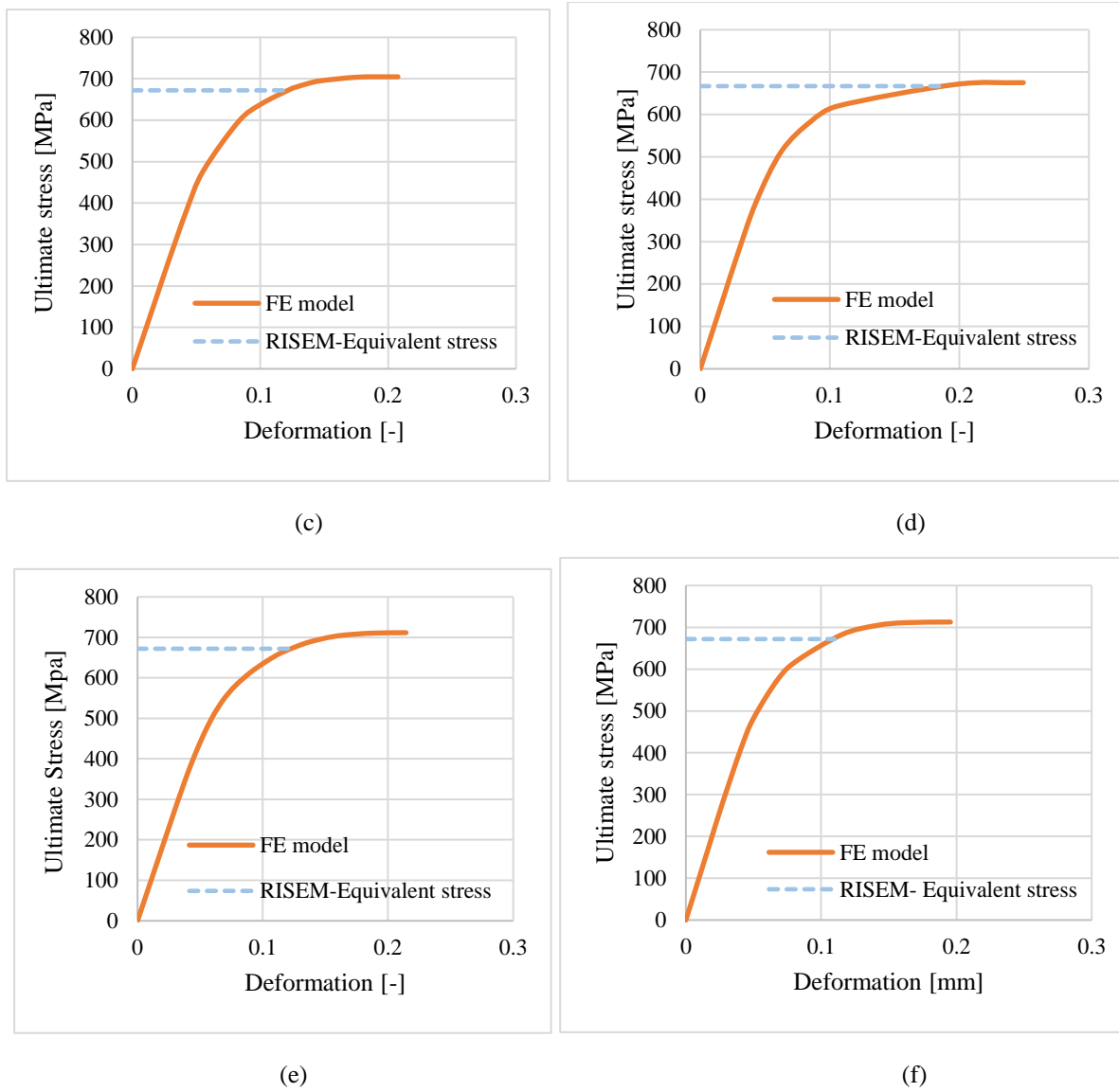


Fig. 65. Force-strain diagram of transverse fillet lap-welded connections; (a) TS-1, (b) TS-2, (c) TS-3, (d) TS-4, (e) TS-5, and (f) TS-6.

Table 37 Summary of equivalent stress and resistance of RISEM.

Specimen	Normal stress (σ_n)	Normal shear stress (τ_θ)	Equivalent stress ($\sigma_{eq_in_T}$)	RISEM resistance (R_{RISEM})
	[MPa]	[MPa]	[MPa]	[kN]
TS-1	671	0	671	260
TS-2	671	0	671	191
TS-3	672	0	672	192
TS-4	667	0	667	203
TS-5	672	0	672	227
TS-6	672	0	672	195

CHAPTER 8: VALIDATION AND VERIFICATION

This section presents a comparative analysis of experimental results, analytical models (AM), and numerical results from the regular inclined shell element model (RISEM) based on stress integration method. The verification and validation procedure is based on the principles proposed by Wald et al. [63]. Validation compares the analytical and numerical solution with the experimental data, whereas verification compares computational solutions with highly accurate (analytical or numerical) verification solutions.

8.1 Validation of numerical calculations

This study compares the strength of transverse and longitudinal fillet lap-welded connection on various weld legs by evaluating the strength based on the theoretical weld area of the weld, see Fig. 66. Table 38 summarizes the comparative results and shows that the calculated strength from RISEM and the actual strength from the test agreed well. In all cases, the test to-RISEM ratios were equal to or greater than 1.0, ranging from 1.10 to 1.35, with a mean value of 1.26 in the case of transverse welding connection and 1.97 in the case of longitudinal welded connection.

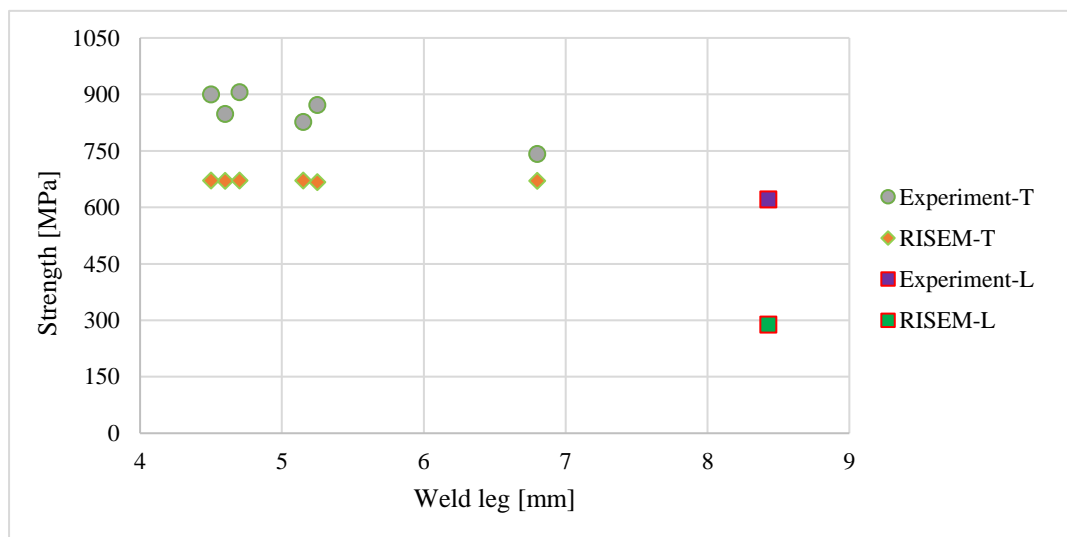


Fig. 66. Comparison the strength of welded connections with the shear leg.

Table 38 Comparison of the strength between test and RISEM results.

Specimen	Strength [kN]		Test/RISEM [-]
	RISEM	Test	
TS-1	260	287.11	1.10
TS-2	191	240.50	1.26
TS-3	192	259.00	1.35
TS-4	203	264.60	1.30
TS-5	227	279.00	1.23
TS-6	195	261.25	1.34
L-100	375	740.00	1.97

Figures 67 and 68 compare strength-deformation curves obtained from testing and numerical calculations. The trend of RISEM curves closely resembles the experimental curve for transverse and longitudinal fillet lap-welded connections. The numerical calculation also revealed that the welded connection's strength and deformation capacity landed on the curve's plastic development platform, and it is conservative with the experimental results' maximum strength and deformation capacity.

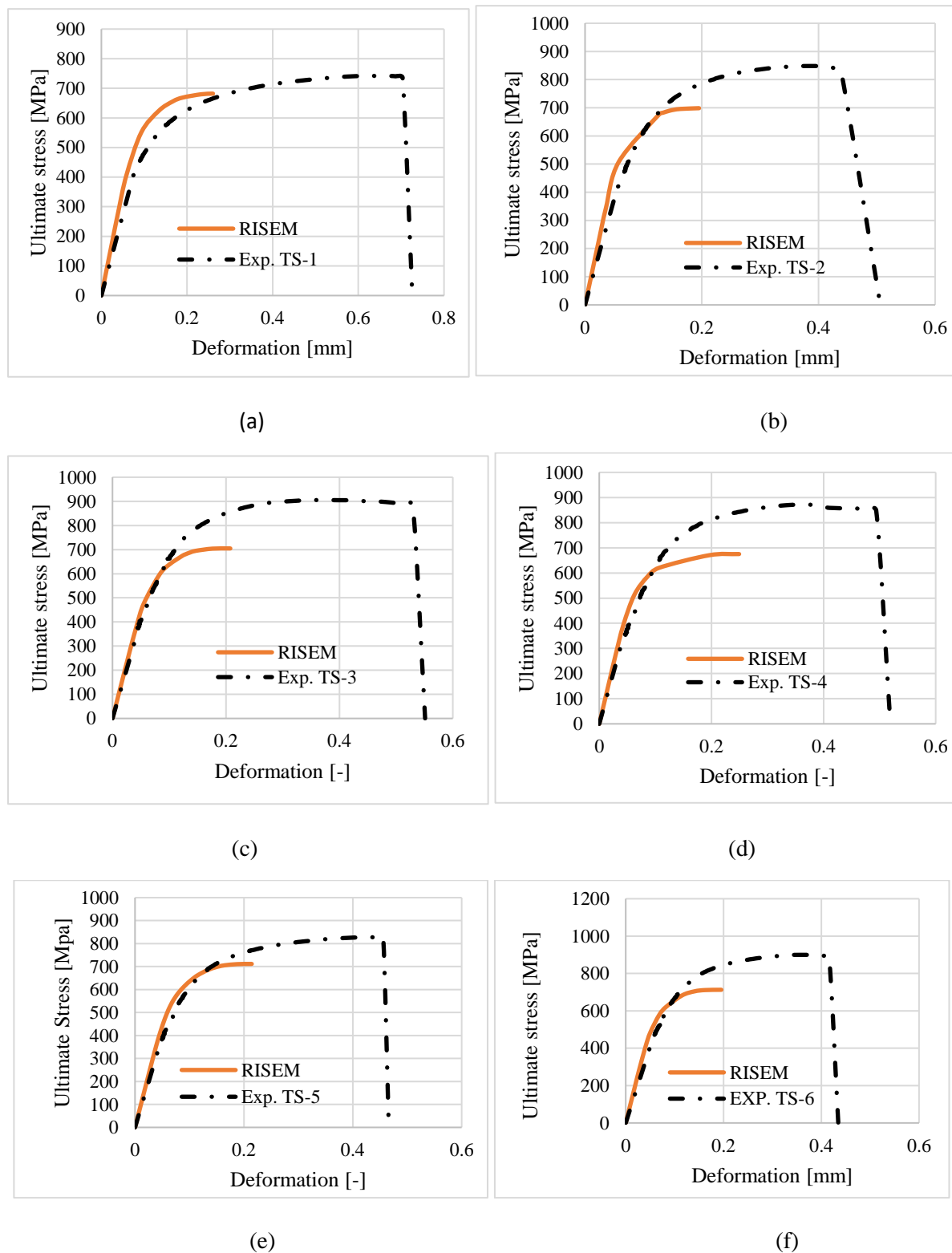


Fig. 67. Force-displacement curves of the transverse fillet lap-welded connection: (a) TS-1, (b) TS-2, (c) TS-3, (d) TS-4, (e) TS-5, and (f) TS-6.

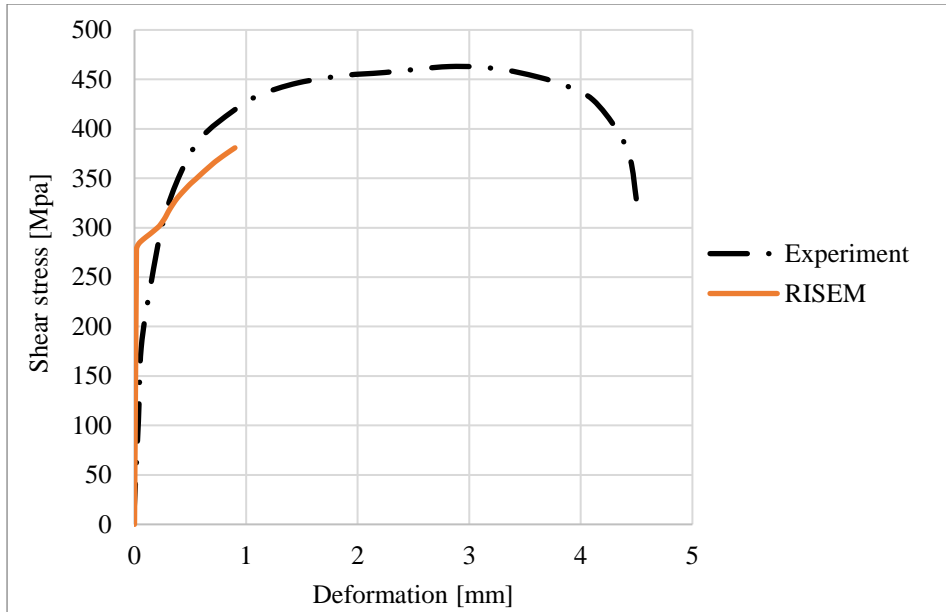
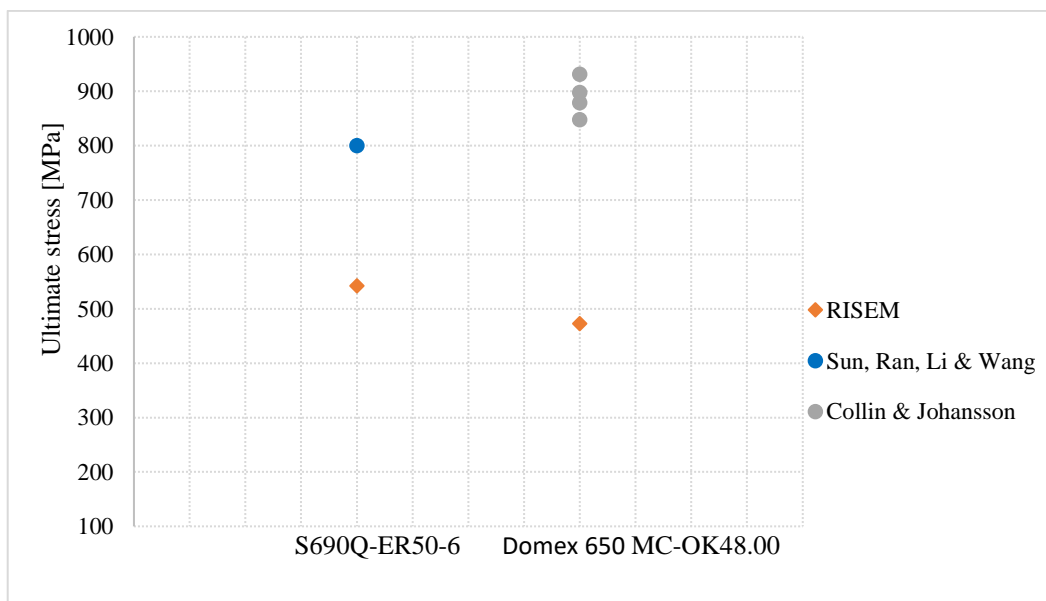


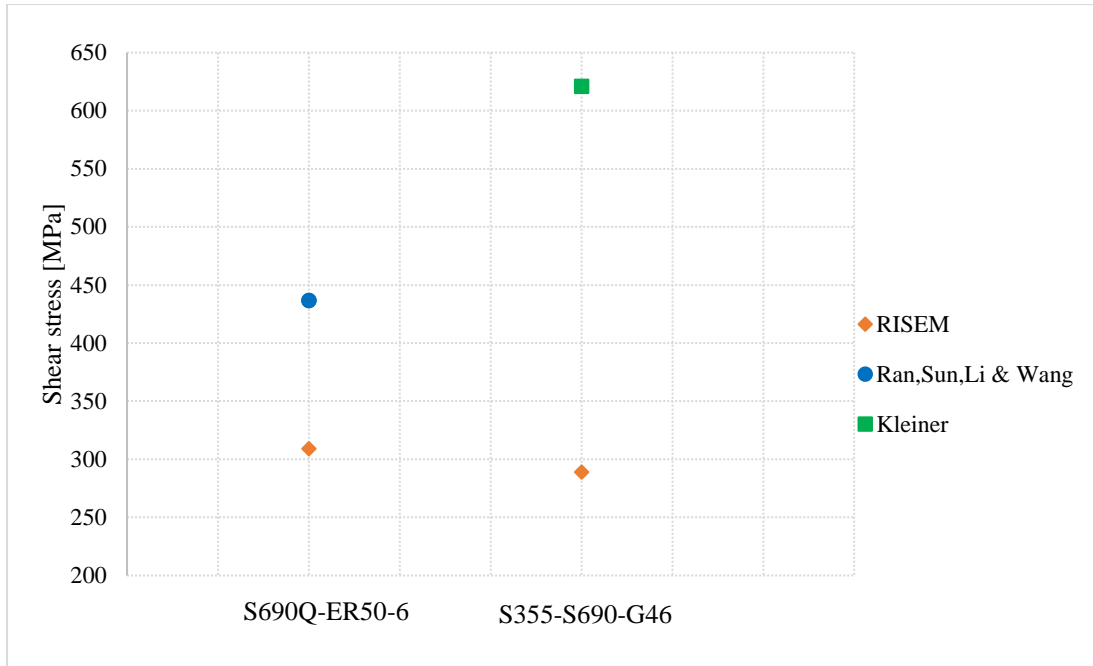
Fig. 68. Force-displacement curves of the longitudinal fillet lap-welded connection.

Moreover, the validation of the proposed RISEM is presented based on the experimental works on HSS fillet welds in the following weld configuration.

1. Transverse welds (loaded in perpendicular): Collin and Johansson [11] and Sun, Ran, Li, and Wang [37] examined the transverse fillet welded connection behavior from HSS. The experiments involved lapped splice specimens with different welding consumables. The strength of transverse fillet welds computed from RISEM is conservative in both experimental results, as shown in Fig. 69a.
2. Longitudinal welds (loaded in parallel): Kleiner [13] and Ran, Sun, Li, and Wang [38] experimented with various welding consumables on longitudinal welds. Compared to the observed behavior in both experiments, the weld model used in RISEM leads to conservative estimations in strength (see Fig. 69b) for an example with one welding electrode type from each experiment.



(a)



(b)

Fig. 69. (a) Comparison of strength from experiments and RISEM on transverse weld [11], [37], and (b) Comparison of strength from experiments and RISEM on longitudinal weld [13], [38].

8.2 Verification of numerical calculations

In this study, the resistance of the RISEM model was compared to the analytical resistance of the weld, which was calculated according to prEN1993-1-8:2020 [27]. The RISEM resistance was computed by limiting the ultimate stresses in an inclined shell element. However, since the method assumes a uniform stress distribution in the element, it may not account for the maximum values of end stresses, especially shear stress. Due to this, the shear stress tends to be negligible when integrating and taking a uniform average value, especially for transverse welded connections. Consequently, the equivalent uniform stress acting on an inclined shell element is significantly higher than the theoretical weld stress. The current analytical model is too conservative since it assumes the uniform stress distribution in the weld.

Table 39 Comparison of the weld resistance by RISEM and AM.

Specimen	Weld Resistant [kN]		RISEM/AM [%]	Remarks
	RISEM	AM		
TS-1	260	162	1.60	CTU Experiment (Transverse weld - T)
TS-2	191	119	1.61	
TS-3	192	120	1.60	
TS-4	203	127	1.60	
TS-5	227	141	1.61	
TS-6	195	121	1.61	
L-100	375	380	99	Kleiner (Longitudinal weld - L)

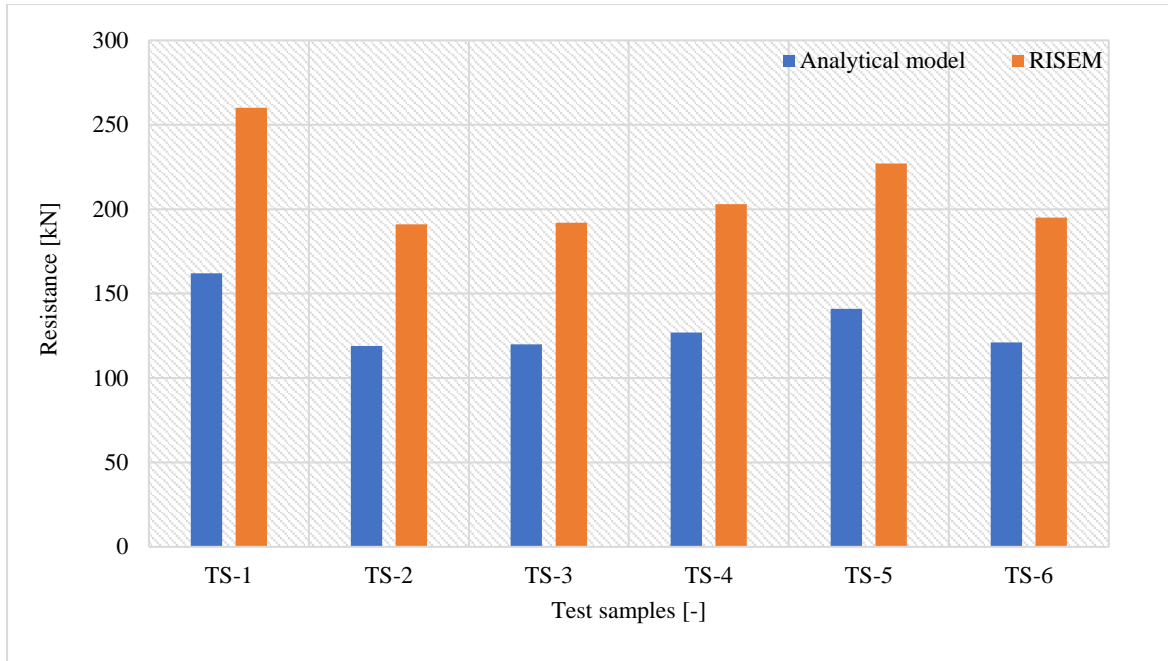


Fig. 70. Comparison of the RISEM and analytical weld resistance of transverse fillet weld-CTU experiment.

The experimental results of AM and RISEM are presented in Figure 70. According to Table 39, the RISEM resistance is 1.6 times more economical than AM resistance when using a correlation β as per design standards. However, it is essential to establish the RISEM in practice by calculating its new correlation β . Unfortunately, this study will not cover this calculation. In addition, the results for longitudinally welded connections show good agreement with AM.

8.3 Benchmark examples

An overview of the geometric configuration of benchmark examples is presented in Fig. 71, Fig. 72, and Table 40 for fillet weld connections in transverse and longitudinal fillet welds. The weld configuration T is for transverse weld and L for longitudinal weld. The changing parameter of the connection is weld length with a constant weld throat thickness of 3mm. The material properties of verification examples are taken from tensile test results of S700 MC Plus for the base and cover plate and OK AristroRod 13.12 for weld metal. The connection resistance is always governed by the weld failure mode in the analytical model.

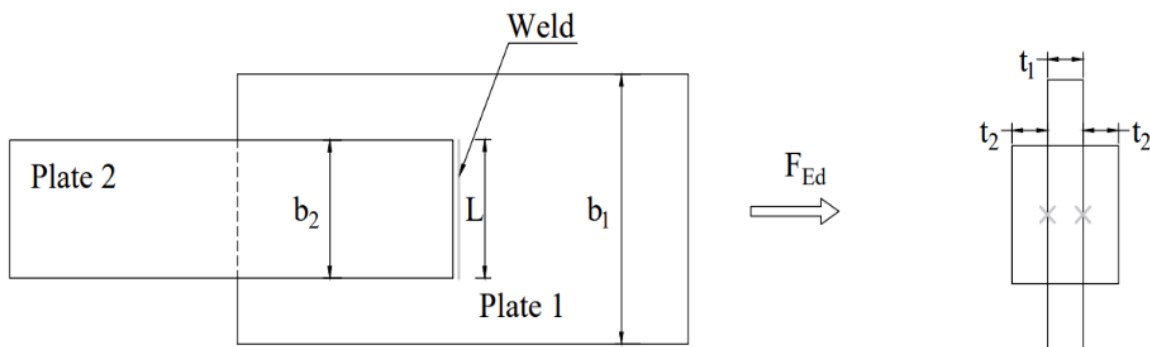


Fig. 71. Geometric configuration of fillet weld transverse weld.

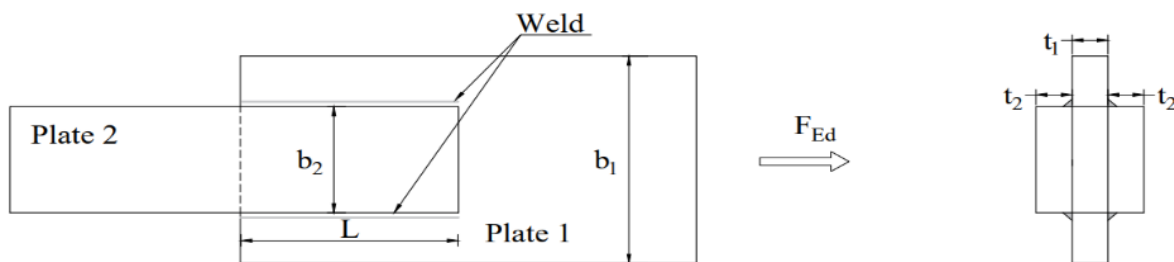


Fig. 72. Geometric configuration of fillet weld longitudinal weld.

Table 40 Overview of transverse and longitudinal fillet weld.

Examples	Weld		Plate 1		Plate 2	
	a	L	b_1	t_1	b_2	t_2
	[mm]	[mm]	[mm]	[mm]	[mm]	[mm]
T60	3	60	300	20	60	20
T120	3	120	300	20	120	20
T180	3	180	300	20	180	20
T240	3	240	300	20	240	20
T300	3	300	300	20	300	20
L 30	3	30	60	30	40	30
L 100	3	100	360	30	320	30
L 200	3	200	360	30	320	30
L 300	3	300	360	30	320	30
L 400	3	400	360	30	320	30
L 450	3	450	360	30	320	30

The design resistance of high-strength welds calculated in RISEM from the FE shell model in Abaqus is compared with the AM from European standards prEN1993-1-8:2020 [27]. RISEM gives good agreement results with AM in longitudinal fillet welded connections and higher resistance in transverse welded connections (see Table 41).

Table 41 Comparison of the design resistance of RISEM with an AM for transverse and longitudinal fillet weld.

Example/Length [mm]	Weld L/a [-]	Design Resistance		Difference
		AM [kN]	RISEM [kN]	RISEM/AM [%]
T60	20	151	242	160
T120	40	301	485	161
T180	60	452	728	161
T240	80	602	971	161
T300	100	753	1213	161
L 30	10	123	120	98
L 100	33	410	428	104
L 200	67	820	904	111
L 300	100	1230	1398	114
L 400	133	1640	1907	116
L 450	150	1845	2165	117

The result shows that the most significant difference in transverse fillet welded connection is 1.6 times with analytical models (see Fig. 73). The integration interval of the weld length does not have any significant influence on the design resistance. However, in longitudinal welded connections, the difference between RISEM and AM results increase with the increase of the weld length (see Table 41) and the integration interval of weld length (see Fig. 74). Figure 75 depicts the sensitivity study on weld length corresponds to design resistance of longitudinal welded connections.

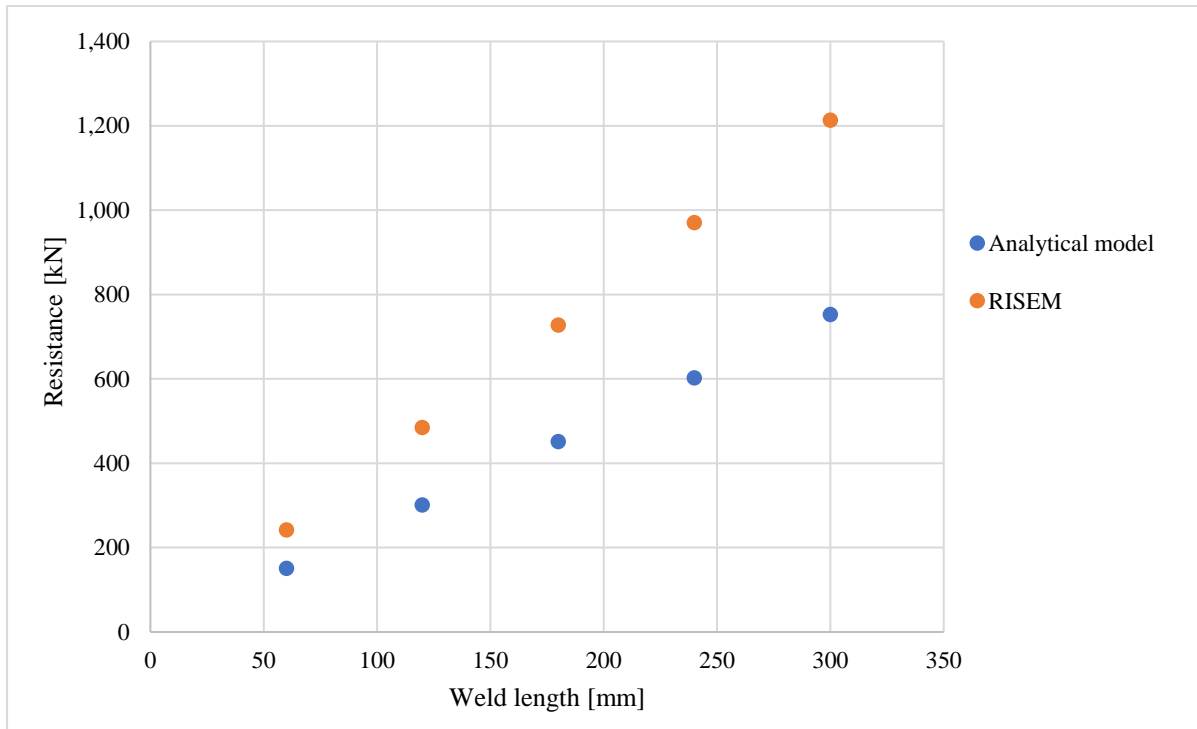


Fig. 73. Sensitivity study on weld length for transverse welded connection.

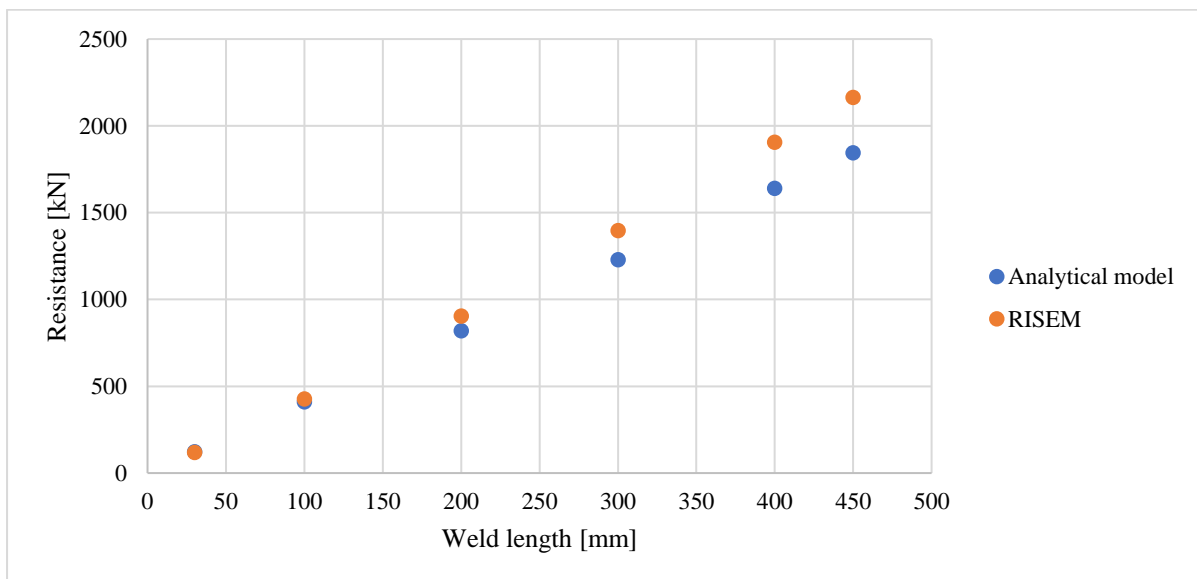


Fig. 74. Sensitivity study on weld length for longitudinal welded connection.

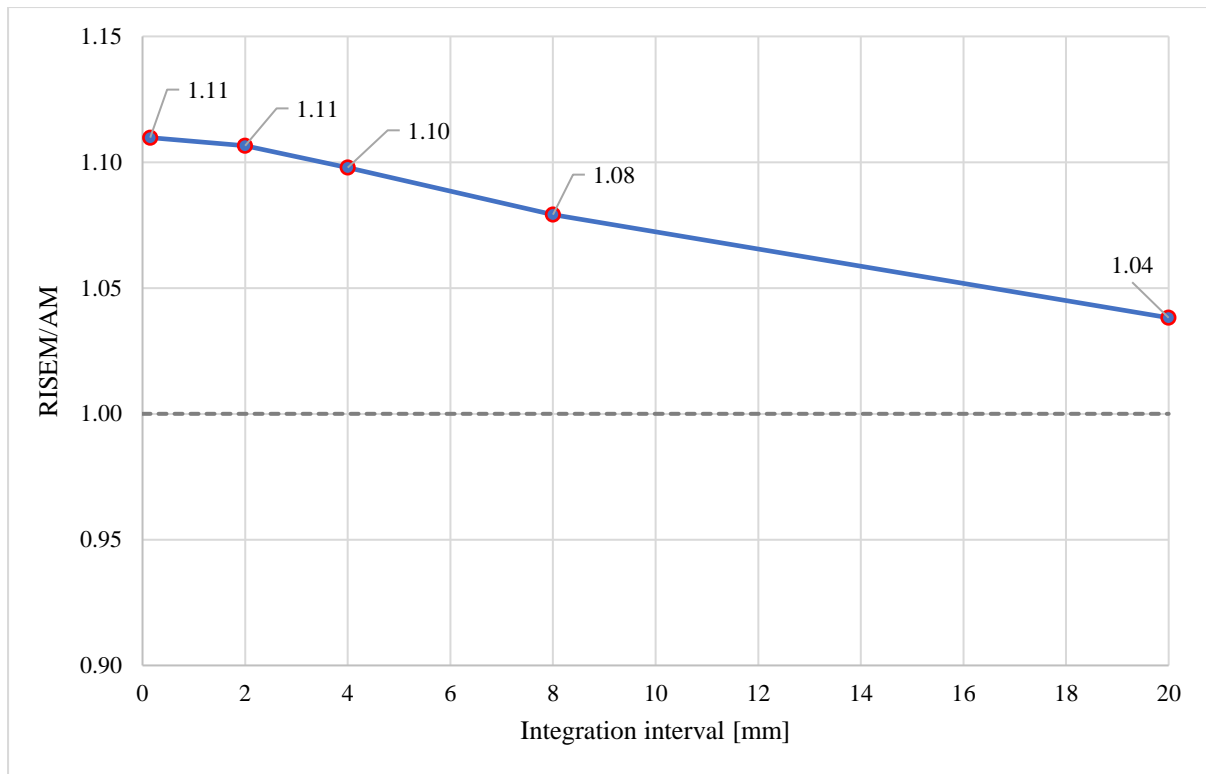


Fig. 75. Influence on the ratio of two calculation approach for longitudinal welded resistance over the integration interval of the weld length.

CHAPTER 9: PLASTIC STRAIN

9.1 General

This study aims to assist designers in selecting the appropriate steel grade by predicting the minimum required ductility of the material that guarantees the safe performance of welded connections subjected to tensile loading fabricated through high-strength steel (HSS). Choosing the suitable steel grade is crucial in ensuring the safe performance of structural details and predicting the loading resistance of the structure. One of the most straightforward failure criteria is limiting the principal membrane strain (at the mid-plane of the plate) in the regions subjected to tensile stresses, which is provided in Eurocodes (Annex C of EN 1993-1-5 [52] and EN1993-1-6 [64]). They rely on von Mises equivalent plastic strain or principal plastic strain.

This section examines and assesses the plastic strain limit criteria for designing welded connections from HSS through FE methods using strain (such as equivalent plastic strain) as a measure. The most challenging part is predicting the strain level at ductile failure, which depends on several factors, such as mesh size, element type selection, and stress triaxiality. Consequently, this study investigates the influence of mesh sizes on the weld resistance at different strain limit state.

9.2 Numerical model

To determine the strain limit criteria for transverse and longitudinal fillet lap-welded connections from HSS, solid and shell finite element models are being prepared and studied. Chapter 6: Finite Element Model explains the numerical model's details. This chapter will also describe and analyze the corresponding results related to the minimum elongation at failure and the purpose strain limits for each model.

9.2.1 Minimum elongation at failure

The minimum elongation at the point of failure is essential in connection design as it ensures safety. To ensure safe design, the amount of ductility required is determined by predicting a single parameter: the maximum equivalent plastic strain (PEEQ) at the critical cross-section of the tensile test [65]. Table 42 shows the maximum equivalent plastic strain of both FE models at the point of weld failure.

Table 42 Comparison of the maximum equivalent plastic strain of solid and shell model.

Specimen	Volume model	Shell model	Volume/Shell
	[-]	[-]	[-]
	ϵ_{real}	ϵ_{eff}	$\frac{\epsilon_{\text{real}}}{\epsilon_{\text{eff}}}$
TS -1	0.065	0.074	0.87
TS -2	0.065	0.062	1.06
TS -3	0.069	0.067	1.02
TS -4	0.068	0.063	1.09
TS -5	0.065	0.068	0.95
TS -6	0.063	0.065	0.96
Average	0.066	0.066	1.00
L100	0.122	0.124	0.98

Similarly, Fig. 75 illustrates the relationship between the maximum equivalent strain of the FE model and the ultimate strain of filler metal OK AristoRod 13.12. The average maximum values of both FE models are almost equal to the ultimate strain ϵ_u of filler metal, making it a suitable failure criterion. Ran et al. [38] have also made a similar statement for the longitudinally welded connection.

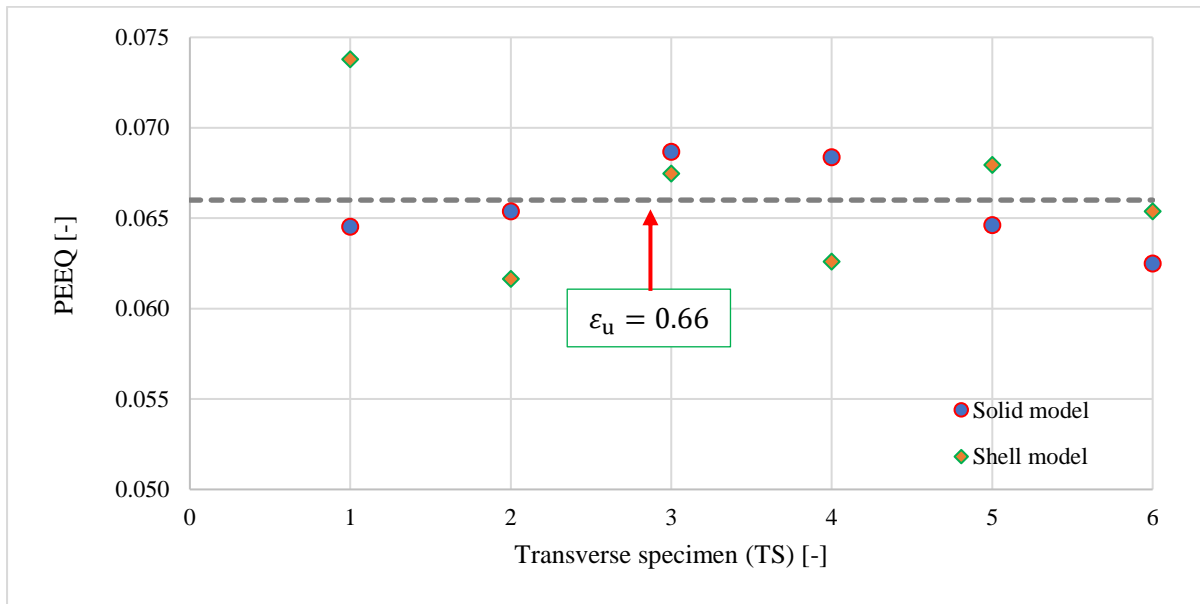


Fig. 76. Comparison of the maximum equivalent plastic strain of solid and shell model with ultimate plastic strain of OK Aristorod 13.12.

9.2.2 Evaluation the purposed strain limits

Experimental results on 5% principal membrane strain and elongation at failure are used to evaluate two strain limit criteria. These criteria determine a safe calculation limit before the welded connection completely fails. Table 43 shows that both proposed strain limits have nearly identical results. However, the 5% strain limit criteria are preferred for verification due to their simplicity and the lack of need for further material tests. Only three basic parameters are required for the material model: E , f_y , and f_u to compute the weld's design resistance in FEM, as mentioned in Fig. 77.

Table 43 Evaluating the strain limit by comparison with experimental results.

Specimen	5% limit- Force [kN]			Elongation at failure limit- Force [kN]		
	Experiment	FEM	Exp./FEM	Experiment	FEM	Exp./FEM
TS-1	600	790	0.76	650	868	0.75
TS-2	660	773	0.85	734	815	0.90
TS-3	718	725	0.99	798	812	0.98
TS-4	718	764	0.94	787	847	0.93
TS-5	679	705	0.96	736	783	0.94
TS-6	706	706	1.00	791	791	1.00

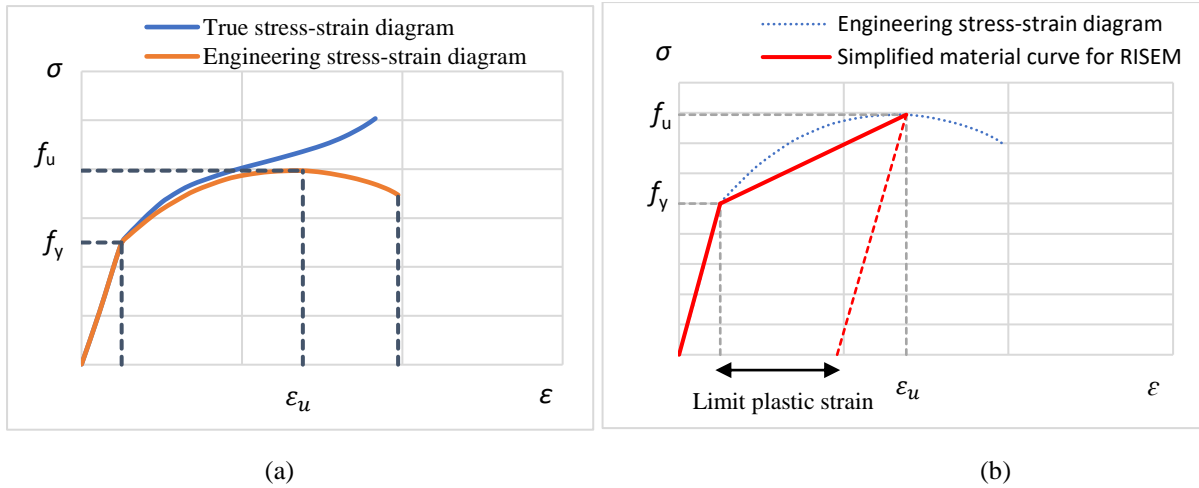


Fig. 77. Stress-strain curve of the material.

9.2.3 Verification

Material model

In RISEM, the elastic-plastic isotropic behavior and bilinear stress-strain diagram of the material is considered during analyses. Table 44 summarises the material model parameters, and Fig. 78 shows the nominal stress–plastic strain curves for each material. The Poisson’s ratio is considered 0.3 for all materials. The stress at the end of the yield plateau is represented by σ_o , whereas the ultimate load and plastic strain of the material are represented by F_u and ϵ_p^u , respectively.

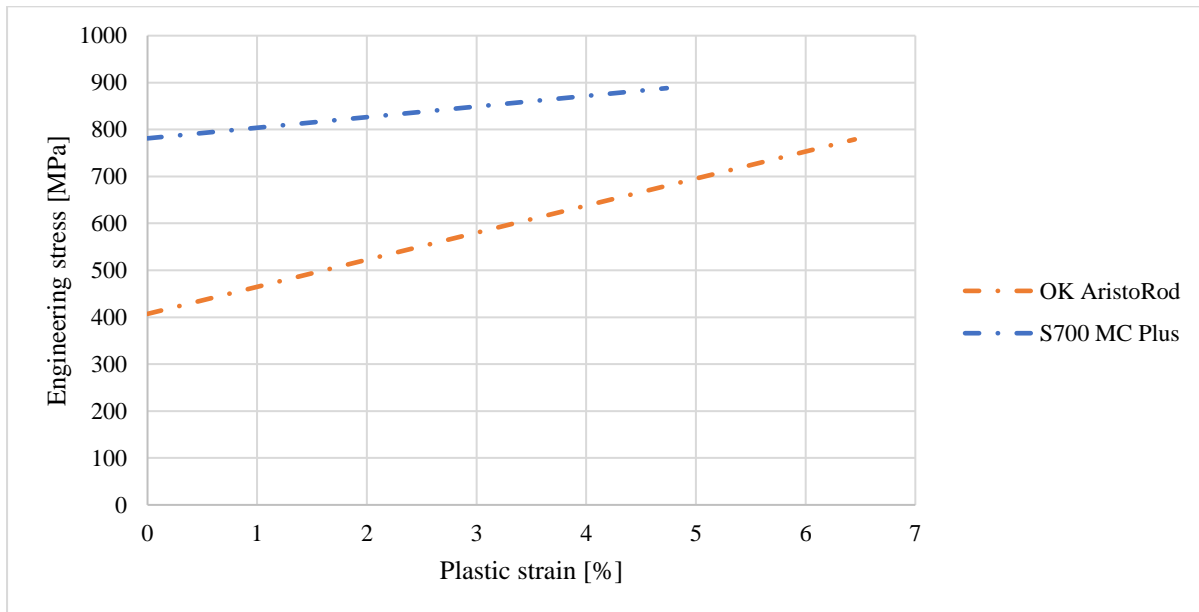


Fig. 78. Nominal stress-plastic strain curve of materials used in RISEM.

Table 44 Material parameters of the base and filler metal in finite element model.

Material	σ_o	F_u	ϵ_p^u	E
	[MPa]	[MPa]	[-]	[MPa]
Steel S700 MC Plus	781.17	888.16	0.047	215200
OK AristoRod 13.12	407.04	778.95	0.064	203523

Geometry and configuration

A transverse fillet lap-welded connection fabricated from HSS is considered to evaluate and verify the proposed strain limit for the weld resistance of welded connections. Chapter 4.2 provides a detailed explanation of the geometry and configuration of welded connections.

Mesh sensitivity study

The mesh size represents in terms of the weld's throat thickness a , which makes consistency to perform and comparison the results of all the specimens which have different throat thickness. The mesh size varies from $\frac{a}{2}$, $\frac{a}{5}$, $\frac{a}{10}$, $\frac{a}{15}$, $\frac{a}{20}$, and $\frac{a}{5.7}$, which corresponds to mesh size (MS): 1.65 mm X 1.65 mm, 0.66 mm X 0.66 mm, 0.33 mm X 0.33 mm, 0.22 mm X 0.22 mm, 0.17 mm X 0.17 mm respectively. The influence of the mesh sizes on the resistance is present in Fig. 79. The mesh size range from 0.17 mm to 0.22 mm provides more consistency results, for more accurate results comparable to the analytical results, it is advisable to utilize a mesh size of inclined shell element within the range of $\frac{a}{15}$ - $\frac{a}{20}$.

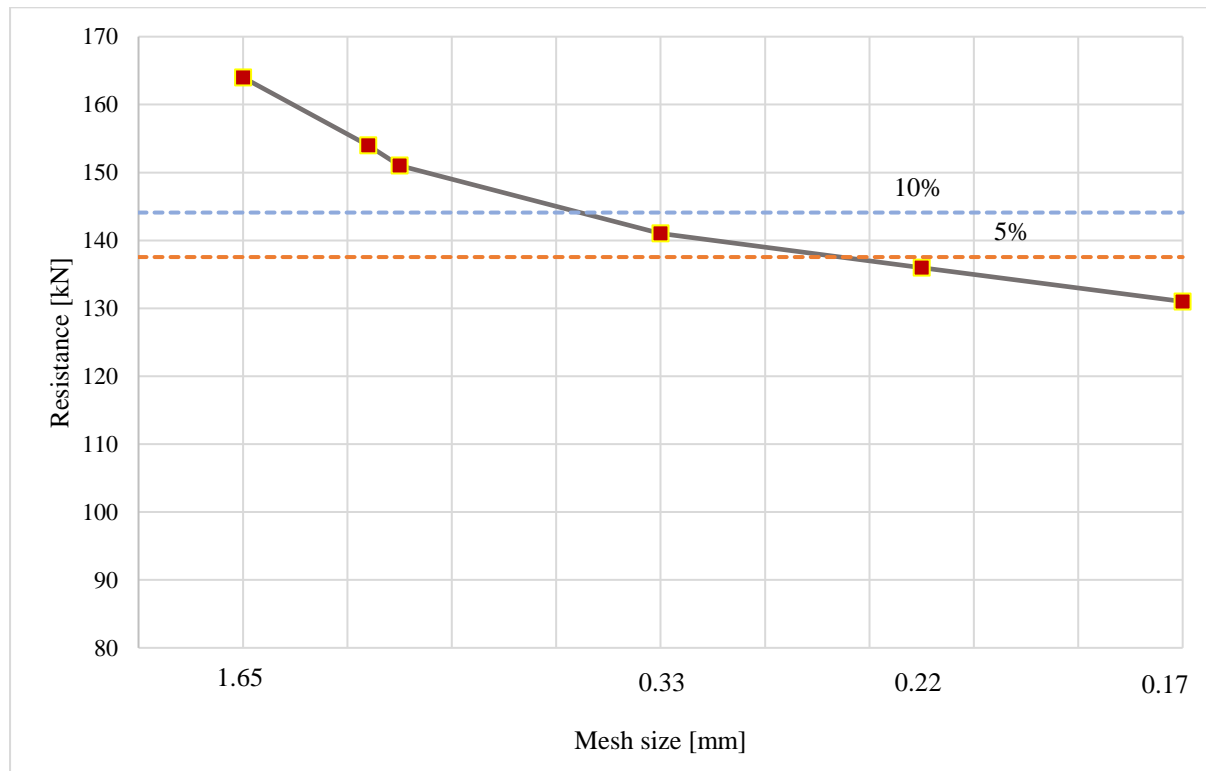


Fig. 79. Influence mesh size on resistance of welded connection.

Sensitivity on plastic limit strain

The plastic strain limit is a topic of much discussion, with Fig. 80 showcasing the effects of varying the limit. The limit for plastic strain can range from 2% to 6.4%. Despite changes in the plastic strain limit, the weld resistance only experiences a relatively small change that falls below the 8% threshold for transverse welding configurations. The 5% strain limit criteria are preferred for verification purposes due to its simplicity and the fact that there is no need for further laboratory performance of material tests. As mentioned in Fig. 77, only three basic parameters for the material model are required (E , f_y , and f_u) to compute the weld's design resistance in FEM.

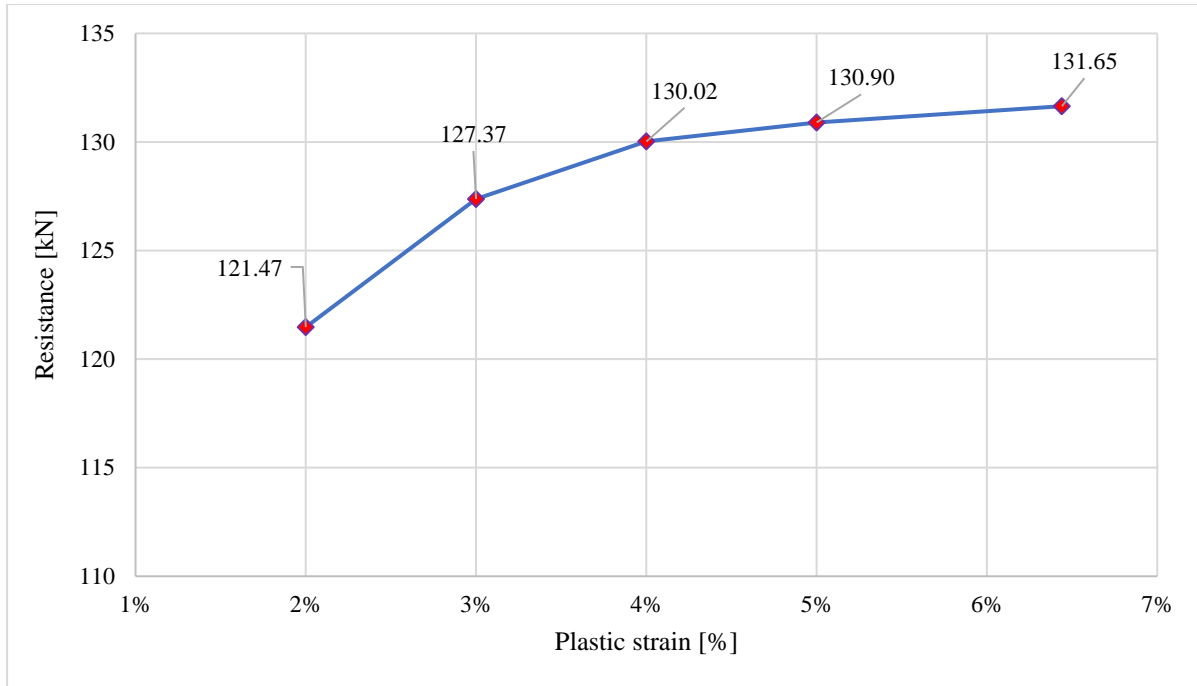


Fig. 80. Influence of the limit value of plastic strain on the weld resistance.

Verification with analytical results

After studying the effects of limiting plastic strain and mesh size of the inclined shell element, it has been concluded that the 5% plastic limit of the filler material and mesh size $\frac{a}{20}$ is appropriate for providing the necessary weld resistance compared to the AM of Eurocode. Table 45 shows the design resistance of high-strength welds calculated in RISEM from the FE shell model in Abaqus and compares it with the AM from European standards prEN1993-1-8:2020 [27]. The design weld resistance from RISEM and AM match up well, with only an 8% difference. Therefore, the proposed NDC with a 5% plastic limit strain is preferred for easy numerical analysis of HSS welds.

Table 45 Comparison of the design resistance of RISEM with an analytical model for transverse fillet weld.

Specimen [mm]	Design Resistance		Difference
	AM [kN]	RISEM [kN]	RISEM/AM [%]
TS 1	162	167	103
TS 2	119	125	105
TS 3	120	127	106
TS 4	127	129	101
TS 5	141	152	108
TS 6	121	131	108

9.3 Benchmark examples

This chapter examines the reliability of the proposed strain limit to compute the weld resistance in transverse and longitudinal fillet welded connections made from HSS. The weld length is the variable parameter for both welding configurations. The same benchmark examples are used here, which is already explained in Chapter 8.3.

The recommended mesh size $\frac{a}{20}$ considered for the transverse fillet lap-welded connection, whereas a mesh sensitivity study was performed to find the appropriate mesh size. In both welded connections, the plastic strain of the inclined shell element is limited to 5%.

Table 46 presents the design resistance of transverse fillet lap-welded connections calculated in RISEM from the FE shell model in Abaqus and compares it with the AM from European standards prEN1993-1-8:2020 [27]. The design weld resistance from RISEM and AM are in good agreement, within an 8% difference.

Table 46 Comparison of the design resistance of RISEM with an analytical model for transverse fillet weld.

Benchmark Example [mm]	Design Resistance		Difference
	AM [kN]	RISEM [kN]	RISEM/AM [%]
T60	151	162	107
T120	301	324	108
T180	452	485	107
T240	603	648	107
T300	753	808	107

A comparison is made between the outcomes of an analytical model and RISEM, along with a presentation of the sensitivity study. Fig. 81 demonstrates the impact of weld length on the ratio of design resistance (RISEM/AM) of a welded connection. The study indicates that all weld configurations are in good agreement. To demonstrate the precision of the RISEM model, a summary of the study results is presented in a diagram comparing the design resistances by RISEM and AM (refer to Fig. 82). In most cases, the difference between the two calculation methods is less than 8%.

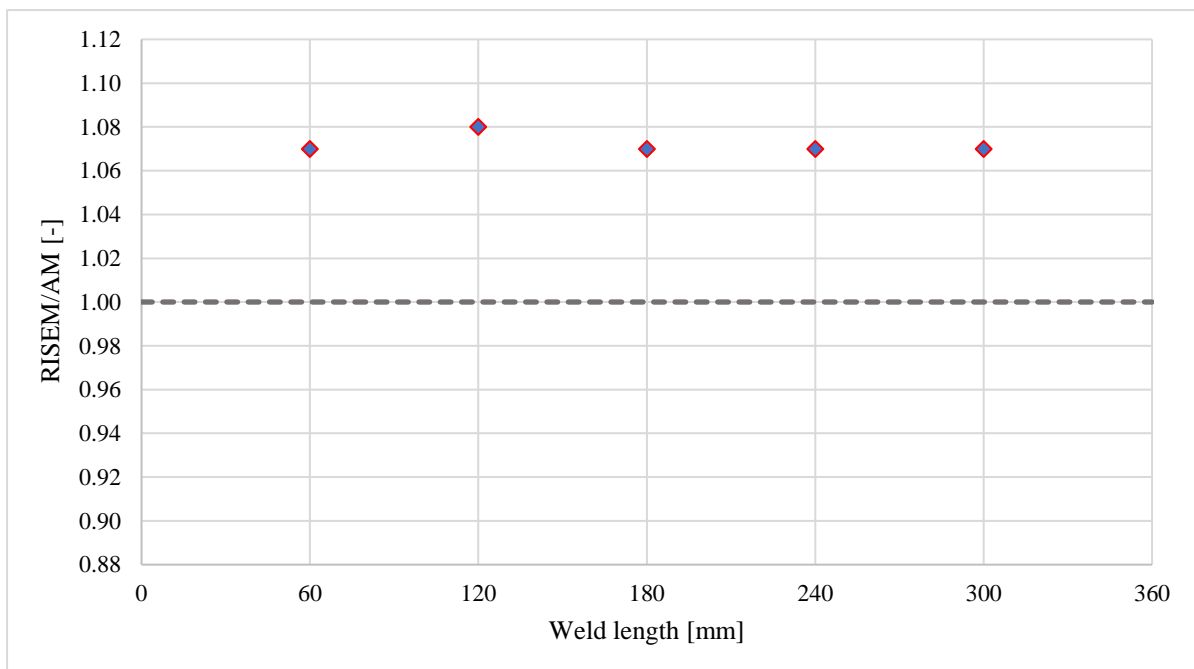


Fig. 81. Sensitivity study of weld length.

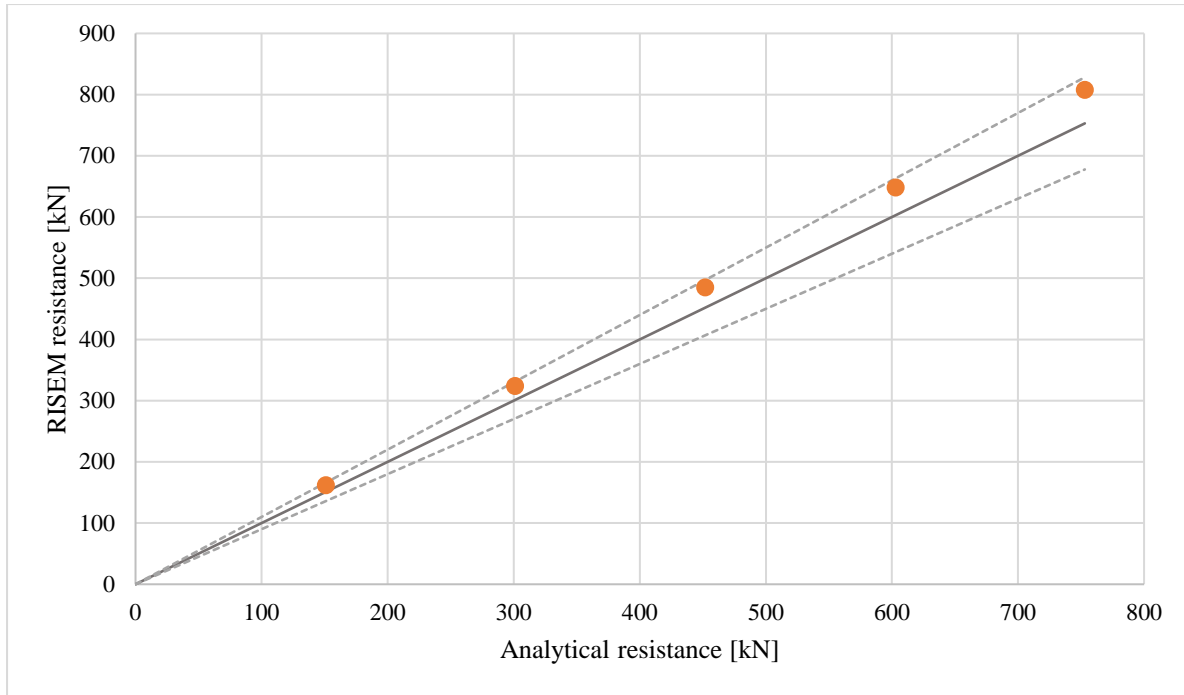


Fig. 82. Verification of RISEM to AM.

The influence of the mesh sizes on the weld resistance of longitudinal fillet lap-welded connection is present in Fig. 79. The mesh size represents in terms of the weld's throat thickness a , which makes consistency to perform and compare the results of all the specimens which have different throat thickness. The mesh size varies from $\frac{a}{2}$, $\frac{a}{5}$, $\frac{a}{6}$, $\frac{a}{7}$, $\frac{a}{7.5}$, and $\frac{a}{8}$, which corresponds to mesh size (MS): 1.5 mm X 1.5 mm, 0.6 mm X 0.6 mm, 0.5 mm X 0.5 mm, 0.43 mm X 0.43 mm, 0.40 mm X 0.40 mm, 0.375 mm X 0.375 mm respectively. The mesh size range from 0.375 mm to 0.43 mm provides more consistent results. For more accurate results comparable to the analytical results, it is advisable to utilize a mesh size of inclined shell elements within the range of $\frac{a}{7} - \frac{a}{8}$.

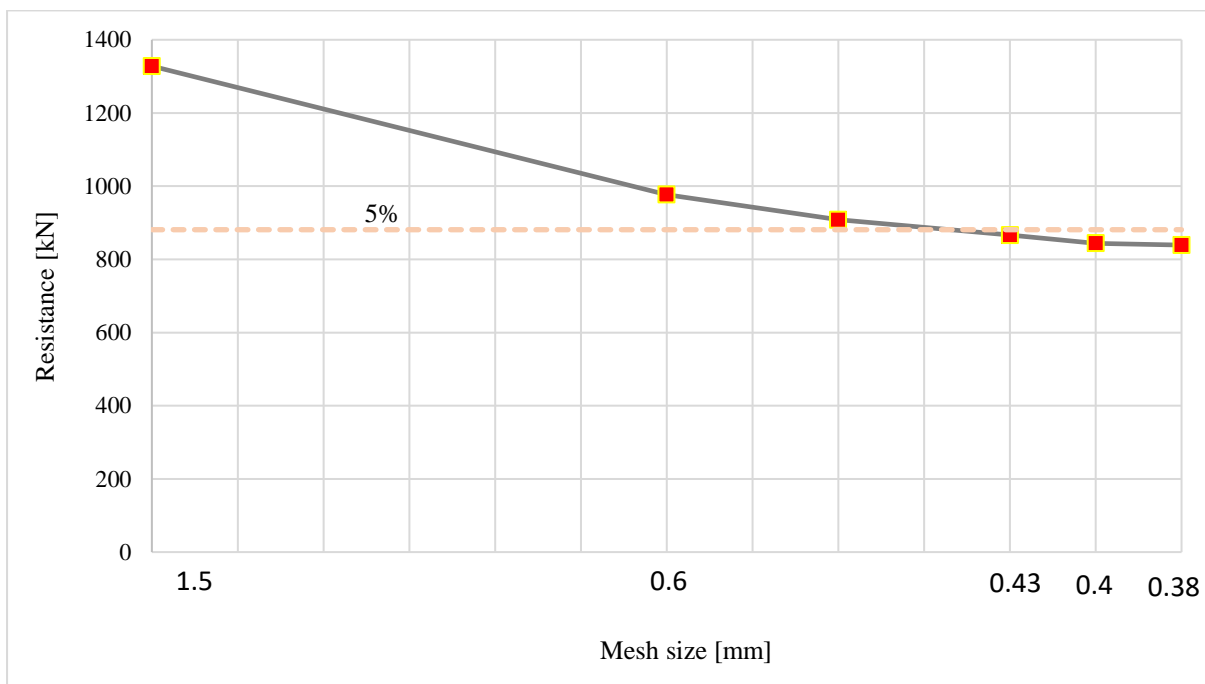


Fig. 83. Influence of mesh size on prediction of resistance of longitudinal welded connections.

Table 47 displays the design resistance of longitudinal fillet lap-welded connections, calculated in RISEM from the FE shell model in Abaqus. The table also compares the design resistance with the AM from European standards prEN1993-1-8:2020 [27]. The design weld resistance from RISEM and AM shows good agreement, with only an 11% difference.

Additionally, the study presents the results of an analytical model and RISEM, along with a sensitivity analysis. The study examines the influence of weld length on the ratio of design resistance (RISEM/AM) of a welded connection, as illustrated in Fig. 84. The study shows good agreement for all weld configurations.

Table 47 Comparison of the design resistance of RISEM with an analytical model for longitudinal fillet weld.

Benchmark Example [mm]	Design Resistance		Difference
	AM [kN]	RISEM [kN]	RISEM/AM [%]
L 30	123	112	91
L 100	410	396	97
L 200	820	866	106
L 300	1230	1349	110
L 400	1640	1819	111
L 450	1845	2027	110

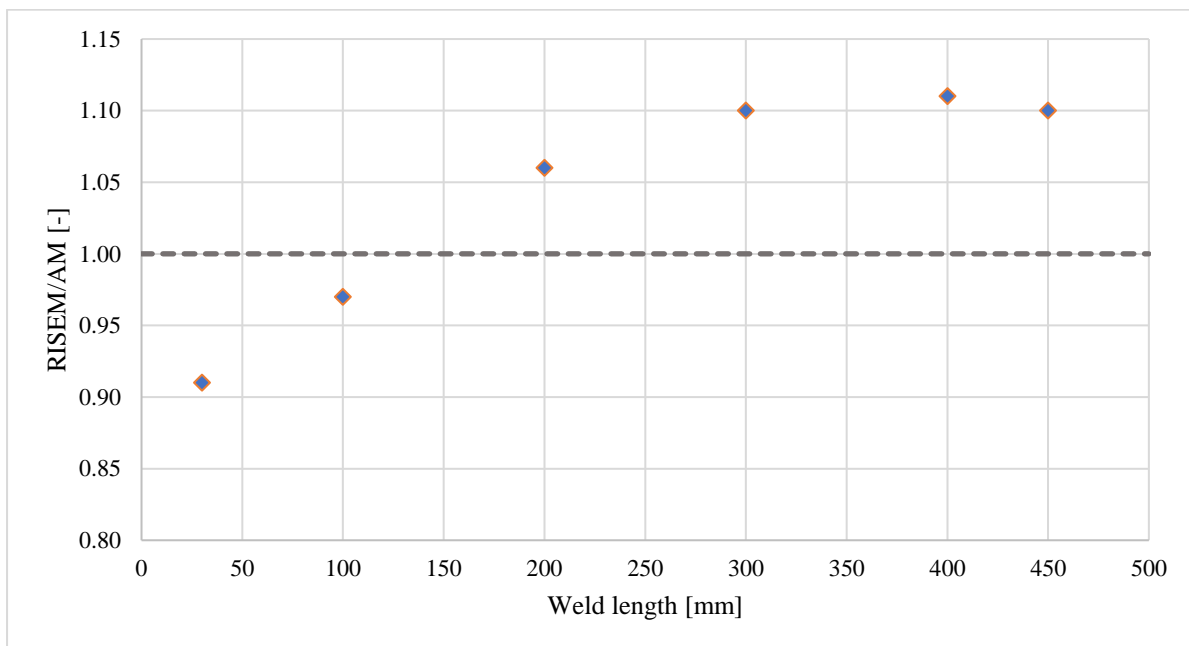


Fig. 84. Sensitivity study of weld length.

To demonstrate the accuracy of the RISEM model, the study summarizes the results in a diagram that compares design resistances by RISEM and AM (See Fig. 85). The results show that the difference between the two calculation methods is generally less than 11%.

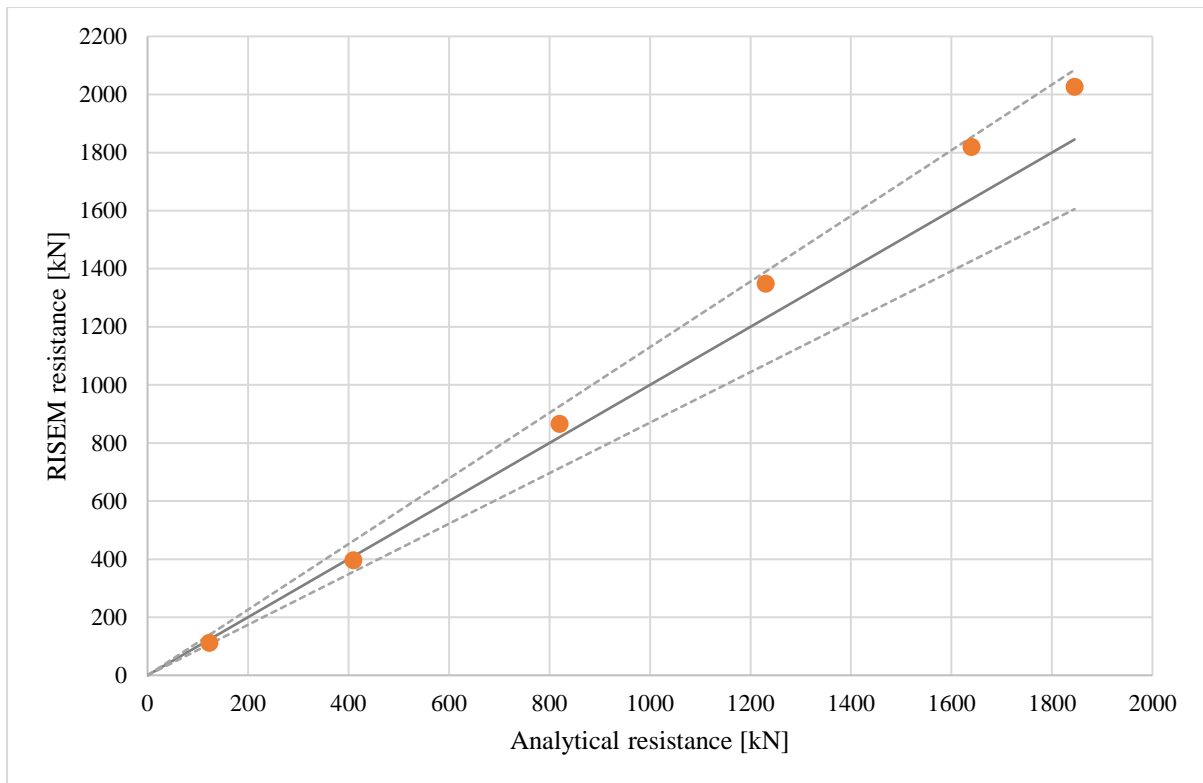


Fig. 85. Verification of RISEM to AM.

CHAPTER 10: SUMMARY AND OUTLOOK

10.1 Summary

This study investigates the resistance of fillet welds in high strength structural steels through analytical, experimental, and numerical investigations. The objective is to develop a reliable numerical design calculation (NDC) for determining the resistance of fillet welds in high-strength structural steel S700 MC Plus based on the principle of design standards. The evaluation includes analytical, experimental, and finite element model (FEM) investigations of transverse fillet welds for resistance and deformation capacity. Numerical modeling has become a valuable tool in design practice, providing reliable results on the proposed system and its components. However, there is a need for well-established methods to determine the resistance of welds in structural steels using numerical models. The objective of this study is to develop NDC of weld resistance in transverse fillet lap welded joints of high strength steels (HSS), validate, and verify the applicability of the analytical model (AM).

Chapter 2 discusses the development trends of high strength steels (HSS), their application benefits, and the welding properties of welded joints. The chapter also provides an overview of previous experimental research on HSS welds, current European and U.S. design rules for determining the strength of fillet welds, and numerical modeling techniques for welds. These explanations form the basis for the interpretation and description of the test results in the following chapters.

Chapter 4 presents an experimental study of a transverse fillet lapped HSS joint. The chapter thoroughly describes the geometry, material properties, test setup, and measurement procedure. The strength and ductility of the welded joint were analyzed. The DIC technique was used to measure the deformation by determining the relative displacement of two arbitrary points between the base plate and the top plate. The deformation of HSS transverse fillet lap welds is always less than 1 mm. In addition, the fractured area more accurately represents the strength of the weld than the effective theoretical area. The predicted strength based on EC3 and AISC is more conservative than the test strength. The expected weld strength calculated using AISC provides a better prediction value.

Chapter 5 tabulates the analytical calculation of weld resistance on each specimen based on the European standards HSS design equation. This weld resistance is essential to verify the applicability of the proposed NDC in the following chapters.

Chapter 6 presented solid and shell finite element models and validated and verified both models using appropriate mesh sizes. The shell FE model is constructed with an inclined plate, which plays a primary role in this model. Therefore, the Regular Inclined Shell Element Model (RISEM) was named for further study. The inclined shell element in RISEM represents the geometry and stiffness of the welds, which allows stress control in the plane. RISEM utilizes finite shell elements and elastic-plastic isotropic behavior of steel plates and welds to provide reliable and economical results comparable to design codes with minimal computational requirements instead of simulating real behavior.

NDC uses FEM to design connections according to standardized procedures. Chapter 7 introduces a new strength criterion based on stresses on inclined shell elements. The criterion uses the maximum uniform equivalent stress as an indicator, called the stress integration method. It is important to note, however, that the calculations do not consider residual stresses and weld shrinkage. An inclined shell element between multipoint constraints represents the geometry and stiffness of the weld. The part behaves based on the code's assumption that stresses are uniformly distributed in the weld throat. This assumption considers the thickness, location, and orientation of the weld throat. This chapter also discusses the maximum equivalent stress method, which uses maximum stress values as an indicator. However, this method does not assume a uniform stress distribution in the weld.

Chapter 8 focused on the validation and verification of numerical calculations. The proposed model was validated using experimental results from the author's experiment and those of other researchers. The test to RISEM strength ratios were consistently between 1.1 and 1.35, with an average of 1.26. Weld strength was determined using NDC, which limits the ultimate stresses in a RISEM. In the case of transverse welds, the NDC weld resistance was 1.6 times higher than that obtained with currently used analytical models, using the exact correlation β and the principle followed by the standard. However, for this numerical calculation to be widely accepted, it will be necessary to perform reliability and probability analysis to determine the new correlation β for the numerical model. Similarly, in the case of longitudinally welded joints, the NDC weld resistance was in agreement with the analytical models of prEN1993-1-8:2020, with a variance of 17%.

A 5% plastic strain limit can be used to simplify the design model of transverse and longitudinal fillet welds as described in Chapter 9. With this limit, only three primary parameters (E , f_y , and f_u) are needed for a numerical calculation to determine the design strength of the weld without requiring laboratory material testing in the FE model. Benchmark examples were performed on transverse and longitudinal fillet welds made of S700 MC Plus-OK AristoRod 13.12 using the 5% plastic strain limit. The RISEM results show good agreement with the analytical model for both welding configurations, demonstrating good consistency. The most significant difference between the two welding configurations is 11% for the analytical models.

10.2 Outlook

This study calculates the design of weld resistance for transverse and longitudinal fillet lap-welded connections made with high-strength structural steel (HSS). The study uses a finite element model called the regular inclined shell element model (RISEM) and proposes a new strength criterion based on stresses on the inclined shell element. This criterion uses the maximum uniform equivalent stress as an indicator and applies standardized procedures to design joints using Finite Element Method (FEM). The research shows that the numerical calculation requires three primary parameters (E , f_y , and f_u) only to compute the weld's design resistance without performing laboratory material tests in the FE model by limiting plastic strain.

The RISEM results are more economical than the analytical model in both welded configurations. The transverse welded resistance is 1.6 times higher. The proposed design model indicates that we need to consider the economical design of the connection and conduct a reliability analysis based on current findings. It is necessary to study reliability and probability study on it.

The scope of work is limited to the fillet lap-welded connections. Further investigations on different weld configurations of fillet weld connections from high-strength structural steel can also ensure the design models' applicability. This calculation approach could also be extended to other welded connections, such as long welds, fin plate joints, and connections to unstiffened flanges. This could increase the reliability of the proposed model.

REFERENCE

- [1] Bernuzzi, C., & Cordova, B. (2016). *Structural steel design to Eurocode 3 and AISC specifications*. John Wiley & Sons.
- [2] European Committee for Standardization (CEN). (2006). EN1993-1-8, Eurocode 3: Design of steel structures – Part 1-8: Design of joints. European Standard. Brussels.
- [3] Kanvinde, A. M., Gomez, I. R., Roberts, M., Fell, B. V., & Grondin, G. Y. (2009). Strength and ductility of fillet welds with transverse root notch. *Journal of Constructional Steel Research*, 65(4), 948-958.
- [4] Saufnay, L., Jaspard, J. P., & Demonceau, J. F. (2021). Economic benefit of high strength steel sections for steel structures. *ce/papers*, 4(2-4), 1543-1550.
- [5] Spiegler, J., & Kuhlmann, U. (2018). Innovative high-strength steel construction using mixed connections. *Steel Construction*, 11(4), 272-277.
- [6] Günther, H.P., Hildebrand, J., Rasche, C., Christian, V., Wudtke, I., Kuhlmann, U., Vormwald, M., & Werner, F. (2012). Welded connections of high-strength steels for the building industry. *Welding in the World*, 56(5), 86-106.
- [7] Griskevicius, P., Urbas, M., Capas, V., & Kozlovas, A. (2011, February). Modeling of welded connections in SolidWorks Simulation. In *Proceedings of 16th International Conference. Mechanika*.
- [8] Krejsa, M., Brozovsky, J., Mikolasek, D., Parenica, P., Flodr, J., Materna, A., Halama, R., & Kozak, J. (2018). Numerical modeling of steel fillet welded joint. *Advances in Engineering Software*, 117, 59-69.
- [9] Aygül, M. (2012). *Fatigue analysis of welded structures using the finite element method*. Chalmers Tekniska Hogskola (Sweden).
- [10] Barsoum, Z., & Khurshid, M. (2017). Ultimate strength capacity of welded joints in high strength steels. *Procedia Structural Integrity*, 5, 1401-1408.
- [11] Collin, P., & Johansson, B. (2005). Design of welds in high strength steel. In *European Conference on Steel and Composite Structures: 08/06/2005-10/06/2005* (pp. 4-10). Verlag Mainz.
- [12] Raoul, J. (2005). *Use and application of high-performance steels for steel structures* (Vol. 8). Iabse.
- [13] Kleiner, A. (2018). Beurteilung des Tragverhaltens von Flankenkehlnahtverbindungen aus normal- und höherfestem Baustahl unter Berücksichtigung statistischer Kriterien.
- [14] Sonsino, C. M. (2007). Light-weight design chances using high-strength steels. *Materials Science and Engineering Technology*, 38(1), 9-22. doi: 10.1002/mawe.200600090.
- [15] Miki, C., Homma, K., & Tominaga, T. (2002). High strength and high performance steels and their use in bridge structures. *Journal of constructional steel research*, 58(1), 3-20.
- [16] Bjorhovde, R. (2004). Development and use of high performance steel. *Journal of Constructional Steel Research*, 60(3-5), 393-400.

- [17] Gogou, E. (2012). Use of high strength steel grades for economical bridge design.
- [18] Shi, G., Hu, F., & Shi, Y. (2014). Recent research advances of high strength steel structures and codification of design specification in China. *International Journal of Steel Structures*, 14, 873-887.
- [19] Baddoo, N., & Anqi, C. (2020). *High strength steel design and execution guide*. SCI.
- [20] Peltonen, M. (2014). *Weldability of high-strength steels using conventional welding methods* (Master's thesis).
- [21] Rasche, C. (2012). Zur Bestimmung der Tragfähigkeit von Kehlnahtverbindungen höherfester Baustähle.
- [22] British Standards. (2004). Hot rolled products of structural steels— Part 3: Technical delivery conditions for normalized/normalized rolled weldable fine grain structural steels (BS EN 10025-3:2004, p. 36).
- [23] European Committee for Standardization (CEN). (2004). Hot rolled products of structural steels (EN 10025-4:2004, vol. 3).
- [24] European Committee for Standardization (CEN). (2004). BS EN10025-6: Hot rolled products of structural steels-Part 6: Technical delivery conditions for flat products of high yield strength structural steels in the quenched and tempered condition.
- [25] British Standards Institution. (2001). EN 1011-2:2001: Welding recommendations for metallic materials—Part 2: Arc welding of ferritic steels.
- [26] European Committee for Standardization (CEN). (2011). Eurocode 3: Design of steel structures— Part 1-12 (Vol. 1, No. 2005).
- [27] European Committee for Standardization (CEN). (2020). prEN 1993-1-8:2020, Eurocode 3: Design of steel structures-Part 1-8: Design of joints. European Standard, March, 2020.
- [28] American Institute of Steel Construction. (2016). AISC360/16 Specification for Structural Steel Buildings, an American National Standard (pp. 1-612).
- [29] Dowswell, B., Cox, C., Gallow, M. S., & Fouad, F. H. (2021). *Fillet and PJP welds: Final report*. American Institute of Steel Construction.
- [30] American Welding Society. (2020). AWS D1.1/D1.1M:2020: Structural Welding Code - Steel. (Year of Original Publication: 1980).
- [31] Wang, Y., Bradford, M. A., & Liu, X. (2020). Strength design of welded high-strength steel beams considering coupled local and global buckling. *Thin-Walled Structures*, 149, 106391.
- [32] Kuhlmann, U., Günther, H. P., & Rasche, C. (2008). High-strength steel fillet welded connections. *Steel Construction: Design and Research*, 1(1), 77-84.
- [33] British Standards Institution (BSI). (1996). BS EN ISO 14341:2008: Welding consumables-Wire electrodes and deposits for gas shielded metal arc welding of non-alloy and fine grain steels-classification.

- [34] International Organization for Standardization. (Year). ISO 16834: Welding consumables — Wire electrodes, wires, rods and deposits for gas shielded arc welding of high strength steels — Classification.
- [35] Björk, T., Toivonen, J., & Nykänen, T. (2012). Capacity of fillet welded joints made of ultra high-strength steel. *Welding in the World*, 56, 71-84.
- [36] Khurshid, M., Barsoum, Z., & Mumtaz, N. A. (2012). Ultimate strength and failure modes for fillet welds in high strength steels. *Materials & Design*, 40, 36-42.
- [37] Sun, F. F., Ran, M. M., Li, G. Q., & Wang, Y. B. (2019). Mechanical behavior of transverse fillet welded joints of high strength steel using digital image correlation techniques. *Journal of Constructional Steel Research*, 162, 105710.
- [38] Ran, M. M., Sun, F. F., Li, G. Q., & Wang, Y. B. (2021). Mechanical behaviour of longitudinal lap-welded joints of high strength steel: Experimental and numerical analysis. *Thin-Walled Structures*, 159, 107286.
- [39] Zamiri Akhlaghi, F. (2009). Fatigue life assessment of welded bridge details using structural hot spot stress method.
- [40] Chillal, R., & Pagar, N. (2016). Hot Spot Stress Assessment At Fillet Welded Joint Using Different Finite Element Weld Modeling Techniques and Its Validation. *World Journal of Engineering Research and Technology*, 2(5), 270-290.
- [41] Weaver, M. A. (1999). Determination of weld loads and throat requirements using finite element analysis with shell element models—a comparison with classical analysis. *WELDING JOURNAL-NEW YORK-*, 116-s.
- [42] Echer, L., & Marczak, R. J. (2014). A formulation and comparison of different shell FE modeling techniques for fatigue life simulation of welded joints. In *Proceedings of the XXXV Iberian Latin-American Congress on Computational Methods in Engineering (CILAMCE 2014)*, Brazil.
- [43] Bennebach, M., Klein, P., & Kirchner, E. (2018). Several seam weld finite element idealizations challenged in fatigue within a French industrial collaborative workgroup. *Procedia engineering*, 213, 403-417.
- [44] Fayard, J. L., Bignonnet, A., & Van, K. D. (1996). Fatigue design criterion for welded structures. *Fatigue & Fracture of Engineering Materials & Structures*, 19(6), 723-729.
- [45] Echer, L., & Marczak, R. J. (2015, May). Optimization of shell FE modeling parameters in the simulation of weld fillets using the structural stress method. In *Proceedings of the 5th International Symposium on Solid Mechanics (MecSol2015)*, Brazil.
- [46] Niemi, E., Fricke, W., & Maddox, S. J. (2018). *Structural hot-spot stress approach to fatigue analysis of welded components*. IIW doc, 13, 1819-00.
- [47] Turlier, D., Klein, P., & Bérard, F. (2010). Seam Sim” method for seam weld structural assessment within a global structure FEA. In *Proc. Int. Conf. IIW2010 Istanbul (Turkey)*. AWST (pp. 651-658).
- [48] Nagiar, H. M. (2013). *Stress analysis of corner welded joints structure by modern numerical-experimental approach*. University of Belgrade, Belgrade.

- [49] Tung, S. H., & Sui, C. H. (2010). Application of digital-image-correlation techniques in analysing cracked cylindrical pipes. *Sadhana*, 35, 557-567.
- [50] Orteu, J. J. (2009). 3-D computer vision in experimental mechanics. *Optics and lasers in engineering*, 47(3-4), 282-291.
- [51] Sutton, M. A., McNeill, S. R., Helm, J. D., & Chao, Y. J. (2000). Advances in two-dimensional and three-dimensional computer vision. *Photomechanics*, 323-372.
- [52] European Committee for Standardization (CEN). (2006). EN 1993-1-5:2006: Eurocode 3: Design of steel structures - Part 1-5: Plated structural elements (Vol. 3).
- [53] Wald, F., Šabatka, L., Bajer, M., Barnat, J., Gödrich, L., Holomek, J., Kabeláč, J., Kočka, M., Kolaja, D., Král, P., Kurejková, M., & Vild, M. (2016). *Benchmark cases for advanced design of structural steel connections*. Czech Technical University in Prague.
- [54] Wald, F., Šabatka, L., Bajer, M., Kožich, M., Vild, M., Golubiatnikov, K., Kabeláč, J., & Kuříková, M. (2021). *Component-based finite element design of steel joints*. Czech Technical University in Prague.
- [55] European Committee for Standardization (CEN). (1996). EN 10149-2: Hot-rolled flat products made of high yield strength steels for cold forming (No. 1)
- [56] European Committee for Standardization. (2022). prEN1993-1-14, Eurocode 3: Design of steel structures – Part 1-14: Design assisted by finite element analysis. European Standard, proposal.
- [57] Hobbacher, A. (2008). *Recommendations for fatigue design of welded joints and components*. International Institute of Welding. IIW-1823-07 ex. XIII-2151r4-07/XV-1254r4-07.
- [58] Ghimire, A., Wald, F., Vild, M., & Kabeláč, J. (2024). Numerical design calculation of the high-strength steel welds. *Engineering Structures*, 300, 117201.
- [59] Ghimire, A., Wald, F., Vild, M., & Kabeláč, J. (2023). Numerical design calculation of the fillet weld resistance. *Welding in the World*, 1-18.
- [60] Meyers, M. A., & Chawla, K. K. (2008). *Mechanical behavior of materials*. Cambridge university press.
- [61] Beer, P.F., Johnston, E.R., DeWolf, J.T., & Mazurek, D.F. (2012). *Mechanics of materials*. McGraw-Hill.
- [62] Philpot, T. A., Hall, R. H., Hubing, N., Flori, R., Oglesby, D. B., & Vikas, Y. (2003). Animated instructional media for stress transformations in a mechanics of materials course. *Computer Applications in Engineering Education*, 11(1), 40-52.
- [63] Wald, F., Kwasniewski, L., Gödrich, L., & Kurejková, M. (2014, May). Validation and verification procedures for connection design in steel structures. In *12th International Conference on Steel, Space and Composite Structures* (pp. 111-120).
- [64] European Committee for Standardization (CEN). (2007). Eurocode 3: design of steel structures– Part 1-6: strength and stability of shell structures. *Brussels, Belgium: European Committee for Standardization*.

- [65] Hradil, P., Fülöp, L., Talja, A., & Kurkela, J. (2017). *Experiences from numerical modelling of details with ductile failure*. Research Report VTT Technical Research Centre of Finland, March, Espoo.

Annex 1 Detail measurement of the specimen.

Measurement before the experiment

A transverse fillet lap-welded connection's typical geometry and configuration are present in Fig. A.1.86 and Fig. A.1.87-Left). The measurements of the weld profile, such as tension leg (TL), shear leg (SL), weld throat (WT), and weld length (L), were taken before testing (see Fig. A.1.87-Right). A vernier caliper was used to determine the dimensions of plates and weld profiles (see Table A.1-48 and Table A.1-49). Table A.1-50 presents the summary of the measurement of each specimen. Six specimens with a transverse fillet lap-welded connection were created, with "TS" denoting the transverse specimen.

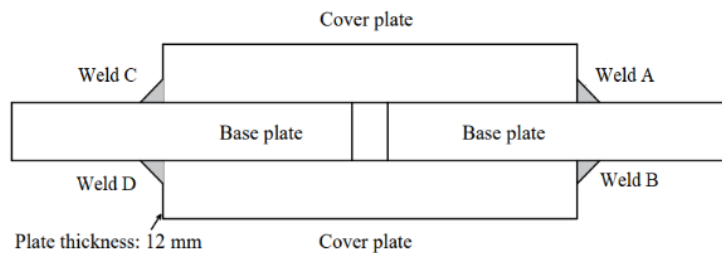


Fig. A.1.86. Section view of the transverse fillet lap-welded connection.

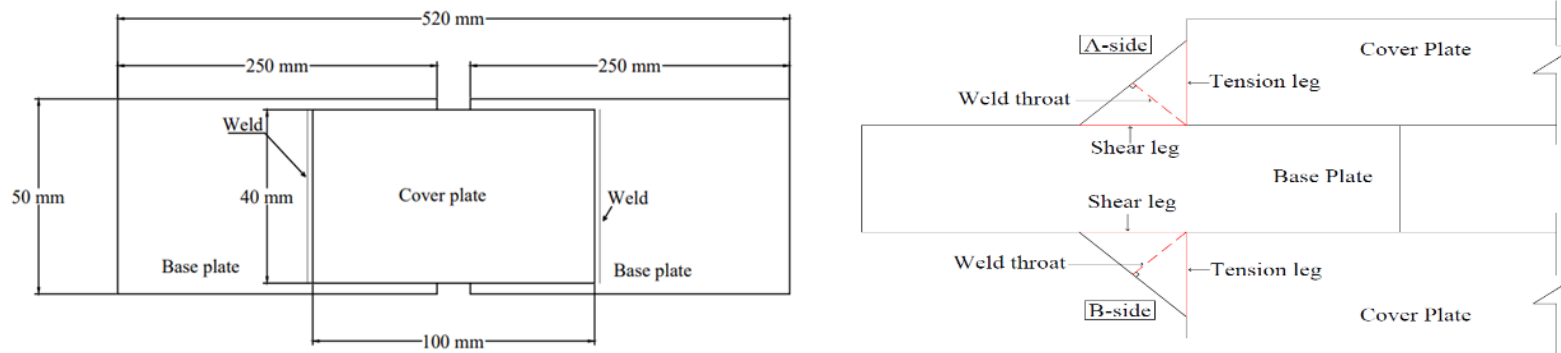


Fig. A.1.87. Plan view (Left) and weld profile measurement before testing (Right) of the transverse fillet lap-welded connection.

Table A.1-48 Measurement of weld profile on transverse fillet lap-welded connections.

Specimen	Weld A				Weld B				Weld C				Weld D			
	L	SL	TL	WT	L	SL	TL	WT	L	SL	TL	WT	L	SL	TL	WT
	[mm]															
TS-1	44.63	5.88	5.43	4.00	44.59	7.70	5.45	4.65	46.64	7.87	6.27	5.00	44.51	6.90	6.53	4.75
TS-2	45.07	4.50	4.50	3.18	44.14	4.70	4.26	3.17	46.18	6.30	6.25	4.44	44.20	6.33	6.10	4.40
TS-3	43.97	5.09	4.70	3.46	43.58	4.29	4.19	3.00	44.23	7.14	3.00	3.59	45.96	5.49	4.50	3.53
TS-4	44.59	5.24	4.54	3.47	44.29	5.29	4.32	3.40	46.75	6.96	3.00	3.52	45.08	6.82	3.16	3.53
TS-5	45.49	5.40	5.20	3.75	45.05	4.87	5.73	3.75	46.18	6.22	6.22	4.40	45.96	6.11	6.20	4.35
TS-6	44.19	4.59	5.23	3.47	44.42	4.43	4.51	3.16	45.70	5.70	4.15	3.48	44.97	6.16	3.97	3.58

Table A.1-49 Measurement of steel plate on transverse fillet lap-welded connections.

Specimen	Base plate			Cover plate		
	Length	width	Thickness	Length	width	Thickness
	[mm]	[mm]	[mm]	[mm]	[mm]	[mm]
TS-1	250	50	12	100	40	12
TS-2	250	50	12	100	40	12
TS-3	250	50	12	100	40	12
TS-4	250	50	12	100	40	12
TS-5	250	50	12	100	40	12
TS-6	250	50	12	100	40	12

Table A.1-50 Summary of average measurement on weld profile of transverse fillet lap-welded connections.

Specimen	Weld A and Weld B					Weld C and Weld D				
	Total length	Shear leg	Tension leg	Weld thickness	Effective area	Total length	Shear leg	Tension leg	Weld thickness	Effective area
	[mm]	[mm]	[mm]	[mm]	[mm ²]	[mm]	[mm]	[mm]	[mm]	[mm ²]
TS-1	90	6.80	5.45	4.30	387.00	92	7.40	6.40	4.90	450.80
TS-2	90	4.60	4.35	3.15	283.50	90	6.30	6.20	4.40	396.00
TS-3	88	4.70	4.45	3.25	286.00	90	6.30	3.75	3.55	319.50
TS-4	88	5.25	4.45	3.45	303.60	92	6.90	3.10	3.55	326.60
TS-5	90	5.15	5.45	3.75	337.50	92	6.15	6.20	4.40	404.80
TS-6	88	4.50	4.90	3.30	290.40	90	5.95	4.05	3.55	319.50

Measurement after the experiment

The failure of all the specimens occurred in the fillet weld. In six specimens, failure of the weld occurred on both sides of the specimen. The fracture surface of the weld area was measured by photogrammetry, which means a 3D scan from photos. In this process, photos of the specimens were taken and created a 3D model of it. After having the 3D model of the specimens, the target surface area of the specimens was cut off, as shown in Fig. A.1.88a, and extracted the fracture surface area of the weld (see Fig. A.1.88b) for the analysis. To get precise data, mesh the weld's fracture surface area and measure its area. After the test, the fracture surface area of each specimen is summarized in Table A.1-51, which is measured by the photogrammetry method.

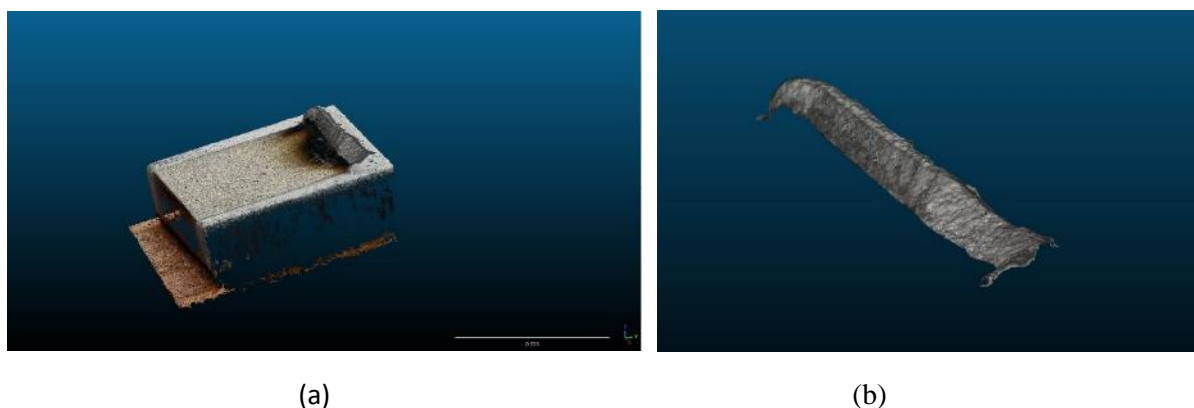


Fig. A.1.88. A typical example of (a) a Cut piece of a 3D model of the specimen and (b) a Fracture surface area of the weld.

Table A.1-51 Summary of the fracture surface area measurement after the experiment.

Specimen	Weld area [mm ²]		Total fracture surface area of the weld [mm ²]
	A	B	A _{fr}
TS-1	312	208	520
TS-2	178	160	338
TS-3	167	261	428
TS-4	179	219	398
TS-5	252	227	479
TS-6	225	248	473

Annex 2 Material properties

A Strain gauge and extensometer were installed on the specimen to determine the strain during loading. The load - curve was determined accordingly. Three tension coupons test for the base and cover plate S700 MC Plus and three for weld metal OK AristoRod 13.12 were performed according to Eurocode to characterize the base and cover plates and weld metal's material properties. The base metal and weld metal tension coupon specimens were prepared with a nominal gauge length (L_o) of 50 mm, diameter (D_o) of 11 mm, and total length (L) of 165 mm. Fig. A.2.89 represents the typical geometric configuration of tension coupon test specimens. The tensile test was performed in the UTS 100 KN testing machine. According to the Eurocode, the loading speed of the machine is 0.17 mm/min.

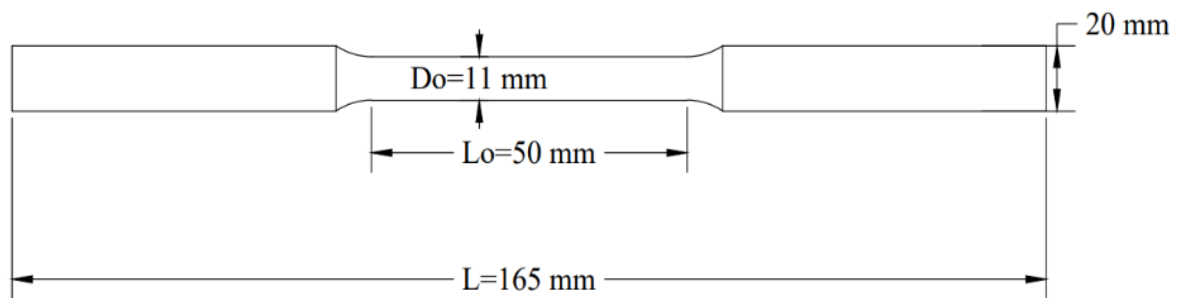


Fig. A.2.89. Typical geometry of the coupon test specimen.

From testing, the ultimate tensile strength was determined by dividing the maximum tensile load by the original cross-sectional area of the specimen. Since the yield strength was not clearly distinguished during the test, the proof stress was determined at the specified offset at 0.2% strain, as shown in Fig. A.2.90.

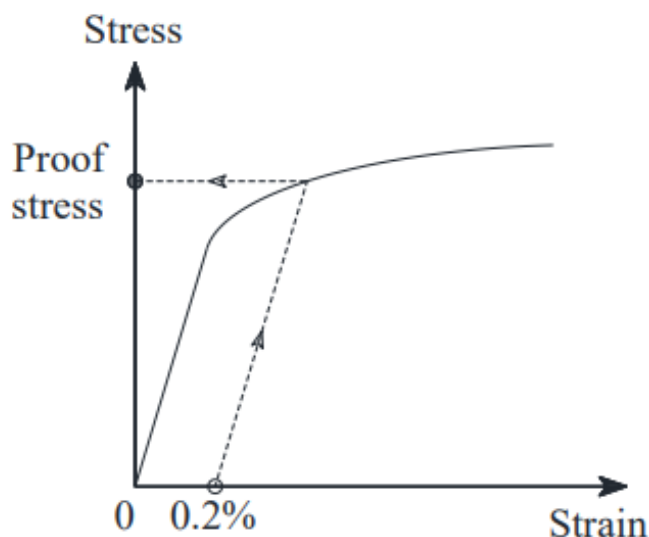


Fig. A.2.90. Proof Stress Calculation.

Steel: S700 MC Plus

Fig. A.2.91 represents the stress-strain curve of the steel material S700 MC Plus. Three tension coupon tests were conducted at the Department of the Steel and Timber Structure laboratory in at Czech Technical University in Prague. The mechanical properties of each tensile test and the average mechanical properties are presented in Table A.2-52.

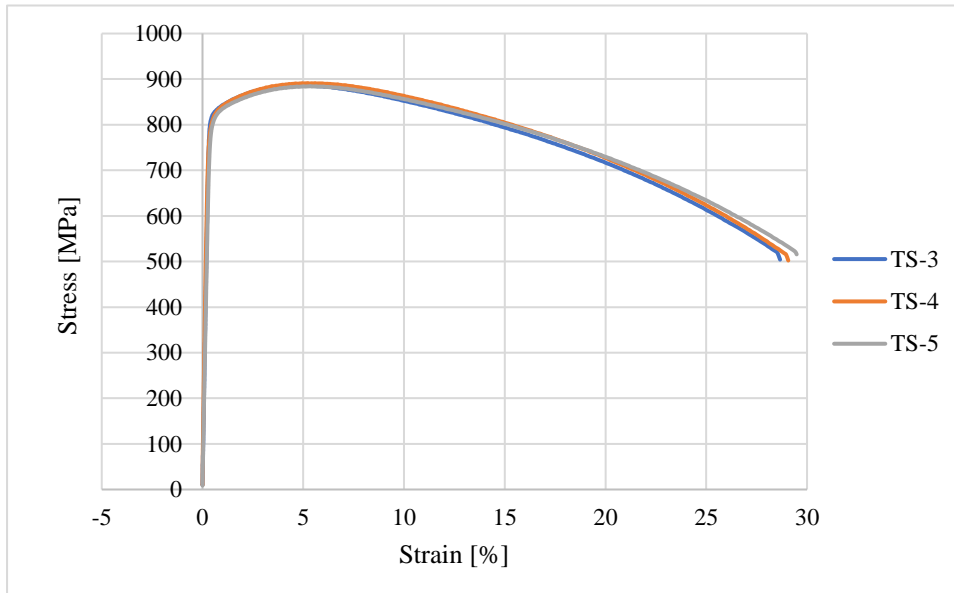


Fig. A.2.91. Stress-strain curve of material Strenx S700 MC Plus.

Table A.2-52 Mechanical properties of material S700 MC Plus.

Description	Young Modulus of Elasticity	Yield Stress	Yield Strain	Ultimate Tensile Stress	Ultimate Strain	Elongation Percentage
	[MPa]	[MPa]	[-]	[MPa]	[-]	[%]
TS-3	205745	798.40	0.0058	886.82	0.047	28.66
TS-4	227865	824.75	0.0055	891.15	0.050	29.06
TS-5	214732	811.49	0.0058	886.50	0.053	29.48
Average	216114	811.55	0.0057	888.16	0.050	29.06

OK AristoRod 13.12

The stress-strain curve of the weld metal OK AristoRod 13.12 is depicted in Fig. A.2.92. The Department of Steel and Timber Structure laboratory at Czech Technical University performed three tension coupon tests. Table A.2-53 displays the average mechanical characteristics and the mechanical properties of each tensile test.

During the tensile coupon test of weld material, OK AristoRod 13.12 shows lower yielding stress than the data provided by the production company. However, out of three, two samples satisfy the ultimate tensile stress and elongation percentage specified in production properties. Therefore, sample-4 & sample-5 are considered to find the material properties of weld metal in this study.

Fig.A.2.93 depicts the average stress-strain curve of the steel (S700 MC PLUS) and weld metal (OK AristoRod 13.12).

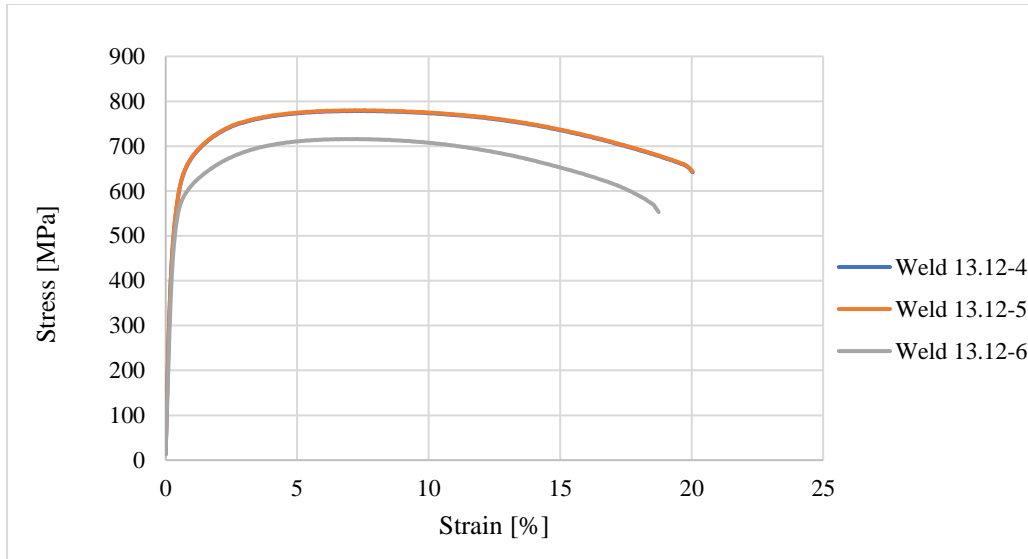


Fig. A.2.92. Stress-strain curve of material OK AristoRod 13.12.

Table A.2-53 Mechanical properties of material OK AristoRod 13.12.

Description	Young Modulus of Elasticity	Yield Stress	Yield Strain	Ultimate Tensile Stress	Ultimate Strain	Elongation Percentage
	[MPa]	[MPa]	[-]	[MPa]	[-]	[%]
Sample-4	232422	570.62	0.0044	778.77	0.065	20.04
Sample-5	232839	571.65	0.0044	778.93	0.068	20.04
Sample-6*	185279	552.58	0.0049	680.86	0.027	18.74
Average	232631	571.14	0.0044	778.85	0.066	20.04

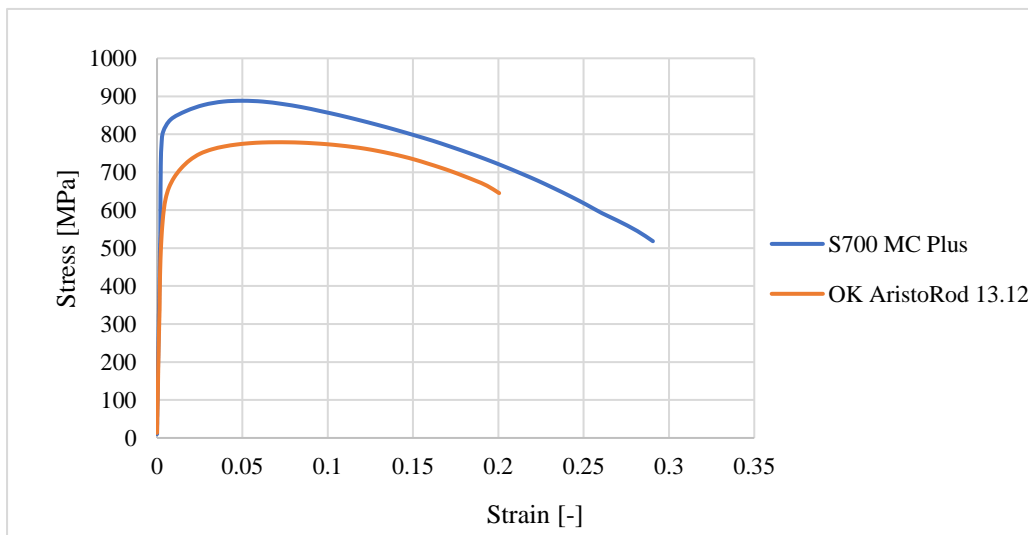


Fig. A.2.93. Average stress-strain curve of S700 MC Plus and OK AristoRod 13.12.

Annex 3 Displacement and strain vs. time

The deformation of the transverse fillet lap-welded connection was measured using DIC. The process involved recording the relative displacement of two points and determining the corresponding strain. Key points in the base plate, cover plate, and weld were assigned and tracked over the loading process to show the displacement, with several key points highlighted in Fig. A.3.94.

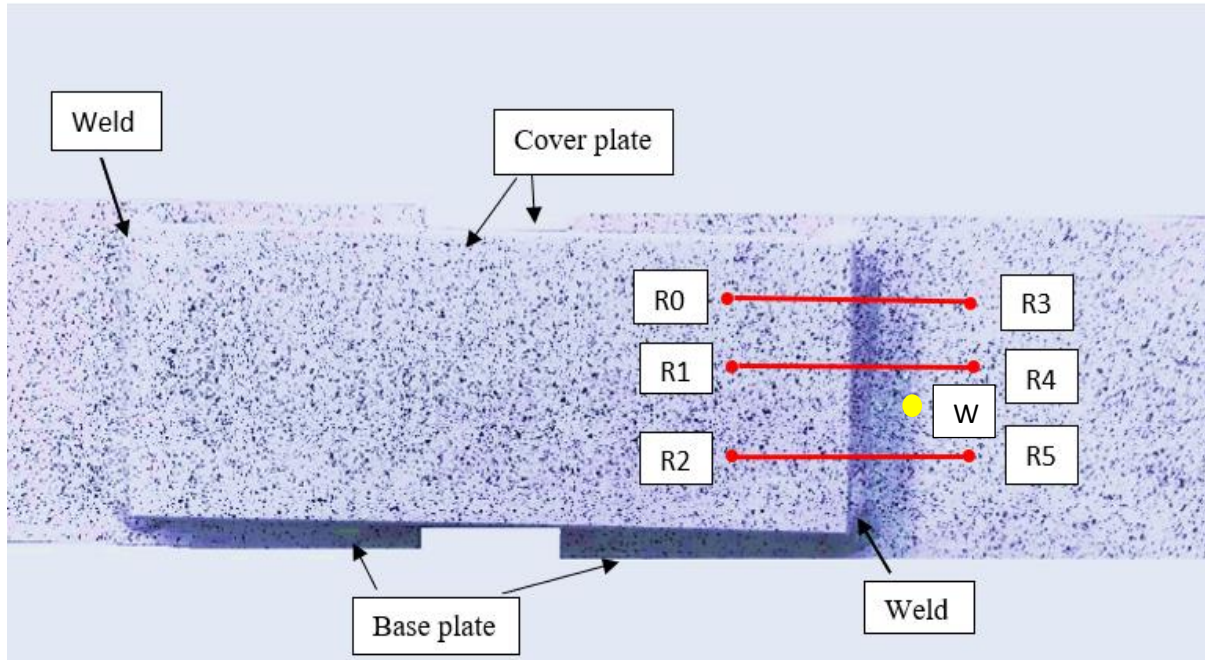


Fig. A.3.94. Several measurement key points were assigned in the test piece.

Fig. A.3.95 to Fig. A.3.100 show that the critical points in the plate underwent the same displacement over time while being loaded. However, the base and cover plates experienced different displacements. Hence the deformation of the transverse fillet lap-welded connection is determined through the relative displacement of two points in both base and cover plates, e.g., R0R3.

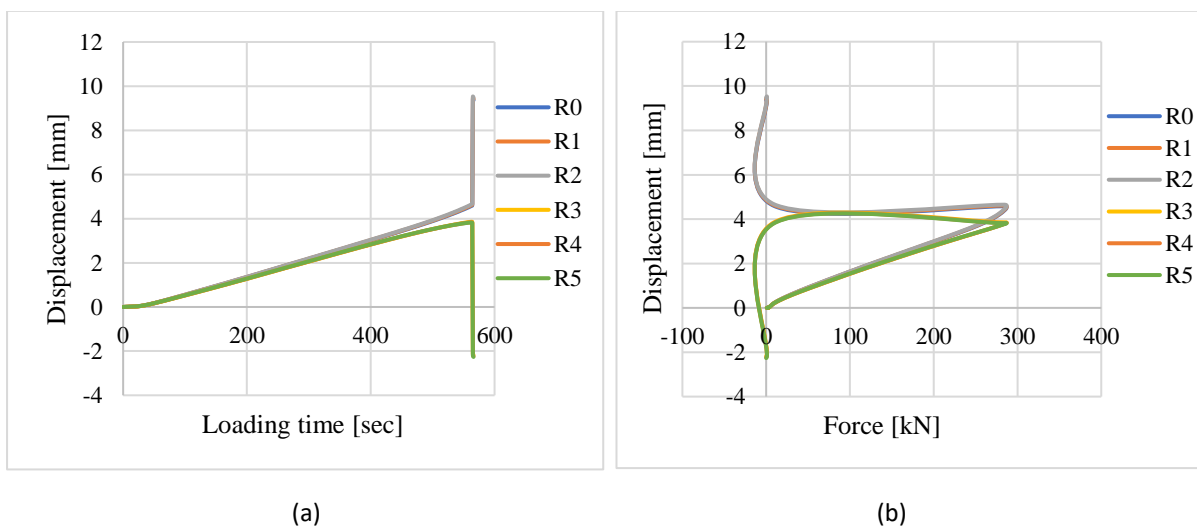


Fig. A.3.95. TS-1 (a) Displacement vs. time and (b) Displacement vs. force.

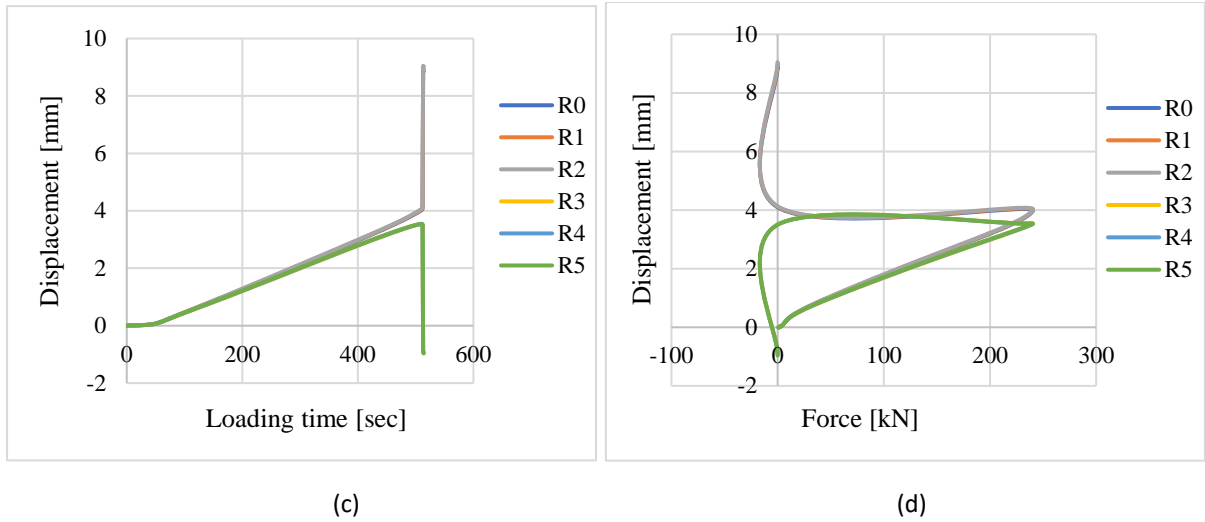


Fig. A.3.96. TS-2 (c) Displacement vs. time and (d) Displacement vs. force.

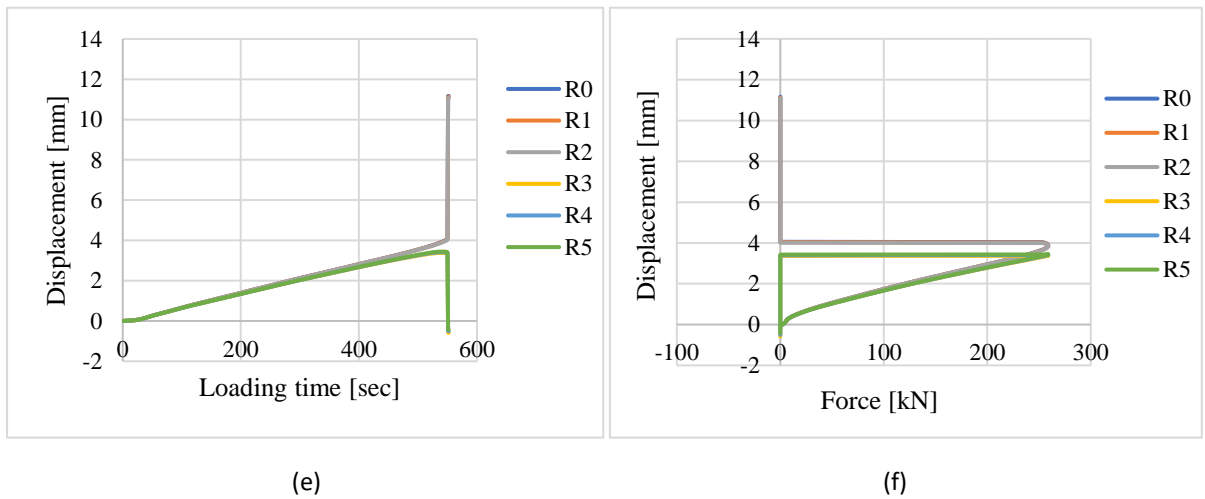


Fig. A.3.97. TS-3 (e) Displacement vs. time and (f) Displacement vs. force.

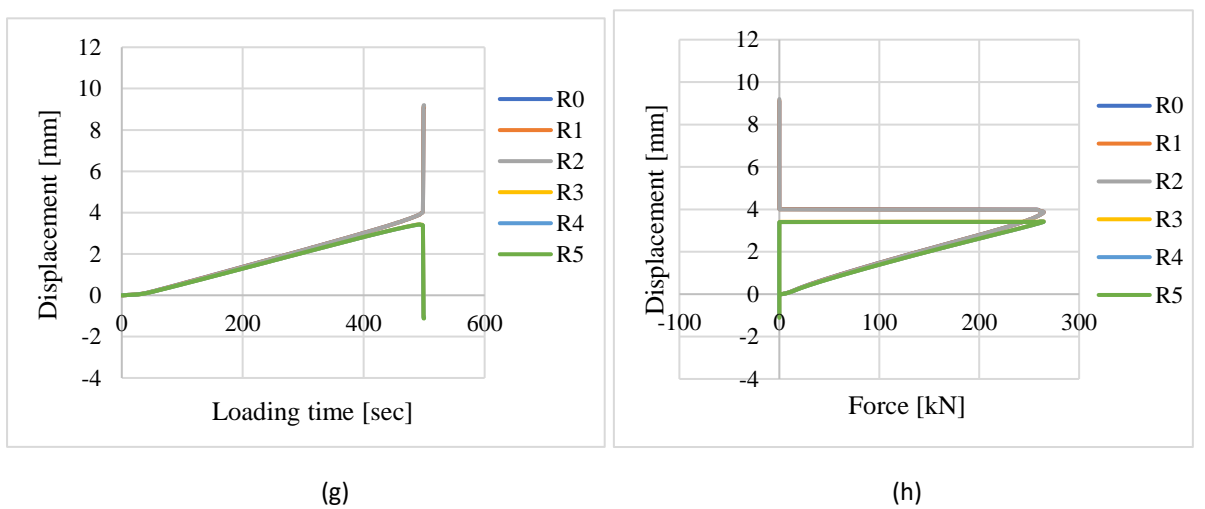


Fig. A.3.98. TS-4 (g) Displacement vs. time and (h) Displacement vs. force.

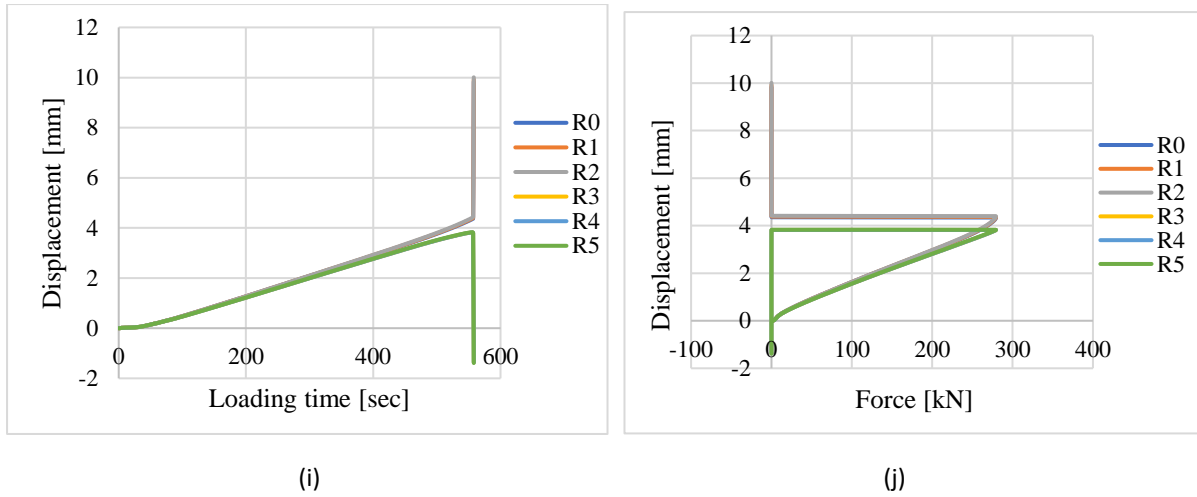


Fig. A.3.99. TS-5 (i) Displacement vs. time for TS-5 and (j) Displacement vs. force.

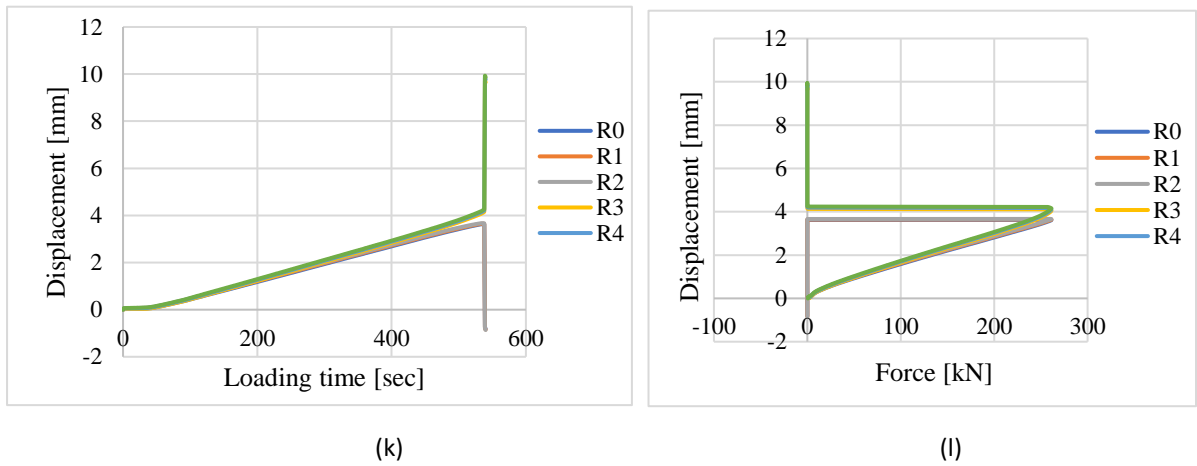


Fig. A.3.100. TS-6 (k) Displacement vs. time and (l) Displacement vs. force.

Fig. A.3.101 to Fig. A.3.106 show that the critical points in the base and cover plates remained unyielding throughout the loading process. This behavior suggests that the base and cover plate deformation is disregarded in transverse fillet lap-welded connections. Therefore, the deformation of the fillet weld can be depicted by the relative displacement of two arbitrary points between the base and cover plate.

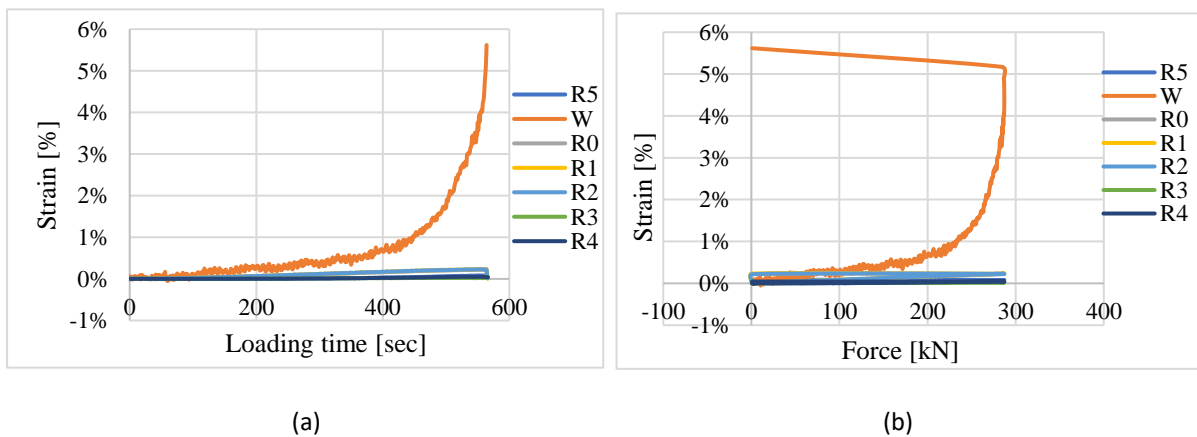
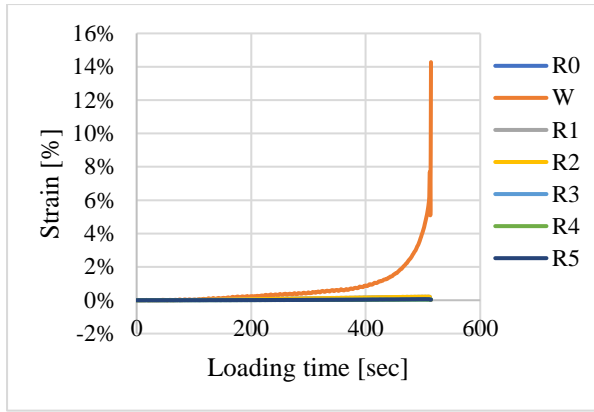
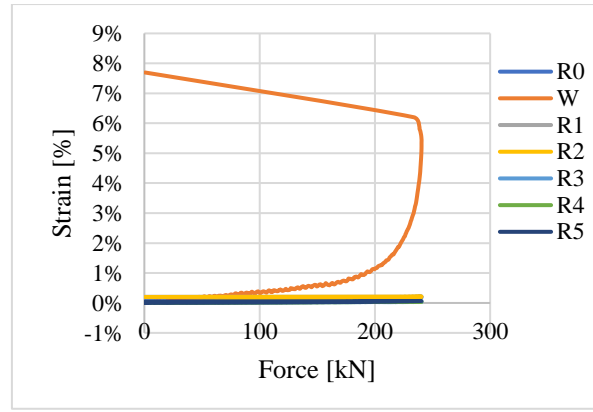


Fig. A.3.101. TS-1 (a) Strain vs. time and (b) Strain vs. force.

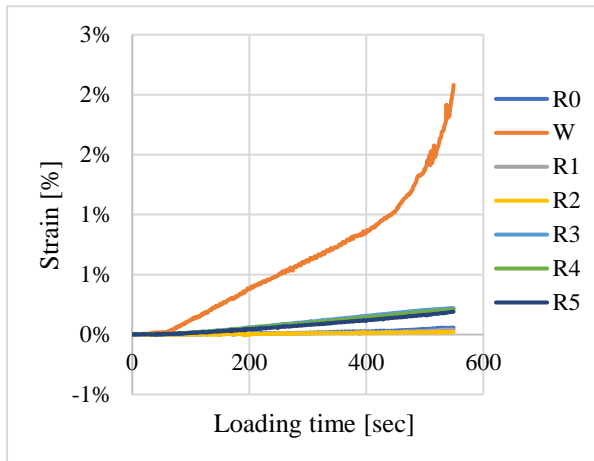


(c)

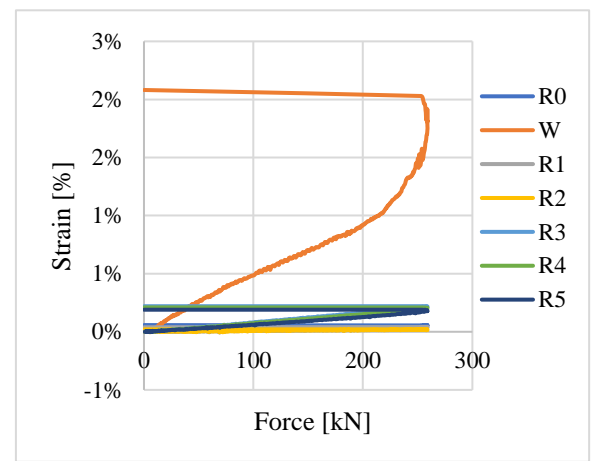


(d)

Fig. A.3.102. TS-2 (a) Strain vs. time and (b) Strain vs. force.

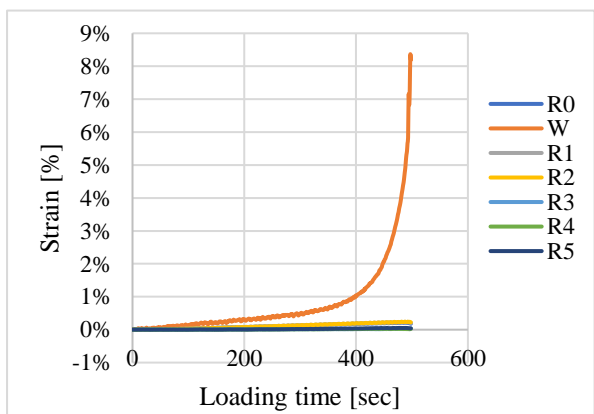


(e)

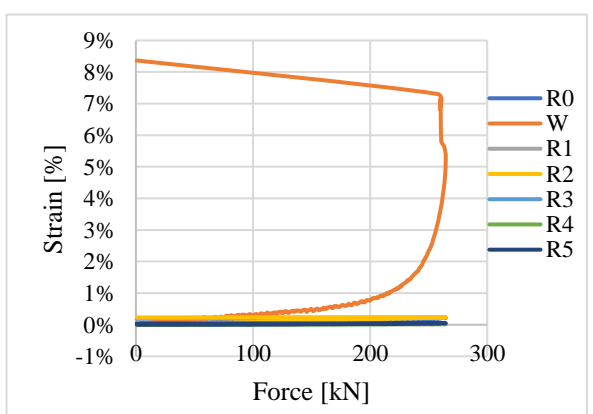


(f)

Fig. A.3.103. TS-3 (a) Strain vs. time and (b) Strain vs. force.

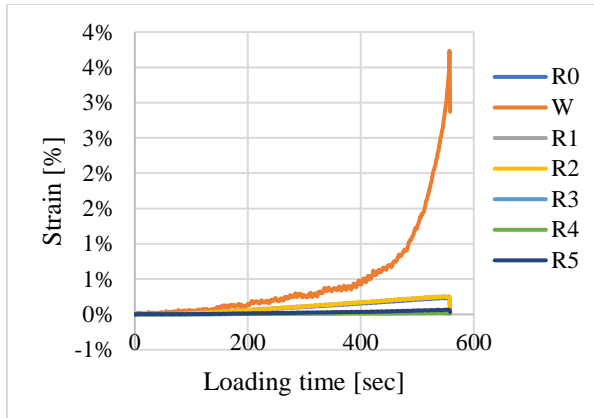


(g)

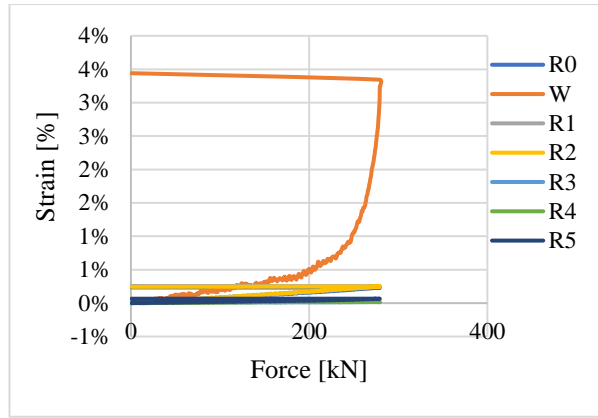


(h)

Fig. A.3.104. TS-4 (a) Strain vs. time and (b) Strain vs. force.

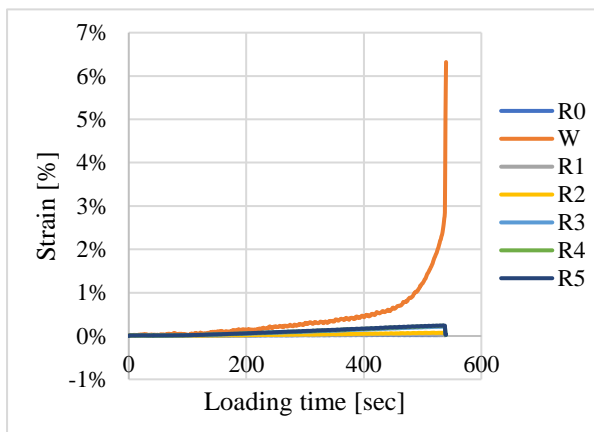


(i)

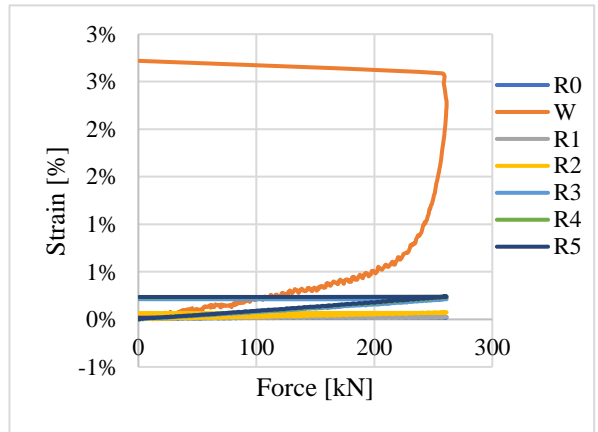


(j)

Fig. A.3.105. TS-5 (a) Strain vs. time and (b) Strain vs. force.



(k)



(l)

Fig. A.3.106. TS-6 (a) Strain vs. time and (b) Strain vs. force.

Annex 4 Force-Deformation curve

The typical force-deformation diagram of the transverse fillet lap-welded connections includes the relative displacement of points R0R3, R1R4, and R2R5 and the average values of three points as recorded by DIC measurement (see Fig. A.4.107). This study utilized the average value of relative displacement of R0R3, R1R4, and R2R5 to measure the deformation of the specimens (see Fig. A.4.108 to A.4.113).

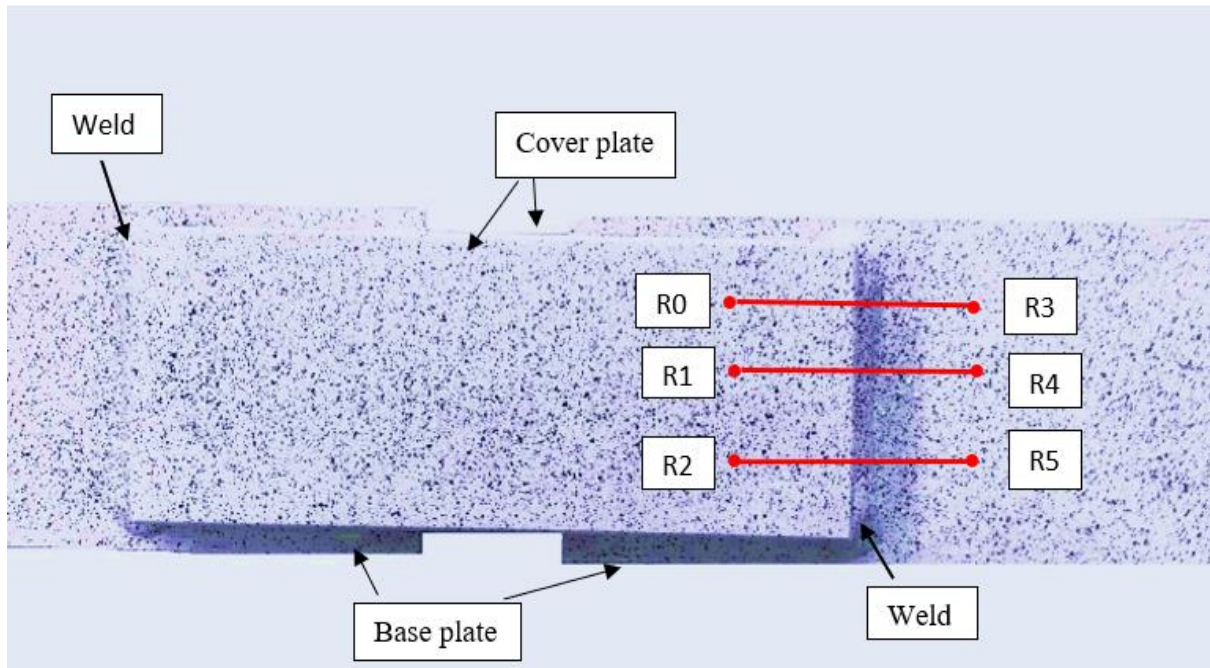


Fig. A.4.107. Measurement points for the deformation of transverse fillet lap-welded connection.

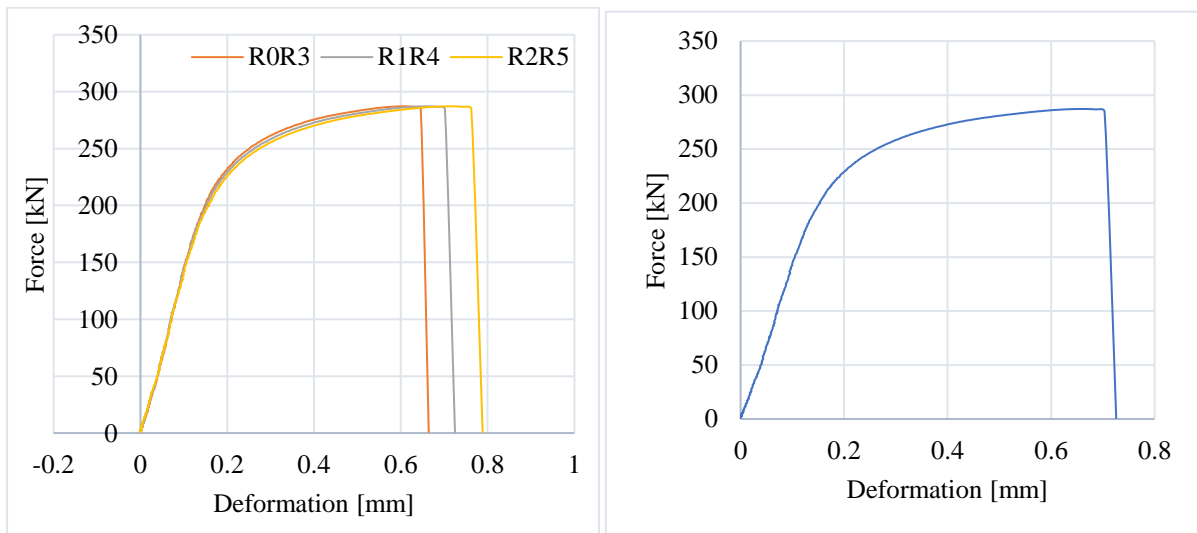


Fig. A.4.108. Force-deformation curve of TS-1, (a) Relative displacement of three distances, (b) Average of relative displacement.

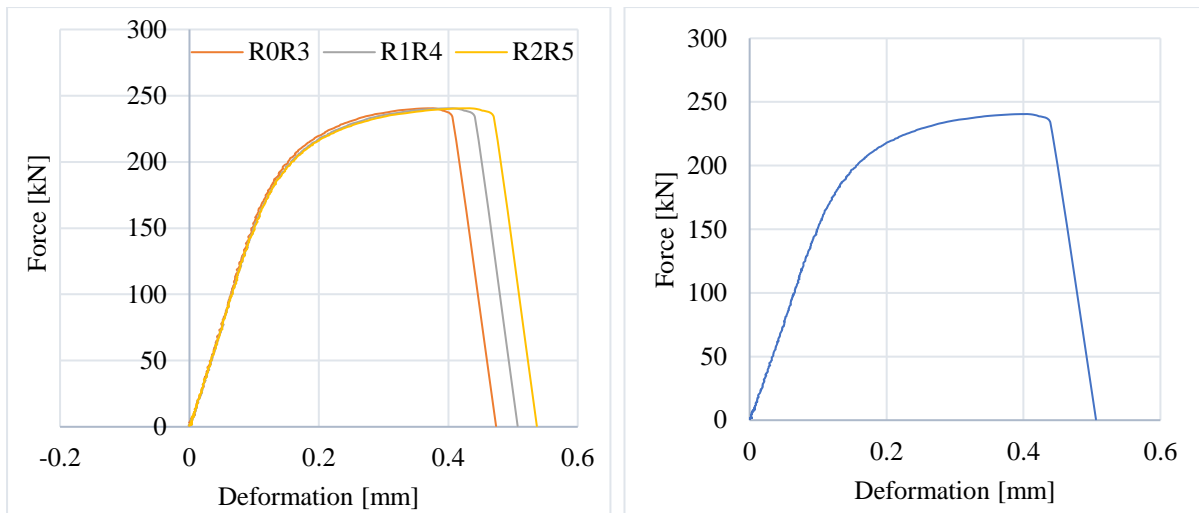


Fig. A.4.109. Force-deformation curve of TS-2, (a) Relative displacement of three distances, (b) Average of relative displacement.

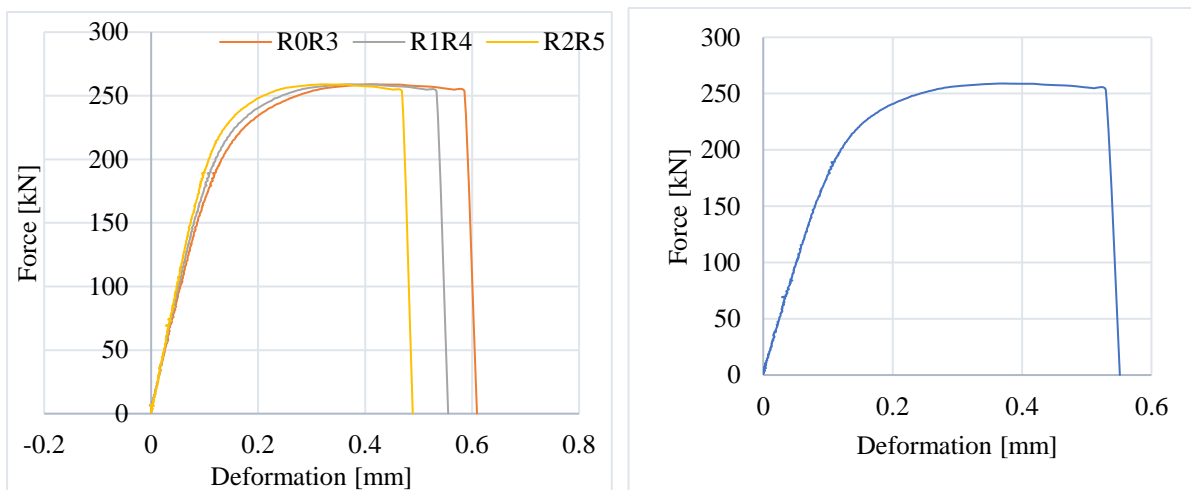


Fig. A.4.110. Force-deformation curve of TS-3, (a) Relative displacement of three distances, (b) Average of relative displacement.

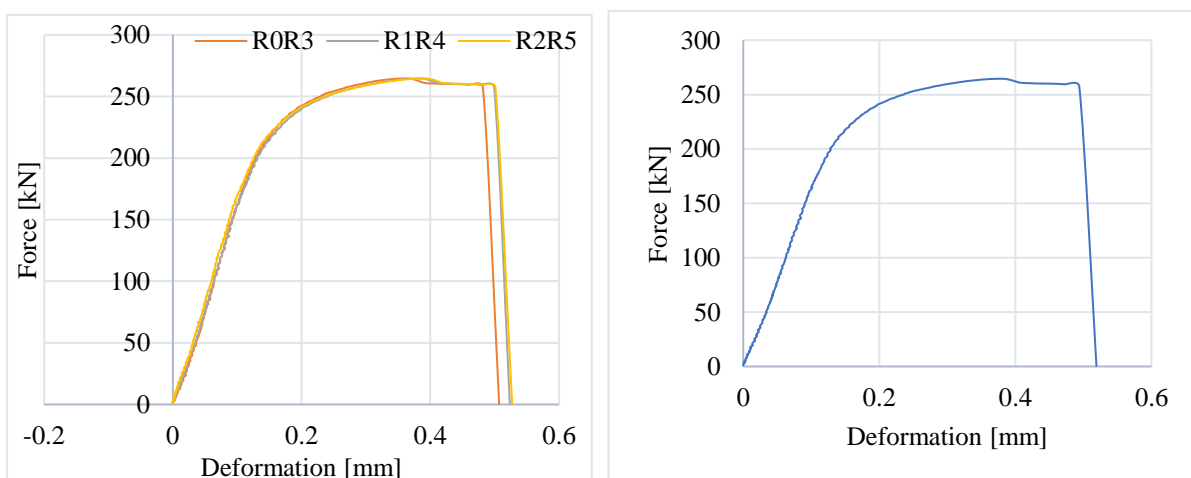


Fig. A.4.111. Force-deformation curve of TS-4, (a) Relative displacement of three distances, (b) Average of relative displacement.

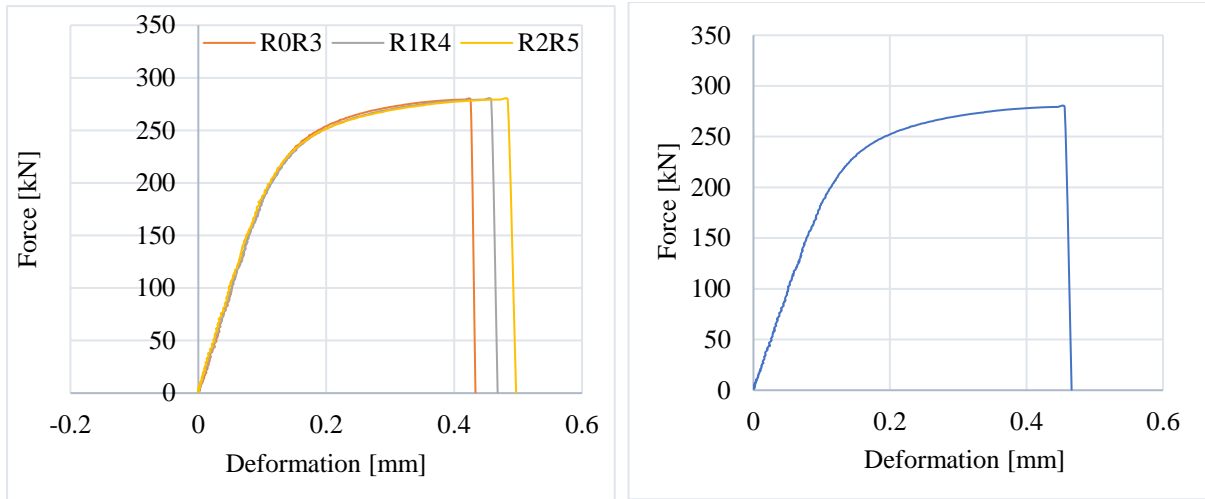


Fig. A.4.112. Force-deformation curve of TS-5, (a) Relative displacement of three distances, (b) Average of relative displacement.

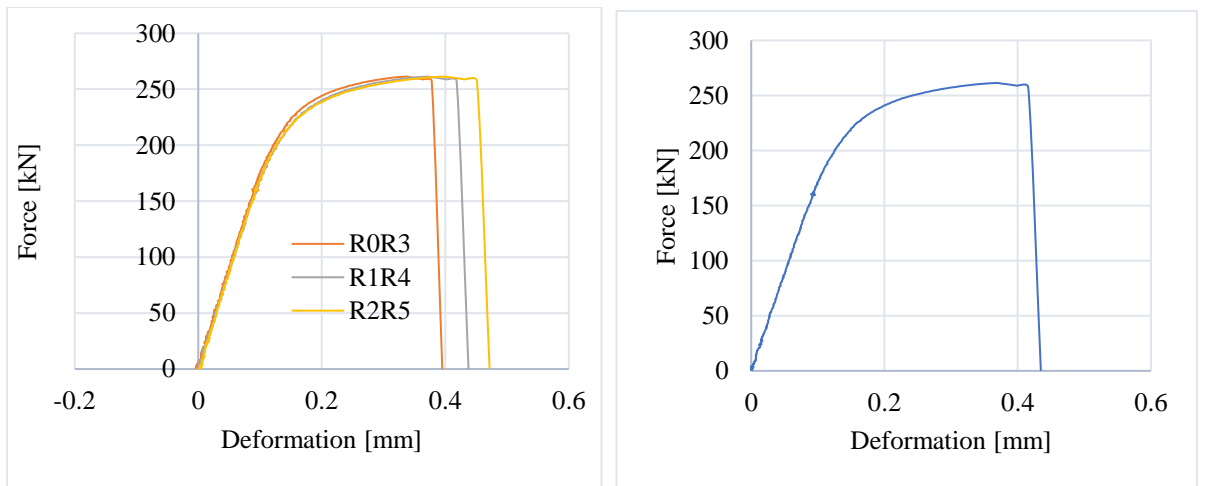


Fig. A.4.113. Force-deformation curve of TS-6, (a) Relative displacement of three distances, (b) Average of relative displacement.

Annex 5 Strength vs. strain

In this section, the strength calculated by dividing the maximum force (F_u) with the theoretical throat area (A_{th}) and the fracture surface area (A_{fr}) of the weld before and after the experiment are presented graphically. Fig. A.5.114 to Fig. A.5.119 depicts the strength corresponding to the strain of each transverse fillet lap-welded connection.

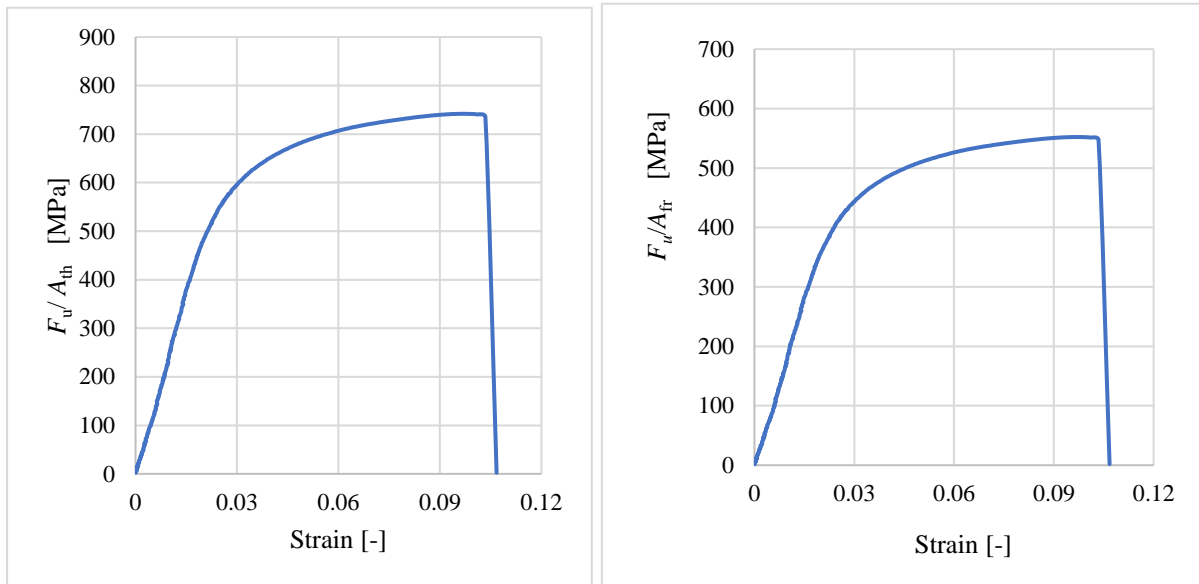


Fig. A.5.114. Strength vs. strain for TS-1.

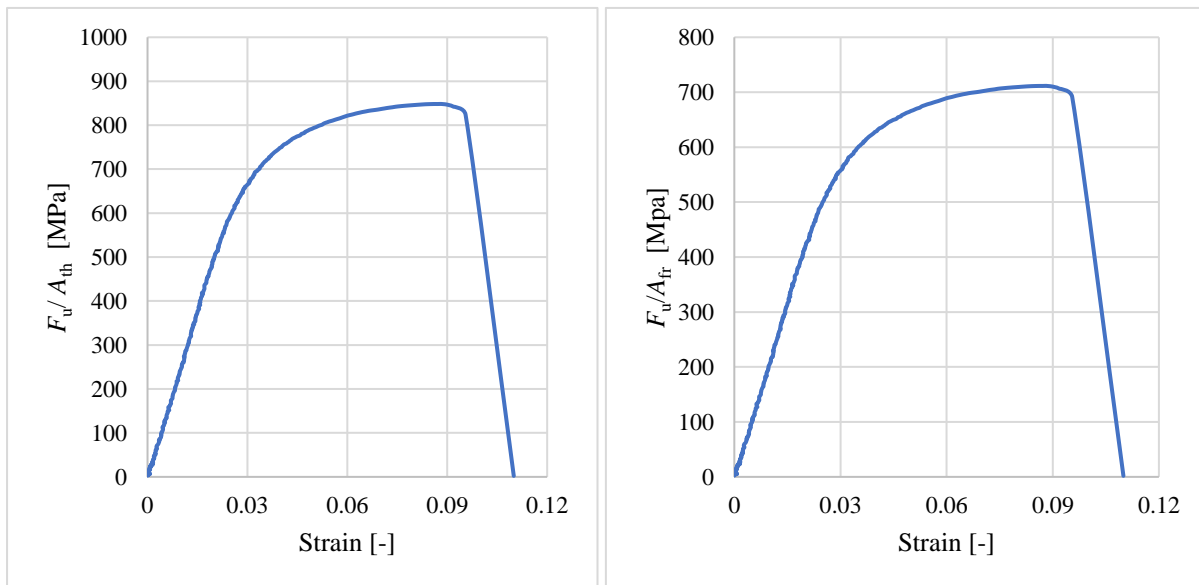


Fig. A.5.115. Strength vs. strain for TS-2.

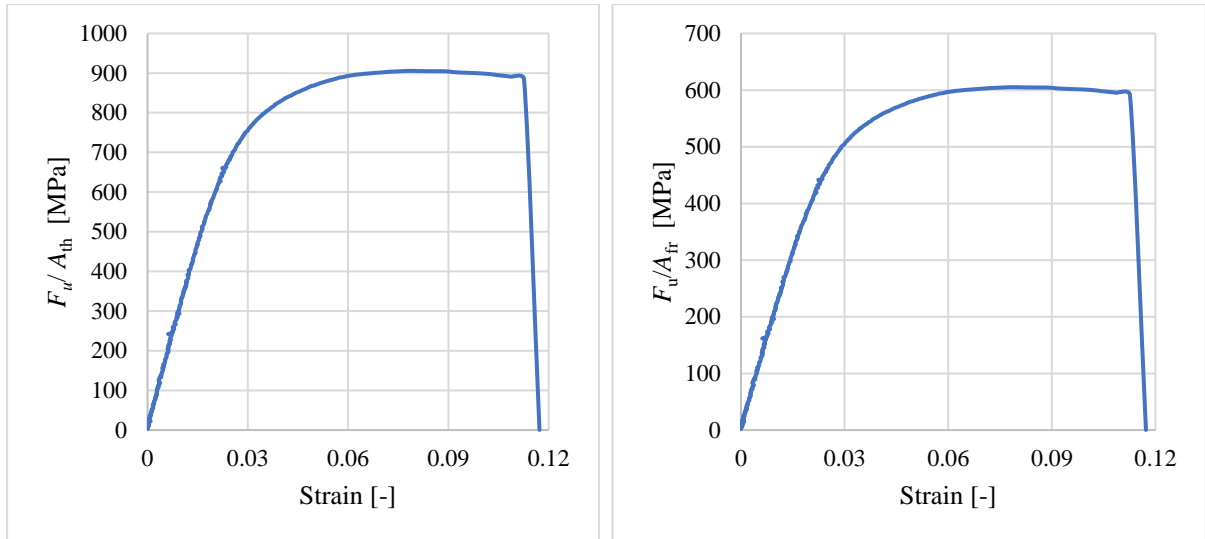


Fig. A.5.116. Strength vs. strain for TS-3.

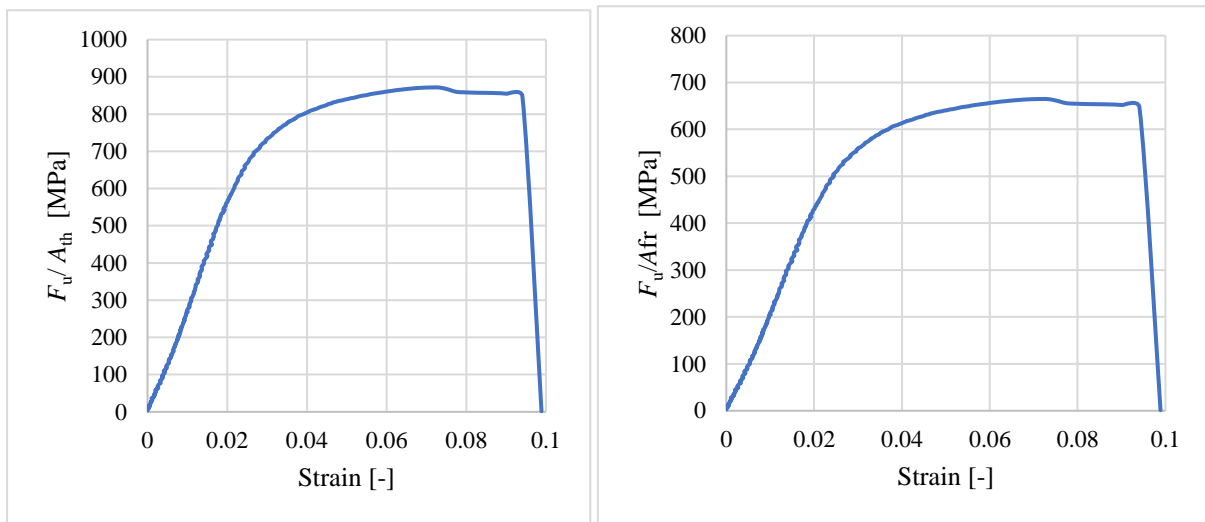


Fig. A.5.117. Strength vs. strain for TS-4.

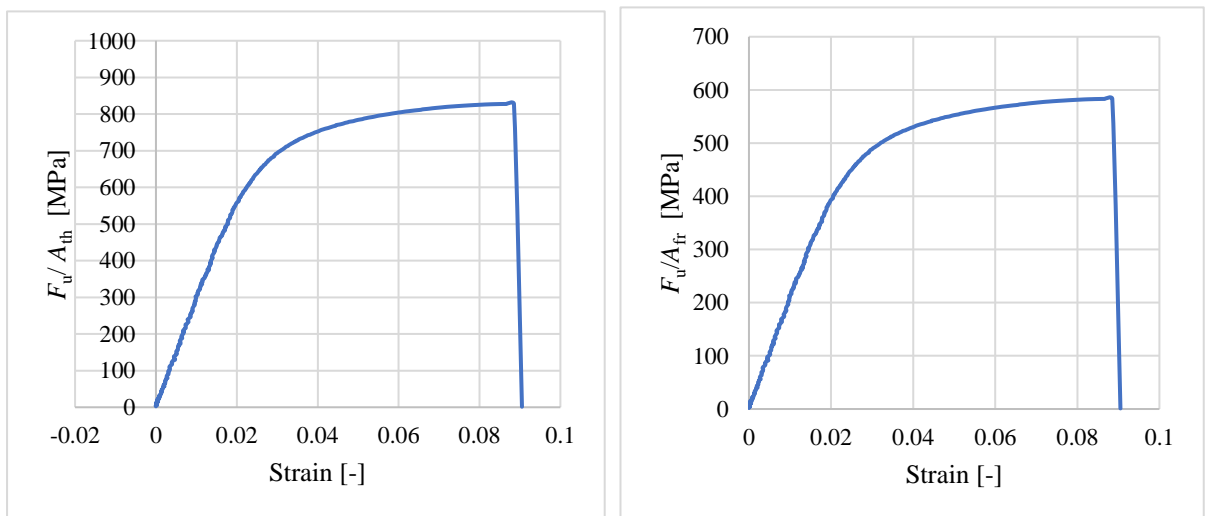


Fig. A.5.118. Strength vs. strain for TS-5.

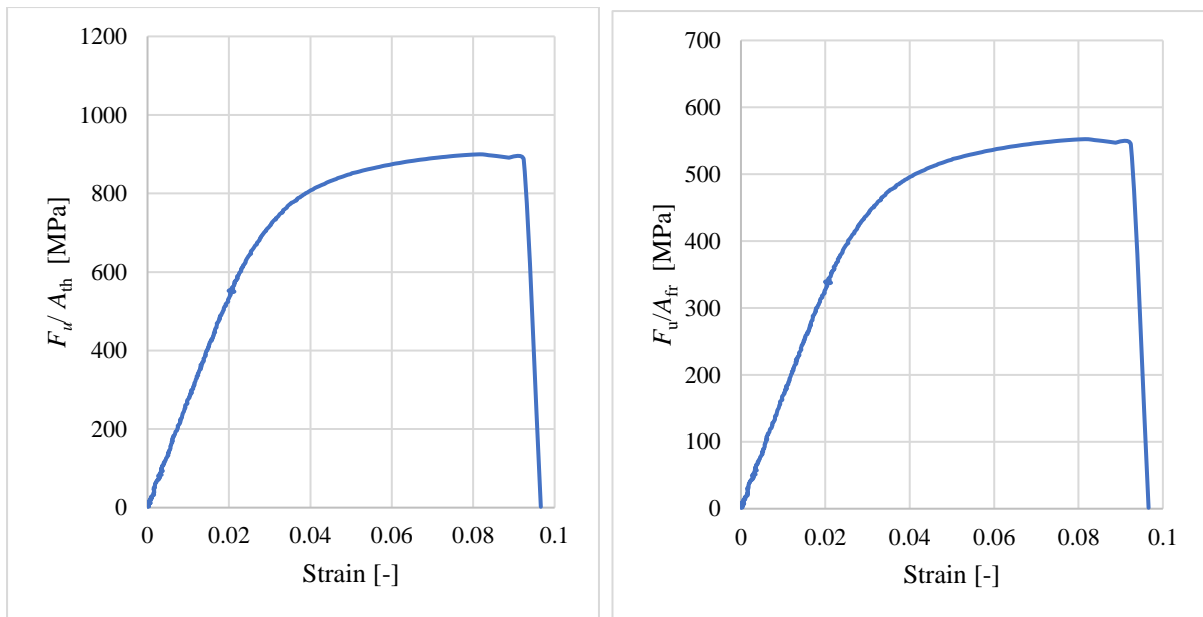


Fig. A.5.119. Strength vs. strain for TS-6.

Annex 6 Summary of experimental results

Table A.6-54 Summary of experimental results.

Present Research (High-Strength Steel- Transverse Fillet weld)							
Filler Metal		OK AristoRod 13.12					
Specimen Designation		TS-1	TS-2	TS-3	TS-4	TS-5	TS-6
Weld Thickness (a)	[mm]	4.30	3.15	3.25	3.45	3.75	3.30
Weld shear leg length (w)	[mm]	6.80	4.60	4.70	5.25	5.15	4.50
Total effective length (L)	[mm]	90	90	88	88	90	88
Theoretical effective area of the weld (A_{th})	[mm ²]	387.0	283.5	286.0	303.6	337.5	290.4
Fracture effective area of the weld (A_{fr})	[mm ²]	520	338	428	398	479	473
Ultimate Load (F_u)	[kN]	287.11	240.50	259.00	264.60	279.00	261.25
Deformation capacity (δ_u)	[mm]	0.66	0.40	0.37	0.38	0.45	0.37
Ductility (δ_u / w)	[%]	9.7	8.7	7.9	7.2	8.7	8.2
Ultimate Strength (F_u / A_{th})	[N/mm ²]	742	848	906	872	827	900
Ultimate Strength (F_u / A_{fr})	[N/mm ²]	552	712	605	665	582	552

Annex 7 Summary of analytical calculation

Table A.7-55 Summary of analytical model results.

Present Research (High-Strength Steel- Transverse Fillet weld)							
Filler Metal		OK AristoRod 13.12					
Specimen Designation		TS-1	TS-2	TS-3	TS-4	TS-5	TS-6
Weld Thickness (a)	[mm]	4.30	3.15	3.25	3.45	3.75	3.30
Total effective length (L)	[mm]	90	90	88	88	90	88
Theoretical effective area of weld (A_{th})	[mm ²]	387.0	283.5	286.0	303.6	337.5	290.4
Tensile strength of base plate ($f_{u,PM}$)	[N/mm ²]	888.16	888.16	888.16	888.16	888.16	888.16
Tensile strength of filler metal ($f_{u,FM}$)	[N/mm ²]	778.85	778.85	778.85	778.85	778.85	778.85
Correlation factor ($\beta_{w,mod}$)	[-]	1.09					
Partial safety factor (γ_{M2})	[-]	1.25					
Weld resistance ($F_{w,Rd,T}$)	[kN]	162	119	120	127	141	122

Annex 8 Summary of numerical design calculation

Table A.8-56 Summary of numerical design calculation results.

		Present Research (High-Strength Steel- Transverse Fillet weld)					
Filler Metal		OK AristoRod 13.12					
Specimen Designation		TS-1	TS-2	TS-3	TS-4	TS-5	TS-6
Weld Thickness (a)	[mm]	4.30	3.15	3.25	3.45	3.75	3.30
Weld shear leg length (w)	[mm]	6.80	4.60	4.70	5.25	5.15	4.50
Total effective length (L)	[mm]	90	90	88	88	90	88
Theoretical effective area of weld (A_{th})	[mm ²]	387.0	283.5	286.0	303.6	337.5	290.4
Equivalent NDC stress (σ_{eqv,in_T})	[N/mm ²]	671	671	672	667	672	672
Weld resistance (R_{RISEM})	[kN]	260	191	192	203	227	195

LIST OF TABLES

Table 1 Maximum specified CEV for normalized HSS, EN 10025-3 [22].	15
Table 2 Maximum specified CEV for thermomechanical rolled HSS, EN 10025-4 [23].	15
Table 3 Maximum specified CEV for quenched and tempered HSS, EN 10025-6 [24].	15
Table 4 Influence of the form of weld on the cooling time $t_{8/5}$ [25].	16
Table 5 Correlation factor β_w depending on standard and steel grade [2].	18
Table 6 Design strength of transverse and longitudinal fillet welds according to EN 1993-1-8:2006 [2].	19
Table 7 Ultimate strength of filler metals f_u , FM and modified correlation factor β_w, mod [27].	19
Table 8 Design resistance of fillet welds based on prEN 1993-1-8:2020 [27].	20
Table 9 Strength of steels with associated welding consumables according to AISC 360-16 [28] (AWS D1.1/D1.1M:2020 [30]).	21
Table 10 Design resistance of fillet welds according to AISC 360-16 [28], (AWS D1.1, 2020 [30]).	21
Table 11 Mechanical properties of materials [35].	25
Table 12 Proposal for the correlation coefficient for fillet weld connections S460 and S690 according to EN 1993-1-8:2006 [2] and 1993-1-12:2007 [26] from Rasche [21].	26
Table 13 Proposal for the correlation coefficients according to EN 1993-1-8:2006 [2] and 1993-1-12:2007 [26] from Rasche [21].	26
Table 14 Mechanical properties of base and filler materials [36].	27
Table 15 Comparisons of correlation factors β_w, mod according to Rasche [21] and $\beta_w, \text{mod, mix}$ for mixed connections.	28
Table 16 Mechanical properties of base materials [13].	29
Table 17 Mechanical properties of filler materials [13].	29
Table 18 Measured average mechanical properties of steel plates and all-weld coupons.	29
Table 19 Chemical composition	37
Table 20 Nominal mechanical properties	38
Table 21 Measured average mechanical properties.	38
Table 22 Chemical composition of wire (%).	39
Table 23 Nominal mechanical properties	39
Table 24 Measured average mechanical properties.	40
Table 25 Average dimension measurement for weld A and weld B before testing.	42
Table 26 Average measurement of the fracture surface area after an experiment	45
Table 27 Summary of the mean measurement before and after an experiment.	45

Table 28 Summary of the strength of transverse fillet weld made from HSS.	47
Table 29 Mean strength and ductility of the transverse weld from high-strength steel.	50
Table 30 Material properties of base and filler materials.	51
Table 31 Average measurement of weld profile and effective area of the weld.	52
Table 32 Weld resistance by using the theoretical effective area of the weld.	53
Table 33 Material properties of base and filler materials for solid finite element model.	55
Table 34 Comparison on strength between experiment and solid finite element model.	59
Table 35 Material properties of base and filler materials for FEM.	59
Table 36 Comparison on deformation capacity between volume and shell finite element model.	64
Table 37 Summary of equivalent stress and resistance of RISEM.	73
Table 38 Comparison of the strength between test and RISEM results.	74
Table 39 Comparison of the weld resistance by RISEM and AM.	77
Table 40 Overview of transverse and longitudinal fillet weld.	79
Table 41 Comparison of the design resistance of RISEM with an AM for transverse and longitudinal fillet weld.	79
Table 42 Comparison of the maximum equivalent plastic strain of solid and shell model.	82
Table 43 Evaluating the strain limit by comparison with experimental results.	83
Table 45 Material parameters of the base and filler metal in finite element model.	84
Table 45 Comparison of the design resistance of RISEM with an analytical model for transverse fillet weld.	86
Table 46 Comparison of the design resistance of RISEM with an analytical model for transverse fillet weld.	87
Table 47 Comparison of the design resistance of RISEM with an analytical model for longitudinal fillet weld.	89
Table A.1-48 Measurement of weld profile on transverse fillet lap-welded connections.	99
Table A.1-49 Measurement of steel plate on transverse fillet lap-welded connections.	99
Table A.1-50 Summary of average measurement on weld profile of transverse fillet lap-welded connections.	99
Table A.1-51 Summary of the fracture surface area measurement after the experiment.	100
Table A.2-52 Mechanical properties of material S700 MC Plus.	102
Table A.2-53 Mechanical properties of material OK AristoRod 13.12.	103
Table A.6-54 Summary of experimental results.	115
Table A.7-55 Summary of analytical model results.	116
Table A.8-56 Summary of numerical design calculation results.	117

LIST OF FIGURES

Fig. 1. Stresses on the throat section of fillet weld [2].	17
Fig. 2. Test specimens for longitudinal welds (left) and transverse welds (right) [11].	22
Fig. 3. Typical drawing of lap and cruciform joint (left) [6] and the picture of respective joints (right) [32].	23
Fig. 4. (a) Comparison of ultimate stresses of lap joints of S355J2, S460M, and S690Q, matching condition [32], (b) Comparison of ultimate stresses of cruciform joints with mismatching conditions [32].	24
Fig. 5. a) Comparison of ultimate stress of lap joints with different filler metals [6], b) Comparison of ultimate stresses of cruciform joints S460M and S690Q, matching condition [6].	24
Fig. 6. a) Longitudinal cruciform joint (L-series), b) Load-carrying transverse cruciform joint (X-series) [35].	25
Fig. 7. a) Transverse load-carrying lap joint (T-series), b) Transverse and longitudinal load-carrying lap joint (LT-series) [35].	25
Fig. 8. Geometry and dimension of cruciform specimen [10].	26
Fig. 9. Comparison of the ultimate strength capacity for filler welds based on penetration (a) Under-matching (b) Over-matching filler material [10].	27
Fig. 10. The influence of filler and base metal strength on the load carrying capacities σ_v, \max of fillet-welded cruciform joints [5].	28
Fig. 11. The influence of filler and base metal strength on the load carrying capacities $\tau_{\parallel, \max}$ of longitudinal fillet-welded [5].	28
Fig. 12. Geometry of the lap joint [13].	29
Fig. 13. (a) Transverse lap-welded fillet joint (b) cruciform fillet joints [37].	30
Fig. 14. Longitudinal lap-welded fillet joint [38].	30
Fig. 15. Fillet welds modelled in T-joints, (a) Rigid links [44], and (b) Increased thickness method. ..	31
Fig. 16. Fillet welds modelled in T-joints, (a) Inclined elements having mid-side nodes and Inclined elements connections with rigid links [46].	32
Fig. 17. Three-dimensional measurement system using DIC technique [51].	32
Fig. 18. Typical geometry of the coupon test specimen.	35
Fig. 19. Specimen ready for tensile testing.	36
Fig. 20. Specimens before (Top) and after (Bottom) the tensile test.	37
Fig. 21. Stress-strain curve of Strenx S700 MC Plus.	38

Fig. 22. Typical scheme for a sequence of the beads during the Strenx 700MC Plus steel welding process.	39
Fig. 23. Welding process of Strenx 700 MC Plus steel plates with a sequence of the beads.	39
Fig. 24. Specimens before (Top) and after (Bottom) the tensile test.	40
Fig. 25. Stress-strain curve of OK AristoRod 13.12 electrode.	41
Fig. 26. (a) Layout and geometry of the transverse fillet lap-welded connection (b) weld measurements before fracture.	42
Fig. 27. Transverse fillet lap-welded connection.	42
Fig. 28. Setting of specimens on a test machine.	43
Fig. 29. Preparation of the surface (Left) and speckle pattern on the target measurement surface (Right).	44
Fig. 30. Transverse fillet lap-welded connection after experiment.	44
Fig. 31. Typical example of (a) 3D specimen model and (b) Extracted weld surface area.	45
Fig. 32. The effect of the weld leg on the strength of transverse fillet lap-welded specimen.	46
Fig. 33. Comparison between the ultimate tensile strength of weld 13.12 concerning ultimate strength calculated by (a) F_u/A_{th} and (b) F_u/A_{fr}	46
Fig. 34. Test vs. predicted capacity of transverse fillet weld according to (a) Eurocode and (b) AISC.	47
Fig. 35. The location of the measurement points on the transverse fillet lap-welded specimen at the initial state.	48
Fig. 36. Displacement developed along the measurement points, (a) Loading time and (b) Force (e.g., TS-4).	48
Fig. 37. Strain development along the measurement points, (a) Loading time and (b) Force (e.g., TS-4).	48
Fig. 38. Load-deformation curve of transverse fillet lap-welded specimen, (a) measurement of relative displacement of TS-14, and (b) average load-deformation curve of all specimens.	49
Fig. 39. Stress-strain diagram of the transverse fillet-lap welded connection (a) Stress corresponds to fracture surface area, (b) Stress corresponds to the theoretical effective area of the weld.	49
Fig. 40. Comparison of the weld leg's effect on the transverse fillet weld's ductility.	50
Fig. 41. Stress-strain curve of the material.	51
Fig. 42. Transverse fillet lap-welded specimen (a) Plan view, and (b) Section.	52
Fig. 43. Longitudinal fillet lap-welded connection [13].	54
Fig. 44. Three-dimensional finite element model and boundary conditions for transverse fillet welded connection.	55

Fig. 45. Three-dimensional finite element model and boundary conditions for longitudinal fillet welded connection.	56
Fig. 46. Influence of mesh size on ultimate stress in the transverse fillet lap-welded connection.	56
Fig. 47. Influence of mesh size on maximum equivalent plastic strain in the longitudinal fillet lap-welded connection.	57
Fig. 48. Strength-deformation diagram of transverse fillet lap-welded connections; (a) TS-1, (b) TS-2, (c) TS-3, (d) TS-4, (e) TS-5, and (f) TS-6.	58
Fig. 49. Strength-deformation diagram of longitudinal fillet lap-welded connections.	58
Fig. 50. Typical scheme used for NDC, (a) real structural parts, (b) option 1, (c) option 2, and (d) option 3.	60
Fig. 51. Regular inclined shell element model (RISEM) with boundary conditions for transverse welded connections.	61
Fig. 52. Regular inclined shell element model (RISEM) with boundary conditions for longitudinal welded connections.	61
Fig. 53. Influence of mesh size on the equivalent plastic strain of the inclined shell elements for transverse weld.	62
Fig. 54. Influence of mesh size on the equivalent plastic strain of the inclined shell elements for longitudinal weld.	62
Fig. 55. Strength-deformation diagram of transverse fillet lap-welded connections; (a) TS-1, (b) TS-2, (c) TS-3, (d) TS-4, (e) TS-5, and (f) TS-6.	64
Fig. 56. Strength-deformation diagram of longitudinal fillet lap-welded connections.	64
Fig. 57. Strength-deformation diagram of transverse fillet lap-welded connections: verification with analytical model.	65
Fig. 58. Strength-deformation diagram of longitudinal fillet lap-welded connections: verification with analytical model.	66
Fig. 59. Stresses acting on the inclined surface of the weld.	67
Fig. 60. Numerical model of the specimen TS-5.	68
Fig. 61. Representation of stresses computation path along the length of the inclined shell element. .	69
Fig. 62. Representation of converted equivalent uniform stresses along the length of the inclined shell element (transverse welded connection – TS5).	71
Fig. 63. Representation of converted equivalent uniform stresses along the length of the inclined shell element (longitudinal welded connection).	71
Fig. 64. Numerical model of the specimen TS-5.	72
Fig. 65. Force-strain diagram of transverse fillet lap-welded connections; (a) TS-1, (b) TS-2, (c) TS-3, (d) TS-4, (e) TS-5, and (f) TS-6.	73

Fig. 66. Comparison the strength of welded connections with the shear leg.....	74
Fig. 67. Force-displacement curves of the transverse fillet lap-welded connection: (a) TS-1, (b) TS-2, (c) TS-3, (d) TS-4, (e) TS-5, and (f) TS-6.	75
Fig. 68. Force-displacement curves of the longitudinal fillet lap-welded connection.....	76
Fig. 69. (a) Comparison of strength from experiments and RISEM on transverse weld [11], [37], and (b) Comparison of strength from experiments and RISEM on longitudinal weld [13], [38].....	77
Fig. 70. Comparison of the RISEM and analytical weld resistance of transverse fillet weld-CTU experiment.....	78
Fig. 71. Geometric configuration of fillet weld transverse weld.	78
Fig. 72. Geometric configuration of fillet weld longitudinal weld.	79
Fig. 73. Sensitivity study on weld length for transverse welded connection.....	80
Fig. 74. Sensitivity study on weld length for longitudinal welded connection.....	80
Fig. 75. Influence on the ratio of two calculation approach for longitudinal welded resistance over the integration interval of the weld length.	81
Fig. 76. Comparison of the maximum equivalent plastic strain of solid and shell model with ultimate plastic strain of OK Aristorod 13.12.....	83
Fig. 77. Stress-strain curve of the material.	84
Fig. 78. Nominal stress-plastic strain curve of materials used in RISEM.	84
Fig. 79. Influence mesh size on resistance of welded connection.	85
Fig. 80. Influence of the limit value of plastic strain on the weld resistance.....	86
Fig. 81. Sensitivity study of weld length.	87
Fig. 82. Verification of RISEM to AM.....	88
Fig. 83. Influence of mesh size on resistance of longitudinal welded connections.	89
Fig. 84. Sensitivity study of weld length.	89
Fig. 85. Verification of RISEM to AM.....	90
Fig. A.1.86. Section view of the transverse fillet lap-welded connection.	98
Fig. A.1.87. Plan view (Left) and weld profile measurement before testing (Right) of the transverse fillet lap-welded connection.....	98
Fig. A.1.88. A typical example of (a) a Cut piece of a 3D model of the specimen and (b) a Fracture surface area of the weld.	100
Fig. A.2.89. Typical geometry of the coupon test specimen.	101
Fig. A.2.90. Proof Stress Calculation.	101
Fig. A.2.91. Stress-strain curve of material Strenx S700 MC Plus.....	102
Fig. A.2.92. Stress-strain curve of material OK AristoRod 13.12.....	103
Fig. A.2.93. Average stress-strain curve of S700 MC Plus and OK AristoRod 13.12.	103

Fig. A.3.94. Several measurement key points were assigned in the test piece.....	104
Fig. A.3.95. TS-1 (a) Displacement vs. time and (b) Displacement vs. force.	104
Fig. A.3.96. TS-2 (c) Displacement vs. time and (d) Displacement vs. force.	105
Fig. A.3.97. TS-3 (e) Displacement vs. time and (f) Displacement vs. force.....	105
Fig. A.3.98. TS-4 (g) Displacement vs. time and (h) Displacement vs. force.	105
Fig. A.3.99. TS-5 (i) Displacement vs. time for TS-5 and (j) Displacement vs. force.	106
Fig. A.3.100. TS-6 (k) Displacement vs. time and (l) Displacement vs. force.....	106
Fig. A.3.101. TS-1 (a) Strain vs. time and (b) Strain vs. force.....	106
Fig. A.3.102. TS-2 (a) Strain vs. time and (b) Strain vs. force.....	107
Fig. A.3.103. TS-3 (a) Strain vs. time and (b) Strain vs. force.....	107
Fig. A.3.104. TS-4 (a) Strain vs. time and (b) Strain vs. force.....	107
Fig. A.3.105. TS-5 (a) Strain vs. time and (b) Strain vs. force.....	108
Fig. A.3.106. TS-6 (a) Strain vs. time and (b) Strain vs. force.....	108
Fig. A.4.107. Measurement points for the deformation of transverse fillet lap-welded connection. .	109
Fig. A.4.108. Force-deformation curve of TS-1, (a) Relative displacement of three distances, (b) Average of relative displacement.....	109
Fig. A.4.109. Force-deformation curve of TS-2, (a) Relative displacement of three distances, (b) Average of relative displacement.....	110
Fig. A.4.110. Force-deformation curve of TS-3, (a) Relative displacement of three distances, (b) Average of relative displacement.....	110
Fig. A.4.111. Force-deformation curve of TS-4, (a) Relative displacement of three distances, (b) Average of relative displacement.....	110
Fig. A.4.112. Force-deformation curve of TS-5, (a) Relative displacement of three distances, (b) Average of relative displacement.....	111
Fig. A.4.113. Force-deformation curve of TS-6, (a) Relative displacement of three distances, (b) Average of relative displacement.....	111
Fig. A.5.114. Strength vs. strain for TS-1.....	112
Fig. A.5.115. Strength vs. strain for TS-2.....	112
Fig. A.5.116. Strength vs. strain for TS-3.....	113
Fig. A.5.117. Strength vs. strain for TS-4.....	113
Fig. A.5.118. Strength vs. strain for TS-5.....	113
Fig. A.5.119. Strength vs. strain for TS-6.....	114